MULTIPLE SCATTERING OF PROTONS AND NITROGEN IONS ON METAL FOILS

Tetsuo Yamazaki

MULTIPLE SCATTERING OF PROTONS AND NITROGEN IONS ON METAL FOILS

by

Tetsuo Yamazaki

Electrotechnical Laboratory

Tanashi, Tokyo

February 1974

Contents

Chapter I. Introduction

When a particle travels through matter it successively changes the direction of motion colliding with medium atoms. This phenomenon is called multiple scattering, which is dominated in the case of charged particle of MeV energy region by Coulomb field produced by the projectile and medium nucleus together with screening electrons. Therefore, much knowledge about screened Coulomb field is obtained from multiple scattering of charged particles.

High-energy and small-angle multiple scattering on moderately thin foil is especially simple from both theoretical and experimental points of view. For example, major difficulties in the theoretical treatment are reduced by the use of small-angle approximation. Since the yield of the scattered particles is dominant in the forward direction, experiment on small-angle multiple scattering has much advantage. In this case, outgoing particles make a Gaussian-like angular distribution whose center is the initial beam direction.

Observation of multiple scattering began when Rutherford[1] investigated this phenomenon in the first decade of this century, though there was no concept of "nucleus". In a few years after the discovery of nucleus by Rutherford,[2] some experiments on multiple scattering were carried out (e.g. by Mayer[3] by means of alpha-particles from polonium).

Bohr[4] suggested an intimate relationship between stopping phenomena and multiple scattering. A more detailed theory of multiple scattering was first given by Williams[5,6]* by fitting together a Gaussian curve for the central part of the angular distribution and a single scattering tail. His theory was greatly

improved by Goudsmit and Saunderson,[7,8] Molière[9,10] and Snyder and Scott.[11] The last three theories were closely related to one another, and the relation was discussed in some detail by Lewis[12] and Bethe.[13] Among them, Molière's theory is most useful because of its analytic and simple feature, but it is not applicable in the region of small mean number of scatterings (plural scattering). Therefore, Keil et al.[14] developed the theory for this region.

Nigam, Sundaresan and Wu (NSW)[15] obtained their multiple scattering theory using Born approximation to the second order and it has been developed and numerically calculated by Marion and Zimmerman.[16]

Recently Meyer[17] has derived a new angular distribution function adopting a classical single-scattering theory proposed by Lindhard, Nielsen and Scharff (LNS).[18]

Many experiments on multiple scattering of electrons or positrons have been done (e.g. refs.19-21) for the adequacy of above theories to be examined, while those of protons or heavier ions are not so many.

One of the merits of Molière's theory, as compared with NSW's theory, is that it is applicable to the cases of fairly large α values, where α is the Born parameter defined in the next chapter. The applicability has been demonstrated by Simon[22] using ^{16}O and ^{40}Ar ions of 10 MeV/amu in energy and by Lassen and Ohrt[23] with high energy (5 MeV/amu) alpha particles. On the other hand, Bernhard et al.[24] and Andersen and Bøttiger[25] have experimented on low energy heavy ions and found their results consistent with Meyer's theory. The observations on intermediate energy particles have been reported by Bichsel,[26] Bednyakov et al.[27-29] and

author's group.[30,31]

We have carried out the experiments on multiple scattering of MeV protons and nitrogen ions upon aluminium, copper, silver and gold foils.[30,31] One of the main ogjects of the present paper is to discuss the applicability of the theories by comparing them with our data. Especially, Molière's original theory is reconsidered by taking the advanced Thomas-Fermi radius into account.

We have also simulated several multiple scattering processes using Monte-Carlo method.[32] The procedure and the results are also described in the present report.

Since the theories of multiple scattering have some complicated notations and expressions, they are outlined briefly in Chapter II. The present experimental method and the results are described in Chapter III. The procedure of simulation and the results are dealt with in Chapter IV. In Chapter V, this report is summarized and problems left are pointed out.

---

* Though the papers of Williams appeared earlier than the paper of Bohr, the theory was obtained later than the treatment of Bohr

Chapter II. Theories

§2-1. Introduction

Williams[5,6] first dealt with multiple-scattering theory in some detail. A little later, the theory was greatly improved by Goudsmit and Saunderson,[7,8] who exploited the addition theorem for spherical harmonics and evaluated the sum over the orders of scattering for arbitrarily large angles using Legendre polynomial expansions. However, their theory has difficulties that related observations are only possible in track-visualization devices and that the presence of boundaries is not considered.

Snyder and Scott[11] derived their distribution function solving numerically the Boltzmann transport equation. This is, however, equivalent to Wentzel[33]-Molière[10] summation method, and the latter is simpler. Molière's theory is most useful in the above theories when a target of foil is assumed, but it is not applicable to the case of small mean number of scatterings as discussed in a later section. Keil et al.[14] modified the theory in this region.

Nigam et al. (NSW)[15] developed the theory using Born approximation to the second order. The theory is, however, not applicable to our cases, as described in the next chapter.

Meyer,[17] adopting the single scattering formula developed by Lindhard et al. (LNS),[18] derived a new formula for multiple-scattering angular distribution. It has been found consistent with the experiments on low energy heavy ions.[24,25]

In this chapter, the theories of Molière and Keil et al. are described in some detail, and the theories of NSW and Meyer briefly. Further details of the theories up to 1963 are given in a review

article by Scott.[34] Some explanations about notations of angles and distribution functions and about small angle approximation would be necessary here.

The spatial angle θ, the projected angles ϕ_x and ϕ_y and the azimuth β are defined as shown in Fig.2-1. We deal with both the spatial-angle distribution function, $F(\theta,\beta,t)$, and the projected-angle function, $f(\phi,t)$. These are based on the single scattering function, $W(\theta,t)$, where t is the foil thickness measured along the initial direction and ϕ is the angle of the track when projected on a given plane containing the original direction (e.g. ϕ_x in Fig.2-1).

The small angle approximation means

(a) replacing $\sin\theta$ by θ and $\cos\theta$ by 1,

(b) replacing the relations for the projected angles $\phi=\phi_x$ and ϕ_y,

$$\tan\phi_x=\tan\theta\cos\beta$$
$$\tan\phi_y=\tan\theta\sin\beta\ , \qquad (2\text{-}1\text{-}1)$$

by

$$\phi=\phi_x=\theta\cos\beta$$
$$\phi_y=\theta\sin\beta\ , \qquad (2\text{-}1\text{-}2)$$

and

(c) replacing the upper limit π for θ and the limits $\pm\pi$ for ϕ by the values ∞ and $\pm\infty$, respectively.

This last substitution involves the assumption that all the functions of θ and ϕ, over which integrals are taken, fall off sufficiently rapidly for large arguments.

We hereafter treat only the cases of amorphous foils and no polarization, and so the dependence of F and f on β may be neglected. The functions F and f are normalized, with the use of above approximations and assumptions, according to

$$2\pi\int_0^\infty F(\theta,t)\theta d\theta=1 \ , \qquad (2\text{-}1\text{-}3)$$

$$\int_0^\infty f(\phi,t)d\phi=1 \ . \qquad (2\text{-}1\text{-}4)$$

If ϕ_x is chosen for ϕ, the relation between F and f becomes

$$f(\phi,t)=2\int_{-\infty}^\infty F\left[(\phi^2+\phi_y^{\,2})^{1/2}\ ,t\right]d\phi_y \ . \qquad (2\text{-}1\text{-}5)$$

For the probability of one scattering occurring in dt at t through an angle between χ and $\chi+d\chi$, we use the notation $2\pi\chi d\chi \times w(\chi,t)dt$. This quantity is related to a differential cross section $2\pi\sigma(\chi,t)\chi d\chi$ by

$$w(\chi,t)dt=N(t)\sigma(\chi,t)dt \ , \qquad (2\text{-}1\text{-}6)$$

where N(t) represents the number of independent scattering atoms per unit volume of foil in the neighbourhood of t. Since there is no theory including energy loss process and since we use homogenious foils hereafter, the dependence of W, σ and N on t can be neglected.

Since "Wentzel's summation method"[33] is used in all the theories discussed in the following sections, its final formulae would be necessary to be presented. For the spatial-angle distribution we introduce a Hankel transform of order zero multiplied by 2π :

$$\tilde{F}(\xi,t)=2\pi\int_0^\infty J_0(\xi\theta)F(\theta,t)\theta d\theta \ . \qquad (2\text{-}1\text{-}7)$$

On the other hand, the absolute value of Fourier transform,

$$\tilde{f}(\xi,t)=\int_0^\infty \cos(\xi\phi)f(\phi,t)d\phi \ , \qquad (2\text{-}1\text{-}8)$$

is used for the projected angle distribution. Finally, by means of the summation method, $\tilde{F}(\xi,t)$ becomes

$$\tilde{F}(\xi,t)=\exp\left\{\Omega(\xi,t)-\Omega_0(t)\right\} \ , \qquad (2\text{-}1\text{-}9)$$

$$\Omega(\xi,t)=2\pi t\int_0^\infty J_0(\xi\chi)W(\chi)\chi d\chi \ , \qquad (2\text{-}1\text{-}10)$$

$$\Omega_0(t)=\Omega(0,t)=2\pi t\int_0^\infty W(\chi)\chi d\chi \ . \qquad (2\text{-}1\text{-}11)$$

The expression for $\tilde{f}(\xi,t)$ is obtained similarly, and the result is quite the same.

The scattering of a fast charged particle by an atom is dominated by a modified form of Rutherford law. The law yields, for the scattering of a non-relativistic particle of charge ze by a nucleus of charge Ze into the angular range χ to $\chi+d\chi$, the cross section

$$\sigma_R(\chi)2\pi\sin\chi d\chi=\frac{(zZe^2/E)^2}{\left[2\sin(\chi/2)\right]^4}\,2\pi\sin\chi d\chi \ , \qquad (2\text{-}1\text{-}12)$$

where E is the kinetic energy of the particle. When only small angles are involved, we have for the single-scattering probability $W_R(\chi)$ (the variable t is omitted here from the reason stated before),

$$W_R(\chi)=N\sigma_R(\chi)=4N\alpha^2/(k^2\chi^4) \ , \qquad (2\text{-}1\text{-}13)$$

where the so-called Born parameter, α, is defined by

$$\alpha=zZe^2/(\hbar v) \ , \qquad (2\text{-}1\text{-}14)$$

k and v being the wave number and the velocity of scattered particle, respectively.

Since the screening effect of atomic electrons on nuclear Coulomb field is neglected in (2-1-13), it should be modified. Usually this correction factor (screening factor) is written by $q(\chi)$, and (2-1-13) is modified as

$$W(\chi)=\left[4N\alpha^2/(k^2\chi^4)\right]\cdot q(\chi) \ . \qquad (2\text{-}1\text{-}15)$$

The screening factor goes to zero as $\chi \longrightarrow 0$ (small angles of

scattering occur classically for passage of the scattering particle far from the nucleus where the screening is most effective) and goes to 1 for large angles (where the screening effect is negligible).

§2-2. Theory of Molière

Molière[9] proposed an interaction potential of

$$V(r)=\frac{zZe^2}{r}\left[0.10\exp\left(-\frac{6.0r}{a_{TF}}\right)+0.55\exp\left(-\frac{1.2r}{a_{TF}}\right)+0.35\exp\left(-\frac{0.3r}{a_{TF}}\right)\right] \qquad (2\text{-}2\text{-}1)$$

by fitting carefully to the Thomas-Fermi function, where a_{TF} is the Thomas-Fermi radius. The radius was given in his original paper by

$$a_{TF}=0.8853a_o Z^{-1/3} , \qquad (2\text{-}2\text{-}2)$$

where a_o is the first Bohr radius of hydrogen atom. Bohr[4] suggested another type of the radius taking account of both projectile and the target atom, and it was corrected by multiplying a constant factor by LNS.[18] The radius is

$$a_{TF}=0.8853a_o(z^{2/3}+Z^{2/3})^{-1/2} , \qquad (2\text{-}2\text{-}3)$$

which is more appropriate than (2-2-2) for the cases of our experiment, as discussed in the next chapter.

Molière derived a differential single-scattering cross section using (2-2-1) and applying the first Born approximation and WKB-type approximation. Finally he derived a simple functional form for $q(\chi)$;

$$q(\chi)=\chi^4/(\chi^2+\chi_\alpha^2)^2 , \qquad (2\text{-}2\text{-}4)^*$$

where χ_α is the so-called "Molière's screening angle" given by

$$\chi_\alpha=\chi_o(1.13+3.76\alpha^2)^{1/2} \qquad (2\text{-}2\text{-}5)$$

with χ_o defined by

$$\chi_o=(ka_{TF})^{-1} \ . \qquad (2\text{-}2\text{-}6)$$

If the combination of (2-1-15) and (2-2-4) is substituted into (2-1-9)$\sim$(2-1-11) and careful approximations are used, we have

$$\Omega(\xi,t)-\ \Omega_o(t)=\frac{1}{4}\chi_c^{\,2}\,\xi^2\ln\left(\frac{\gamma^2\chi_\alpha^{\,2}\,\xi^2}{4e}\right) , \qquad (2\text{-}2\text{-}7)$$

where e and lnγ are the base of natural logarithums and Euler's constant, respectively. The characteristic (or critical) angle, χ_c, is obtained from

$$\chi_c=(\pi e^4 z^2 Z^2 NtE^{-2})^{1/2} \ , \qquad (2\text{-}2\text{-}8)$$

which has a meaning that the probability of getting one scattering in length t of angle χ_c or greater is just unity.

Since $\tilde{F}(\xi,t)$ of (2-1-9) has been obtained already, the multiple scattering distribution is derived from its inverse Hankel or Fourier transform (cf. (2-1-7) and (2-1-8)). Molière[10] expanded the integrand in the inverse transform carefully, and obtained the distribution functions. Here, he introduced the reduced angular variables ϑ and φ given by

$$\vartheta=\theta/(\chi_c B^{1/2}) \ , \qquad (2\text{-}2\text{-}9)$$

$$\varphi=\phi/(\chi_c B^{1/2}) \ , \qquad (2\text{-}2\text{-}10)$$

together with the normalized "reduced" distribution functions

$$2\pi F_{red}(\vartheta,t)\vartheta d\vartheta=2\pi F(\theta,t)\theta d\theta \ , \qquad (2\text{-}2\text{-}11)$$

$$f_{red}(\varphi,t)d\varphi=f(\phi,t)d\phi \ . \qquad (2\text{-}2\text{-}12)$$

Then we have for the spatial distribution

$$F_{red}(\vartheta,t)=\frac{1}{2\pi}\int_0^\infty\left[1+\frac{\eta^2}{4B}\ln\frac{\eta^2}{4}+\frac{1}{2}\left(\frac{\eta^2}{4B}\ln\frac{\eta^2}{4}\right)^2+\cdots\right]$$

$$\times\exp(-\frac{\eta^2}{4})J_0(\vartheta\eta)\eta d\eta$$

$$=\frac{1}{\pi}\left[D_0(1,1,-\vartheta^2)+\frac{1}{B}D_1(2,1,-\vartheta^2)+\frac{1}{2B^2}D_2(3,1,-\vartheta^2)+\cdots\right], \tag{2-2-13}$$

and for the projected distribution, we have

$$f_{red}(\varphi,t)=\frac{2}{\pi}\int_0^\infty\left[1+\frac{\eta^2}{4B}\ln\frac{\eta^2}{4}+\frac{1}{2}\left(\frac{\eta^2}{4B}\ln\frac{\eta^2}{4}\right)^2+\cdots\right]$$

$$\times\exp(-\frac{\eta^2}{4})\cos(\varphi\eta)d\eta$$

$$=\frac{2}{\pi}\left[D_0(\frac{1}{2},\frac{1}{2},-\varphi^2)+\frac{1}{B}D_1(\frac{3}{2},\frac{1}{2},-\varphi^2)\right.$$

$$\left.+\frac{1}{2B^2}D_2(\frac{5}{2},\frac{1}{2},-\varphi^2)+\cdots\right]. \tag{2-2-14}$$

Here, D_i's are Dalitz functions as tabulated by Scott,[34] and B is a parameter used for the expansion of Molière given by the transcendental equation

$$B=\ln B+\ln(\Omega_0 e/\gamma^2). \tag{2-2-15}$$

The quantity Ω_0 is defined by

$$\Omega_0=\chi_c^2/\chi_\alpha^2, \tag{2-2-16}$$

which is called the "effective" mean number of scatterings in the foil.**

It should be noted that Ω_0 is proportional to foil thickness and is a very slowly varying function of energy. If $\alpha^2\gg1.13$ /3.76 holds, the term 1.13 in (2-2-5) can be neglected and χ_α is

nearly proportional to E^{-1}. On the other hand, χ_c is clearly proportional to E^{-1} (cf. (2-2-8)). Then, Ω_0 is almost independent of E when α is large enough.***

---

* Though the formula is somewhat different from the one which was explicitly used by Molière in the derivation of multiple scattering distribution, Scott[34] verified that the use of (2-2-4) leads to the same result (of (2-2-7)) as Molière's.

** The notation Ω_0 is not equal to $\Omega_0(t)$ in (2-1-11) and Molière called this ratio Ω_b, but Scott[34] used Ω_0 for it.

*** The values of α in our experiment range from 1.71 to 215 (cf. Tables I and II).

---

§2-3. Theory of Keil-Zeitler-Zinn

Molière's theory described in the preceding section is very ingenious and supported by many experimental results. However, since it uses the expansion of the integrand of (2-2-13) and (2-2-14) in powers of 1/B, it is not applicable to the cases of small B, i.e. of small Ω_0. Keil et al.[14] have made an alternate and numerical calculation for $0.2 \leqq \Omega_0 < 20$ (plural scattering), which is introduced in this section.*

Since the parameter B is not used in this theory, a new angular variable ϑ_K other than (2-2-9) should be used, which is given by

$$\vartheta_K = \theta/\chi_\alpha \ . \qquad (2\text{-}3\text{-}1)$$

Using this new variable, we obtain, instead of (2-2-13), only for integral values of $\Omega_0 = m$,

$$F(\vartheta_K, m) = \int_0^\infty \tilde{F}(y)^m J_0(\vartheta_K y) y dy \ , \qquad (2\text{-}3\text{-}2)$$

where we use the argument m in place of t in (2-2-13). The transform $\tilde{F}(y)$ for m=1 is given by

$$\tilde{F}(y)=\exp\left[yK_1(y)-1\right] \quad , \tag{2-3-3}$$

where K_1 is the modified Bessel function of the second kind.

The device used by Keil et al., who followed Leisengang's treatment[35] but used a computer, is to approximate $\tilde{F}(y)$ to within 0.002 for all y by the formula

$$F(y) \simeq e^{-1}(1+b_1 e^{-c_1 y}+b_2 e^{-c_2 y}) \tag{2-3-4}$$

with the coefficients

$$\begin{aligned} b_1 &= 2.10667 & c_1 &= 0.935 \\ b_2 &= -0.388388 & c_2 &= 5.000 \quad . \end{aligned} \tag{2-3-5}$$

The m'th power of (2-3-4) is then written out:

$$\tilde{F}(y)^m=e^{-m}\sum_{k=0}^{m}\binom{m}{k}b_1{}^k\exp(-kc_1y)\sum_{n=0}^{m-k}\binom{m-k}{n}b_2{}^n\exp(-nc_2y) \quad , \tag{2-3-6}$$

and use is made of Bessel function integral

$$\int_0^\infty \exp(-qy)J_0(\vartheta_K y)y\,dy=\begin{cases} q(q^2+\vartheta_K{}^2)^{-3/2} & (q>0) \\ \delta(\vartheta_K) & (q=0) \quad . \end{cases} \tag{2-3-7}$$

Then we have

$$F(m,\vartheta_K)=e^{-m}\sum_{k=0}^{m}\sum_{n=0}^{m-k}\binom{m}{k}\binom{m-k}{n}b_1{}^k b_2{}^n(c_1k+c_2n)\left[(c_1k+c_2n)^2+\vartheta_K{}^2\right]^{-3/2} \quad . \tag{2-3-8}$$

The term k=n=0 gives the contribution of the unscattered particles $\exp(-m)\delta(\vartheta_K)$, which we call "no scattering" term hereafter. Keil et al. made machine computations of the non-singular part of the distribution $G(\vartheta_K,m)$, given by

$$G(\vartheta_K,m)=F(\vartheta_K,m) - e^{-m}\delta(\vartheta_K) \ . \qquad (2\text{-}3\text{-}9)$$

The greatest error, of the order of 4%, occurs for m=20 and ϑ_K=0, which is due to the error remaining in the approximation (2-3-4). Exact numerical calculation for ϑ_K=0 shows that for m=20 the computations using (2-3-4) are high by 3.2%, whereas the Molière expansion gives results that are 4.3% too low. Since the errors in Molière's method decrease as Ω_o increases, and those of Keil et al. increase, we see that Ω_o=m=20 is a good division point between the two methods.

The omission of the no scattering term in Keil et al.'s theory is significant and it will be discussed in the following chapters.

---

* Since there appears no case of $\Omega_o \leqq 2$ in the present report, the case is eliminated here.

---

§ 2-4. Theory of Nigam-Sundaresan-Wu

NSW's theory[15] is scarcely used in the present paper, but it is described here very briefly.

NSW carefully examined the Dalitz formula[36] which uses the Born approximation to the second order, and got an expression for q(χ) valid for all χ,

$$q(\chi)=\chi^4(\chi^2+\chi_\mu^2)^{-2}\left[1-\beta^2(1+\alpha\pi)\sin^2(\chi/2)+2\alpha\chi_\mu(\chi_\mu^2+\chi^2)/(4\chi_\mu^2+\chi^2)\right.$$
$$\left.+\frac{1}{2}\alpha\beta^2(\chi_\mu^2+4\sin^2(\chi/2))\right]\mathrm{cosec}(\chi/2)\tan^{-1}(\sin(\chi/2)/\chi_\mu) \ , \qquad (2\text{-}4\text{-}1)^*$$

where β=v/c, c being the velocity of light, and χ_μ is given by

$$\chi_\mu=\mu\chi_o \ . \qquad (2\text{-}4\text{-}2)$$

Here NSW used the adjustable factor μ=1.12 and 1.8. Then the

theory gives a formula for χ_α,

$$\chi_\alpha=\chi_\mu\left\{1+4\alpha\chi_\mu\left[(1-\beta^2)\ln\chi_\mu+0.2310+1.448\beta^2\right]\right\}^{1/2}, \qquad (2\text{-}4\text{-}3)$$

instead of (2-2-5) of Molière. Using (2-4-3), they derived their distribution functions in a way similar to Molière's. Some corrections for Molière's theory were made also. The results are so complicated that they are not written here. Further details have been described by Scott.[34)]

One of the major differences between the theories of Molière and NSW exists in the magnitude of χ_α. It is found easily, if (2-4-3) is compared with (2-2-5), that χ_α of NSW is nearly equal to that of Molière when α is very small. However, for large α value, NSW's χ_α is much smaller than Molière's, and finally the angular distribution of NSW becomes much broader than that of Molière. This is an important point as discussed in the next chapter.

---

* Small angle approximation is severely examined in their theory.

---

§ 2-5. Theory of Meyer

Though Molière's theory is applicable even to the cases of fairly large α, there is a limitation of

$$\alpha\chi_0 \ll 1 , \qquad (2\text{-}5\text{-}1)$$

as Scott[34)] has predicted. Meyer[17)] established a theory applicable to the cases of large α values, using LNS's classical single-scattering theory.[18)]

Single-scattering cross section is, in general, a function of scattering angle χ and reduced energy

$$\varepsilon = a_{TF}/b \ , \qquad (2\text{-}5\text{-}2)$$

where

$$b = 2zZe^2(m_1+m_2)/(m_1 m_2 v^2) \qquad (2\text{-}5\text{-}3)$$

is the distance of closest approach in a classical sense written in the center of mass system, where m_1 and m_2 are the masses of projectile and target atom, respectively. LNS showed that this dependence of the cross section on two variables can be reduced in rather good approximation to a dependence on only one quantity

$$\eta = \varepsilon \sin(\chi/2) \ . \qquad (2\text{-}5\text{-}4)$$

They obtained the differential scattering cross section in the form of

$$\frac{d\sigma}{d\eta} = \pi a_{TF}^2 \frac{f(\eta)}{\eta^2} \ . \qquad (2\text{-}5\text{-}5)$$

The function $f(\eta)$ was numerically calculated according to the Thomas-Fermi model and given graphically and by a table. For large values of η, this function approaches the function

$$f_R(\eta) = (2\eta)^{-1} \ , \qquad (2\text{-}5\text{-}6)$$

which corresponds to the Rutherford cross section (cf. the description following (2-1-15)). Molière's cross section in this form is represented by

$$f_M(\eta) = \eta^3 / \left\{2(3.76/16 + \eta^2)\right\}^2 \ , \qquad (2\text{-}5\text{-}7)$$

where it is assumed that $\alpha^2 \gg 1.13/3.76$ and the term 1.13 in (2-2-5) is neglected. The above three functions are shown in Fig.2-2.

The strong decrease of the scattering cross section of Molière with decreasing angle results in a finite value of total scattering cross section. Consequently the number of collisions,

encountered by a particle in Molière's theory, is much smaller than the number of atomic layers penetrated. The differential cross section (2-5-5) calculated from classical mechanics, however, results in a diverging total cross section which has to be cut off on physical grounds.

Meyer assumed that each scattering center is effective within a spherical volume of radius r_0 which is equal to half the distance of immediately neighbouring atoms of amorphous foil;

$$r_0 = N^{-1/3}/2 \ . \qquad (2\text{-}5\text{-}8)^*$$

The restriction to this volume results in a minimum scattering angle η_0 for single scattering, which is determined by

$$\int_{\eta_0}^{\varepsilon} \frac{d\sigma}{d\eta}\, d\eta = \pi r_0^{\,2} \ . \qquad (2\text{-}5\text{-}9)$$

Then we have for the average number of collisions, m, suffered by a particle penetrating a layer of thickness t,

$$m = \pi r_0^{\,2} N t \ , \qquad (2\text{-}5\text{-}10)$$

assuming that the classical impact parameters are uniformly distributed over the cross section $\pi r_0^{\,2}$. The value of m is much greater than that of Ω_0 of Molière.

Using (2-5-5) and (2-1-9), we have for the spatial angle distribution of multiple scattering in laboratory system

$$F(\vartheta,\tau) = \frac{\varepsilon^2}{8\pi}\left(\frac{m_1+m_2}{m_2}\right)^2 \left[f_1(\vartheta,\tau) - \frac{a_{TF}^{\,2}}{r_0^{\,2}} f_2(\vartheta,\tau) \right] \ , \qquad (2\text{-}5\text{-}11)$$

where

$$f_1(\vartheta,\tau) = \int_0^{\infty} \exp\left[-\tau\,\Delta(z)\right] J_0(\vartheta z)\, z\, dz \qquad (2\text{-}5\text{-}12)$$

and

$$f_2(\tilde{\vartheta},\tau)= \frac{\tau}{2} \int_0^\infty \exp\left[-\tau\, \Delta(z)\right] J_0(\tilde{\vartheta}\, z)\Delta^2(z)zdz \ , \qquad (2\text{-}5\text{-}13)$$

both of which have been tabulated by Meyer. Here $\tilde{\vartheta}$ is Meyer's reduced angular variable given by

$$\tilde{\vartheta} = \theta \cdot \frac{\varepsilon}{2} \cdot \frac{m_1+m_2}{m_2} \ , \qquad (2\text{-}5\text{-}14)$$

and τ is the reduced thickness defined by

$$\tau = \pi a_{TF}^{\ 2} N t \ , \qquad (2\text{-}5\text{-}15)$$

which is numerically very close to Ω_0 of Molière and the relation

$$\tau = 3.76\, \Omega_0/4 \qquad (2\text{-}5\text{-}16)$$

holds when $\alpha^2 \gg 1.13/3.76$. The function $\Delta(z)$ in (2-5-12) and (2-5-13) is obtained from

$$\Delta(z)= \int_{\eta_0}^\infty \frac{f(\eta)}{\eta^2} \left[1-J_0(z\,\eta)\right] d\eta \ . \qquad (2\text{-}5\text{-}17)$$

The distribution (2-5-11) is nearly equal to (2-2-13) of Molière for large τ ($\gtrsim 20$) and becomes broader than the distribution of Keil et al. as τ decreases.

---

* Rigorously, $r_0=\pi^{-1}N^{-1/3}$ should be used as in ref.24, but the second term in the brackets of (2-5-11) is so small that the use of (2-5-8) causes little error.

Chapter III. Experiments

§3-1. Arrangement and Measuring System

The schematic view of the present experimental arrangement and the block diagram of measuring system are shown in Figs.3-1 and 3-2, respectively.

Protons or nitrogen ions extracted from a PIG type ion source were accelerated by a 4MV Van de Graaff accelerator of Kyoto University which had been constructed in 1969. The ion beam was deflected and energy-analysed by a 90° magnet and introduced into a collimation system. The ion energy can be determined within an accuracy of about 5keV by an NMR measurement of the analyser magnetic field.

The collimation system was arranged to measure correctly the spatial-angle distribution. Three longitudinal slits having movable knife edges and with the length of 6mm were used. Two of them (S-1 and S-3) were placed vertically, while one (S-2) horizontally, each distance being 900mm. Thus a well collimated ion beam spot of about 0.3mm × 0.3mm in size was obtained, which was clearly seen on a fluorescent screen placed behind. Moreover, we could control the counting rate of the detector SSD, prior to the experiment, by changing the slit widths a little.*

Just behind the slit S-3, a foil exchanger was placed, on which scattering foils were set. Techniques of foil preparation and of thickness measurement are described in the next section.

To move the particle detector SSD (D) exactly on the line passing the beam axis, two small concave cuts were made at the end of the detector holder. If the straight beam travels through the cuts, the detector slit of about 0.2mmØ would be correctly

moved on the line.

The window slit of 2mmØ was made in front of the monitor SSD (M), which was fixed at a position where the counting rate was adequate (usually 300~500 counts/sec). Thus for the scattered ions, the ratio, D/M, of the count of detector (D) to that of monitor (M) as a function of the detector position (i.e. of the angle of the scattered particles) leads to the spatial angle distribution. The counting errors were less than 2%.

The straight beam was examined by removing the scattering foil and using the detector SSD also. It was always 0.2~0.3mm in size** and no appreciable scatterings caused by slit edges were found. During the experiment, energy spectrum of the beam after the foil was frequently checked and measured by means of the multi-channel pulse-height analyser. Moreover, the counting rates of D and M were always checked by the use of a two-pen recorder connected with the rate meters.

The foil exchanger and detector- and monitor-SSD were arranged in a scattering chamber, the vacuum in which was maintained at better than 4×10^{-6} mmHg. The chamber was arranged so that we could measure correctly the angular distribution up to about 0.15 radians.

---

* The size of the straight beam spot during the experiment on multiple scattering is expected to be smaller than 0.3mm × 0.3mm, because we usually reduced the width of slits, after seeing the spot, to get an appropriate counting rate.

** The accuracy of the measurement of straight beam width was not good, because the window before the detector SSD was as large as 0.2mmØ, as described above.

§ 3-2. Foils

Preparation of foil and measurement of its thickness are very important to the experiment on multiple scattering. The present method and technique are described in this section. A number of methods have been reviewed in refs.37 and 38.

(i) Preparation of thin and self-supporting foils

The foils were produced by means of vacuum evaporation. The arrangement is schematically shown in Fig.3-3.

Grains or wires of metallic material of high purity were heated on a tungsten boat. We determined the distance between the glass slide to be deposited and the source to be 307mm in order to have good uniformity of film. The slide was 20mm x 50mm in size, which had been cleaned carefully by the use of cleanser, water, distilled water and ethyl alcohol. This cleaning procedure is necessary to obtain good quality of foil. In the course of evaporation, the thickness of the deposited film was always monitored by means of quartz crystal method. The foil thickness measurement is described in the next subsection.

Small amount of potassium chloride (KCl) was deposited on the slide before the deposition of desired source material so that the removal of foil from the glass might be easy. The vacuum in the evaporation chamber was maintained at better than 1.5×10^{-5} mmHg even in the course of evaporation.

After the vacuum evaporation, the glass coated by KCl and source material was immersed in distilled water diagonally. First, KCl melts, and then the foil floats on the water surface. Since this method takes advantage of the surface tension of water to pull the film away from the glass, sufficient time must be

allowed to permit these forces to act effectively. Before this procedure, the film should be cut by knife into pieces of desired area. The pieces are seperated from one another on the water surface. In the case of very thin foil, the surface tension of water is sometimes too strong for the film to be unbroken. In such a case, a small amount of ethyl alcohol should be added in the water.

Each piece of foil was removed from the water by picking it up with aluminium or copper frame having a hole of about 6mmØ . Care should be taken to remove sharp edges on the frame which may cut the film as it stretches somewhat upon drying.

(ii) Measurement of foil thickness

Accurate measurement of foil thickness is very important for multiple scattering experiment as we have seen in Chap.II.

Foil thickness was monitored and measured by means of quartz crystal method in the course of evaporation. However, this method has a disadvantage that the monitoring is done for the deposited film on the quartz surface. Moreover, the crystal is covered with conductive layer prior to the evaporation, and this may influence the accuracy of measurement. Therefore we calibrate the quartz oscillator by means of multiple-beam interferometer (MBI).

The results obtained from above two methods are compared in Fig.3-4, from which we find that values from quartz crystal method are proportional to those from MBI. In the quartz crystal method, the increase in frequency during the deposition, Δf (kHz), is proportional to the foil thickness ρt ($\mu g \cdot cm^{-2}$). Referring to the specification of our equipment, the relation

$$\rho t = 20 \cdot c \cdot \Delta f \qquad (3\text{-}2\text{-}1)$$

exists for all materials, where c is a constant. We can conclude from Fig.3-4 that different source elements have slightly different values of c for the same thickness in $\mu g \cdot cm^{-2}$. The value for each element is represented in the figure.

On the other hand, we tried to calibrate the thickness by weighing method also, but the accurate measurement of the weight and area of very light foil was so difficult that we could not do. The gross uniformity of foil was also examined carefully by MBI method and was found satisfactory.

(iii) Energy loss

Before multiple-scattering experiment, energy loss of protons or nitrogen ions in the foil was measured for the purpose of confirming the foil thickness and determining the average energy in the foil. Here, the average beam energy, E, in laboratory system is simply given by

$$E = (E_i + E_f)/2 \ , \qquad (3\text{-}2\text{-}2)$$

where E_i and E_f are the initial energy and the energy after passing through the foil, respectively. The resultant values of stopping power are shown in Fig.3-5 (for protons) and Fig.3-6 (for nitrogen ions) together with other authors' curves.

Northcliffe and Schilling[39] have tabulated the electronic stopping power for representative ions in different material media. The tables are based on an investigation of the systematic relationships between many observed data, guided by simple theoretical expectation and extrapolated into regions where no measurements have been made. Unfortunately they did not tabulate the values of copper medium either for protons or for nitrogen ions. Therefore

we referred to a report of Allison and Warshaw[40] for protons. For nitrogen ions on copper, we got the curve by means of interpolation of the table of Northcliffe and Schilling.

In the figures, it seems that our data for aluminium, silver and gold are in good accordance with the curves from the reports of other authors in spite of some scattering caused by experimental errors.* However, the experimental values of stopping power of copper (for both protons and nitrogen ions) deviate a little from those of other authors. One may think that this is because the calibration factor c (=1.32) of (3-2-1) for copper is extraordinarily small compared with the average value (1.37), but the factor from our measurement seems to be adequate if we judge from multiple-scattering data discussed in later sections. Moreover, even if we use the average value of c, still the values of the stopping power of copper are larger than those from other authors. Then we use c=1.32 for copper hereafter.

---

* Experimental values of stopping power are not so accurate, since the energy loss in the foil is fairly small in the present cases.

---

§3-3. Angular Distributions

Multiple-scattering spatial-angle distributions of protons (0.4～1.5MeV) and nitrogen ions (1.3～4.5MeV) on aluminium, copper, silver and gold foils have been measured. The data for protons and nitrogen ions are listed in Tables I and II, respectively. The values of α, χ_α and Ω_o in the tables are calculated according to Molière's method with (2-2-3). The average energy is obtained from (3-2-2). The foil thickness ρt is written in $\mu g \cdot cm^{-2}$ units. The values of $F(0)$, $\theta_{1/2}$ and $F(2\theta_{1/2})/F(0)$ experimentally obtained

are also tabulated, where $\theta_{1/2}$ means the HWHM of distribution.

The typical angular distributions of multiple scattering are shown in Figs.3-7～3-9 together with theoretical curves. Here, they are normalized according to (2-1-3).

Figure 3-7 shows the result of 1.45MeV protons on an aluminium foil of 562μg·cm^{-2} thick. From this figure, we find that the angular distribution according to Molière's theory with the use of a_{TF} of (2-2-3) agrees fairly well with the experimental result. On the other hand, both the distributions according to NSW's theory (with μ=1.12 and μ=1.8) are much broader than the observed distribution.

As described in §2-4, NSW's χ_α is numerically close to Molière's when $\alpha \ll 1$ (cf. (2-4-3) and (2-2-5)). However, NSW's χ_α becomes much smaller than Molière's χ_α as α increases, and consequently the difference between the distributions according to the two theories becomes large as α increases. Though the α value of ion-atom combination of Fig.3-7 is the smallest in our experiment (cf. Tables I and II), still the difference is fairly large.

A few parameters of Molière and of NSW in this case are tabulated and compared in Table III. NSW's Ω_o and B are larger than those of Molière because of smaller χ_α value, and consequently NSW's distribution becomes broader than Molière's.

From what described so far, we deduce that the angular distribution of NSW will become much broader than that of Molière in the case of larger α. In fact, it is clearly seen in Fig.3-8 and Table IV. Figure 3-8 shows the angular distribution of 4.18 MeV nitrogen ions scattered from an aluminium foil of 118μg·cm^{-2}. In this case, the distribution according to NSW's theory is extremely broader than the one according to Molière's theory and

the latter theory is preferable. We conclude, as Simon[22] has already predicted, that the theory of NSW cannot be applied to the case of large α value.

The value of Ω_0 in the case of Fig.3-8 is 21.1 which is close to the boundary value (Ω_0=20) between the regions of applicability for the theories of Molière and Keil et al. Then the two theories are compared in this figure, and the description following (2-3-9) is confirmed here.

Figure 3-9(A) shows the angular distribution of 1.39MeV nitrogen ions scattered from aluminium foil of 90.9μg.cm^{-2}. Here, Keil et al.'s theory is applied* (with Lagrange interpolation** about Ω_0) because of small Ω_0 (=16.2), and the difference between the distribution functions, as obtained using (2-2-2) and (2-2-3), is shown. The Thomas-Fermi radius according to (2-2-3) seems preferable. In our experiment, the difference between (2-2-2) and (2-2-3) is greatest in the case of nitrogen ions on aluminium because of the largest value of z/Z. Our data prefer (2-2-3) to (2-2-2) in almost all the cases, though the difference between them is smaller for the other ion-atom combinations.

The angular distribution of 1.32MeV nitrogen ions scattered from silver foil of 113μg.cm^{-2} thick is shown in Fig.3-9(B). Here, the curves according to Keil et al.'s theory and Meyer's are compared. Keil et al.'s calculation neglects the "no scattering" term described in §2-3, whereas the experimental distribution for $\Omega_0 \lesssim 5$ should include an appreciable number of events classified to no scattering. Therefore, Keil et al.'s theory has little meaning in this case of Ω_0=2.78. On the other hand, Meyer's theory does not include the concept of no scattering as seen from (2-5-10), and one may think that the theory of Meyer is

applicable to the case of $\Omega_0 \lesssim 5$. However, seeing Fig.3-9(B), we find that the curve according to Meyer's theory is too broad.

The angular distributions according to Meyer's theory are in good agreement with our observations when $\Omega_0 \sim 15$ (though the figures are not shown in this report), but broader than the experimental results in the region of $\Omega_0 \lesssim 10$. At least in the present energy region, Meyer's prediction shows a deviation, which would be ascribed to the inadequate concept of classical orbit.

Keil et al.'s distribution in Fig.3-9(B) seems to be a little narrower than our experimental result. Inclusion of "no scattering" term into their formula would lead to still a narrower distribution even if the angular spread of initial beam is taken into account. This problem will be again discussed in the next section.

In conclusion, the theory of Molière-Keil et al. explains the present experimental results more satisfactorily than the theories of NSW and Meyer over the wide ranges of α and Ω_0.

---

* Rigorously, Keil et al.'s distribution should be noted as $G(\theta)$ (cf. (2-3-9)), but the notation $F(\theta)$ is used hereafter for convenience.

** Keil et al.'s table is given for integral values of Ω_0 only, as described in §2-3.

---

§3-4. Comparison with Theories

In this section, we compare the experimental results with the theories of Molière and Keil et al. only, because the inadequacy of the theories of NSW and Meyer has been found in the preceding section.

Since it is very laborious to compare the considerable amount of data in Tables I and II directly with theories as in the preceding section, we take the typical values of $F(0)$, $\theta_{1/2}$ and $F(2\theta_{1/2})/F(0)$. For the theoretical value of $\theta_{1/2}$, there is an approximate formula[41,34]

$$\vartheta_{1/2}{}^2 B = -0.146+1.799 \log \Omega_o \ . \qquad (3\text{-}4\text{-}1)$$

However, the errors in this approximation increase as Ω_o (i.e. B) decreases. Then, the theoretical value of $\vartheta_{1/2}$ was calculated directly for each case by means of Lagrange interpolation method.

Though the ratios of above three values ($F(0)$, $\theta_{1/2}$ and $F(2\theta_{1/2})/F(0)$) experimentally obtained to those from theories have been drawn as functions of projectile energy for the purpose of examining energy dependence, no relationship was found. Therefore the figures are not shown in the present report. On the other hand, we can see some dependence of above three values on the mean number of scatterings in the foil (Ω_o).

The relative value $F(2\theta_{1/2})/F(0)$ is a function of B (i.e. of Ω_o) only, but $F(0)$ and $\theta_{1/2}$ are functions of B and χ_c (i.e. functions of foil thickness, beam energy, z, Z, etc.); $F(0)$ and $\theta_{1/2}$ cannot be expressed as functions of Ω_o only. Then, we take the values of $\chi_\alpha{}^2 F(0)$ and $\theta_{1/2}/\chi_\alpha$ instead of $F(0)$ and $\theta_{1/2}$.

Substitution of (2-2-9) and (2-2-11) into (2-2-13) yields

$$F(0,t) = \frac{1}{\pi \chi_c{}^2 B}\left[D_0(1,1,0) + \frac{1}{B} D_1(2,1,0) + \frac{1}{2B^2} D_2(3,1,0) + \cdots \right] , \qquad (3\text{-}4\text{-}2)$$

where the terms in the brackets are functions of B only. If we combine (3-4-2) with (2-2-16), we know that $\chi_\alpha{}^2 F(0)$ is a function of Ω_o (i.e. of B) only. Since the relative shape of the distri-

bution is determined by the terms in the brackets of (2-2-13) (functions of B and ϑ), we have a relation

$$\theta_{1/2}=\chi_c \cdot \text{ function of B (i.e. of } \Omega_0) \qquad (3-4-3)$$

remembering (2-2-9). Accordingly $\theta_{1/2}/\chi_\alpha$ is universally expressed as a function of Ω_0.

Thus, we have found that $\chi_\alpha^2 F(0)$, $\theta_{1/2}/\chi_\alpha$ and $F(2\theta_{1/2})/F(0)$ are expressed by Ω_0 only in Molière's theory. The same conclusion can be drawn in the theory of Keil et al., if we examine (2-3-8) and (2-3-1).

Experimental values of $\chi_\alpha^2 F(0)$, $\theta_{1/2}/\chi_\alpha$ and $F(2\theta_{1/2})/F(0)$ against Ω_0 are plotted in Figs.3-10～3-12, where theoretical curves are drawn also.

Typical errors are shown by bars. They are due to (a) errors in the measurement of foil thickness, energy and scattering angles, (b) counting statistics ($< 2\%$), (c) errors in the procedure of normalization, (d) errors in reading $\theta_{1/2}$ and $F(2\theta_{1/2})$, and so on. Errors due to (a) influence all the values of F(0), $\theta_{1/2}$ and $F(2\theta_{1/2})/F(0)$. Errors due to (b) are very small, since we accumulated sufficient count during the experiment. Errors due to (c) are serious for F(0). Values of $\theta_{1/2}$ and $F(2\theta_{1/2})/F(0)$ are greatly affected by errors due to (d).

It should be noted that "no scattering" term is not included in Keil et al.'s theory, as described in §2-3. Therefore, Keil et al.'s curves in Figs.3-10～3-12 for very small Ω_0 are drawn only for reference.

Though the present experiment has been done using two kinds of projectiles of different energies and foils of four elements, the observed data in Figs.3-10 and 3-11 are closely distributed along the theoretical curves. This means that the theories treat

multiple scattering fairly reasonably even in the region of large α value and that the expression of (2-2-5) is appropriate enough. However, if we examine Fig.3-11 carefully, we find a little deviation of experimental points of $\theta_{1/2}$ from Keil et al.'s prediction where $\Omega_0 \lesssim 20$ and slight deviation from Molière's curve where Ω_0 is large. It seems that Molière's theory is more appropriate than Keil et al.'s theory where $5 \lesssim \Omega_0 \lesssim 20$, but the former theory is mathematically invalid in this region as predicted in §2-3; this becomes clear if we see Fig.3-12.

Though the experimental points of $F(2\theta_{1/2})/F(0)$ in Fig.3-12 are considerably scattered probably because of reading errors, the data evidently prefer Keil et al.'s theory for Ω_0 less than 20; $\Omega_0=20$ is the boundary value between the regions of applicability for the two theories as pointed out in §2-3.

The observed points in Fig.3-12 are, in general, a little lower than the curve from Keil et al.'s theory where $\Omega_0 \lesssim 20$ and slightly higher than that from Molière's theory where $\Omega_0 \gtrsim 20$. This tendency is considered to be an expanded one of Fig.3-11, which is explained by the use of Fig.2-2.

Molière's single-scattering cross section in Fig.2-2 seems to be underestimated than the real one in the region of very small angle, i.e. an appropriate cut-off is made. Here, a little overestimation is seen for intermediate scattering angle. The cut-off becomes significant in the case of small Ω_0 —— the width $\theta_{1/2}$ of the distribution is underestimated, and the curve of $F(2\theta_{1/2})/F(0)$ becomes higher than the observed points. In the region of large Ω_0, this effect becomes very small compared with the total multiple scattering deflection.

Molière's theory has mathematical validity for large Ω_0, where

a considerable number of medium- to large-angle scatterings are included. Since a small overestimation of the scattering cross section is effective in the region of large Ω_0, the width is estimated to be broader and the curve of $F(2\theta_{1/2})/F(0)$ becomes a little lower than the experimental points.

Experimental values of $F(0)$, $\theta_{1/2}$ and $F(2\theta_{1/2})/F(0)$ are in fairly good agreement with Keil et al.'s theory even in the region of $\Omega_0 \lesssim 5$. However, this agreement is unexpected if we remember that no scattering term is neglected in their theory. The present author cannot explain this fact. Though the theoretical distribution will become a little broader because of the angular spread of initial beam and this effect is relatively large for very small Ω_0, it is not sufficient yet.

In order to compare the experimental results more clearly with theories, the ratios of experimental $F(0)$, $\theta_{1/2}$ and $F(2\theta_{1/2})/F(0)$ to theoretical values are plotted against Ω_0 in Figs.3-13 ~ 3-15. Here, the values according to Molière's theory are used for $\Omega_0 > 20$ and those according to Keil et al. are used for $\Omega_0 \leqq 20$.

In Fig.3-13, the points of $F(0)$ are closely distributed around unity for all Ω_0. The points of $\theta_{1/2}$ in Fig.3-14 are a little higher than unity where $\Omega_0 \lesssim 20$. The difference becomes larger as Ω_0 decreases (though this tendency was obscure in Fig.3-10), and this is consistent with the explanation given before in this section.

In Fig.3-15, we see the same tendency as in Fig.3-12 in spite of fairly large dispersion. It should be noted that both the theories of Molière and Keil et al. are not so accurate in large angle region because of the errors in small angle approximation.

§3-5. Corrections for a_{TF}

Meyer and Krygel[42] have proposed to determine the screening radius a_{TF} from the results of multiple scattering experiment, and they have given formulae for the calculation of the radius from the values of F(0) and $\theta_{1/2}$ using Meyer's theory. Generally, a_{TF} should be a function of z, Z and even E.[18] The Thomas-Fermi radius of (2-2-2) or (2-2-3) is a very rough estimation, since the individual properties of the electronic shells are not accounted for.

Following their method, we tried to find the value of the radius appropriate to each experiment, which we call a_c hereafter. However, since the present experimental results are in better agreement with the theories of Molière and Keil et al. than with the theory of Meyer, as described in §3-3, we calculated the values using the former two theories. We also chose the values of F(0) and $\theta_{1/2}$. Since there is no convenient method to calculate the appropriate values of the screening radius from experimental F(0) and $\theta_{1/2}$ especially in the region of small Ω_o, we calculated them using interpolation method. An example of the computational programs (to obtain a_c's from experimental values of F(0) and $\theta_{1/2}$ according to Keil et al.'s theory) is shown in Appendix I.

The resultant values of a_c/a_{TF} against Ω_o, where a_{TF} is according to (2-2-3), are plotted in Figs.3-16 and 3-17. In the figures, the curves show the boundary values between the regions of applicability for the theories of Molière and Keil et al. If an Ω_o value is calculated using a value of a_c above the line, Ω_o becomes larger than 20, and this means that the a_c is in the region of Molière's theory. Conversely, if the point of a_c is below the boundary curve, the a_c value is considered to be subjected to

Keil et al.'s theory.

The value of a_c according to Keil et al.'s theory is larger than that according to Molière's theory, as far as F(0) and $\theta_{1/2}$ are concerned. Then there is a case in which the a_c value from Molière's theory is smaller than the boundary value and that from Keil et al.'s theory is larger than the boundary value. In such a case, we take the a_c value which yields the Ω_o value nearer to 20.

From these two figures, we find that the theory of Keil et al. becomes invalid with the decrease in Ω_o. The tendencies of a_c/a_{TF} from experimental F(0) and $\theta_{1/2}$ are similar to each other, and this is natural. This again confirms the explanation given in the preceding section.

However, the present author considers that the screening radius should not be a function of foil thickness (i.e. of Ω_o), and the dependence of a_c on Ω_o means that the method in this section is not correct physically. If the value of the screening radius increases, χ_α becomes smaller (cf. (2-2-5) and (2-2-6)) and $q(\chi)$ of (2-2-4) (i.e. single-scattering cross section) becomes larger on the whole though the relative increase is smaller in large angle region in comparison with that in small angle region. As we have seen in this chapter, the cross section should be larger in the small angle region and should be a little smaller in the intermediately large angle region than that derived by Molière. It is not the absolute value of the cross section but the shape of it (cf. Fig.2-2) that should be corrected.

The dependence of a_c/a_{TF} on ions and foil elements cannot be seen from these figures.

We tried to calculate a_c's from the values of $F(2\theta_{1/2})/F(0)$

too, but they are not shown in this report since the results are scattered greatly and the theoretical approximation is not good in the large angle region.

§3-6. Discussion

In this chapter, multiple-scattering angular distributions experimentally obtained have been compared with theories. Our data show fairly good agreement with Molière-Keil et al.'s theory if the Thomas-Fermi radius according to (2-2-3) is used, while the theories of Meyer and NSW differ rather largely from our results.

The use of (2-2-3) instead of (2-2-2) may be regarded as a kind of mixture of the theories of Molière and Meyer. Bednyakov et al.[29] have pointed out that the absence of a dependence on the charge of the projectile in (2-2-2) is a defect of Molière's theory. Therefore they have used for calculation the effective charge, z_{eff}, of the particle from their own charge exchange experiment instead of z, and we have also tried to use the similar method.[30] However, this method seems to be not so meaningful physically.

The theories of Molière and Keil et al. deviate a little from our experimental results. This seems to be attributable to the underestimation (in small angle region) and the overestimation (in intermediately large angle region) of single-scattering cross section.

Bichsel's experimental results of protons of $0.6 \sim 4.7$MeV[26] agree fairly well with Molière's theory. In his experiment, Ω_o's are large. However, his results for $E \lesssim 1.5$ MeV give a little narrower distributions than theoretical ones, and this

tendency is consistent with that of our results.

Bednyakov et al.[27,28] have reported their experimental results of multiple scattering of low energy protons (40 ~ 200keV). The angular distributions are a little narrower in the cases of carbons and slightly narrower in the cases of heavier substances than those from Molière's theory with a_{TF} of (2-2-2). They explained that the discrepancy in the carbon case is a consequance of applying the Thomas-Fermi model in the theory, and they employed the Hartree-Fock model for proton-carbon potential. However, if a_{TF} of (2-2-3) is used instead of (2-2-2), Molière's distributions fairly approach their results, and this method seems preferable. When Z of the foil is large, Molière's theory with (2-2-2) seems to explain their experimental results rather well, but this may be because the difference between (2-2-2) and (2-2-3) becomes smaller as Z increases.

Rigorously, simple estimation (3-2-2) of mean energy will always give an energy value which is higher than the true mean energy calculated by averaging all the transmitted particles. Therefore, Högberg and Norden[43] carefully examined the relation between energy loss and scattering distributions for low energy heavy ions, using Meyer's method. However, since the energy region in our experiment is rather high, no correction for the mean energy seems to be necessary even when energy loss in the foil is relatively large. The dependence of scattering distribution on energy is rather small for high energy particles, as Bernhard et al.[24] have already predicted.

Kerr et al.,[44] in their paper of experiment on multiple scattering of fission fragments, adjusted Ω_0 from the contribution of no scattering, but the method does not seem to be adequate

because the estimation of the contribution of no scattering term from experimental result is very difficult and adjustment of Ω_o only is physically unreasonable. Reasonable estimation of screening effect should be considered, as described before.

Chapter IV. Simulations

§4-1. Introduction

In the preceding chapter, experimental results of multiple scattering have been treated. Our results have supported Molière-Keil et al.'s theory, yet some deviations have been found in the case of $\Omega_0 \lesssim 10$. Therefore, it becomes necessary to know whether the disagreement is attributable to the imperfect expression of single-scattering cross section or it is because of inadequate precedure of approximation in the plural scattering theory.

The rigorous analytical calculation of angular distribution is laborious, and it is much complicated to calculate the projected-angle distribution for small Ω_0. The calculation including energy loss and effect of slit geometry is also difficult. On the other hand, the simulation using Monte Carlo method solves these problems easily, because the procedure needs only one information about differential cross section of single scattering of a projectile by a target atom. Therefore we have carried out the simulation, and some results are discussed in this chapter.

The Monte Carlo method has been widely applied to simulations on various phenomena. For example, penetration of neutrons or gamma rays through matters has been extensively treated by the method and applied to neutron physics, radiation shielding etc.[45] Moreover, we see many reports applying this method to the passage of electrons,[46] and for heavy charged particles there is a famous example of Robinson and Oen[47] who treated the case of single crystal target —— channeling.

Recently Ishitani et al.[48-50] have made simulations on low energy light ions incident upon thick medium and calculated the

range, back scattering coefficients and others using Lindhard et al.'s classical theory.[51,18] Their works are very valuable, but their aims and energy region are different from those of the present study.

§4-2. Method of Simulation

(i) Differential cross section of single scattering

We start from single scattering of a projectile by a target atom. Molière's theory[9] is used as a basis. The combination of (2-1-15) and (2-2-4) yields a single-scattering cross section

$$\sigma(\chi)2\pi\sin\chi d\chi = \frac{4\alpha^2}{k^2(4\sin^2(\chi/2)+\chi_\alpha{}^2)^2}2\pi\sin\chi d\chi \ . \qquad (4\text{-}2\text{-}1)^*$$

Since multiple scattering is a result of successive single collisions, we can simulate the path of a particle until it goes out of a given foil —— a history is known. From such histories, an angular distribution due to multiple scattering is obtained. Of course the simulation needs long time for computation when the number of collisions is large.

(ii) Random numbers

A set of uniform random numbers $\{r_i\}$ $(0 \leqq r_i \leqq 1)$ has been generated by means of a subroutine called KUNIRN in the Data Processing Center of Kyoto University. The subroutine uses a mixed congruential method (mod 2^{35}), the constants of which are chosen so that the random numbers pass a set of statistical tests.[52]

Random numbers $\{y_i\}$ with a probability function f(y) are derived from $\{r_i\}$ by the following inverse transformation method:[52]

$$\int_{-\infty}^{y_i} f(y)dy = r_i \ . \qquad (4\text{-}2\text{-}2)$$

(iii) Mean free path

By means of the differential cross section of (4-2-1), the total cross section, σ_t, is given by

$$\sigma_t = \int_0^{\pi} \sigma(\chi) 2\pi \sin\chi d\chi = \frac{16\pi\alpha^2}{k^2\chi_\alpha^2(4+\chi_\alpha^2)} \quad , \tag{4-2-3}$$

and the mean free path, λ, is obtained from

$$\lambda = (N\sigma_t)^{-1} \quad . \tag{4-2-4}$$

Suppose that a particle starting from x=0 and travelling along the path length x is scattered for the first time at a point in the interval of $x \sim x+dx$. Since the probability, $P(x)dx$, is given by

$$P(x)dx = \exp(-x/\lambda)dx/\lambda \quad , \tag{4-2-5}$$

we obtain the distance x_i from r_i as

$$x_i = -\lambda \ln(1-r_i) \quad , \tag{4-2-6}$$

using (4-2-2).

(iv) Angle of single scattering

The polar deflection angle, θ_i, caused by a scattering is derived from (4-2-1)$\sim$(4-2-3) as

$$\frac{1}{\sigma_t} \int_0^{\theta_i} \sigma(\chi) 2\pi \sin\chi d\chi = r_i \quad , \tag{4-2-7}$$

which leads to

$$\theta_i = \cos^{-1}\left(1 - \frac{2r_i\chi_\alpha^2}{4+\chi_\alpha^2-4r_i}\right) \quad . \tag{4-2-8}$$

Since the scattering is cylindrically symmetric (i.e. amorphous foil and no polarization are assumed), we simply get the azimuthal

deflection angle, ϕ_i, from

$$\phi_i = 2\pi r_i \ . \qquad (4\text{-}2\text{-}9)$$

The angle θ_i is of course given in center of mass system, and it should be converted into laboratory system. Hereafter we treat in laboratory system. Uniform random numbers, r_i's, of (4-2-6), (4-2-8) and (4-2-9) should be chosen independently.

(v) Summing-up of scattering angles

Suppose that a particle travelling in a direction (Θ_i, Φ_i) is scattered in a new direction $(\Theta_{i+1}, \Phi_{i+1})$, the deflection angles of the scattering being $(\theta_{i+1}, \phi_{i+1})$ as given in (iv). Here, Θ_i and Φ_i indicate polar and azimuthal angles of the direction of the particle (after the i-th collision) with respect to the initial direction, as shown in Fig.4-1. The relations combining above angles are given by

$$\cos\Theta_{i+1} = \cos\Theta_i \cos\theta_{i+1} - \sin\Theta_i \sin\theta_{i+1} \cos\phi_{i+1} \qquad (4\text{-}2\text{-}10)$$

and

$$\sin\Theta_{i+1} \sin(\Phi_{i+1} - \Phi_i) = \sin\theta_{i+1} \sin\phi_{i+1} \ , \qquad (4\text{-}2\text{-}11)$$

by means of the law of spherical trigonometry. For the incident particle (i=0) which has not experienced scattering, we put

$$\Theta_0 = \Phi_0 = 0 \ , \qquad (4\text{-}2\text{-}12)$$

i.e. incident particle enters the foil perpendicularly. Thus, with the aid of (4-2-10) and (4-2-11), we know the new direction $(\Theta_{i+1}, \Phi_{i+1})$ successively after each collision (i=0, 1, 2, ···).

(iv) Energy loss

We treat a case in which energy loss process of projectiles

in the foil is taken into account, where the energy of the incident beam is assumed to be monochromatic.

Since there is no appropriate formula of energy loss in the present energy region, the semi-empirical table of Northcliffe and Schilling[39] is used. As described in §3-2, the values in the table agree fairly well with our experimental values. In their table, the stopping power, $-dE/dx$, is given for discrete values of energy, and we assume that the stopping power is a linear function of energy E over each small energy interval. By solving the linear differential equation about E(x), the reasonable energy is given to the projectile as it proceeds in the foil. The lower limit of energy is necessary to be set in the calculation, which we choose as 0.0125MeV/amu. However, the probability that the projectile energy becomes lower than the limit is extremely small ($\sim 1 \times 10^{-4}$), because the foil used is thin enough.

(v) Detection of scattered particles

The particle after passing through the foil enters a detector placed behind. The detector can record the spatial-angle, projected-angle, energy, number of scatterings in the foil, etc. of the particle, which are obtained very easily by the present simulation method.

The schematic arrangement for the measurement of spatial-angle distribution is shown in Fig.4-2. Though the plane A is drawn in the figure, actually in the simulation only the histogram of θ is obtained, and the plane A should be the surface of a sphere whose center is the beam spot on the foil. The counting statistics in the small angle part is not good, since we have graduated the spatial angle uniformly as seen in Fig.4-2 and the solid angle

in this region is very small. This problem will be discussed in §4-7. Lateral deflection is very small, and is neglected.

Practically, we obtain the projected-angle distribution using a longitudinal slit of long but finite length, while the theory treats the case of infinite slit to which the incident beam enters uniformly. Accordingly, for a finite slit we have an angular distribution between spatial- and projected-angle ones; the combination is difficult to be treated analytically —— the slit geometry should be carefully considered.

The present simulation method solves the problem of finite slit easily. The schematic arrangement for measuring the distribution is shown in Fig.4-3. The longitudinal initial beam of length d enters the foil perpendicularly and is scattered. The angular distribution is experimentally measured along the line L. However, it is equivalent to the distribution of initially pin-hole beam aiming at the point O scattered only into the plane P whose width is d. In the simulation we took the latter case. The projected-angle distribution is the special case of $d \longrightarrow \infty$. It should be noted that the line L in Fig.4-3 should be actually a circle whose center is the center of the beam spot, O, on the foil and accordingly the plane P should be a cylinder.

An example of the programs of simulation (including energy loss process and three geometries of slit) is shown in Appendix II.

---

* Small-angle approximation is not necessary in the present method.

---

§4-3. Large Ω_o without Energy Loss

To certify the adequacy of the present method, we first make

the simulation on two cases in either of which the mean number of scatterings, Ω_0, is large enough and the energy loss process is neglected, since such cases have been just treated analytically by Molière. In this and the next sections we use a_{TF} from (2-2-2), and in §4-5 and §4-6 we use a_{TF} from (2-2-3).

Figures 4-4 and 4-6 show the angular distributions of 0.407MeV protons on 869μg·cm^{-2} copper foil and of 1.45MeV protons on the same foil, respectively. The spatial-angle distributions and the projected-angle ones are shown in (A) and (B), respectively, together with theoretical curves from Molière's theory. As described in the preceding section, statistical errors of $F(\theta)$ in the small angle region is rather large. Moreover, errors in Fig.4-6 are larger than those in Fig.4-4 because of smaller number of histories.

The histograms of the number of scatterings, W(n)'s, for the above two cases are shown in Figs.4-5 and 4-7. The solid curve in each figure is the Poisson distribution,

$$W(n)= \exp(-\Omega_0)\cdot \Omega_0{}^n/n! \qquad \left(\sum_{n=0}^{\infty} W(n)=1\right), \quad (4\text{-}3\text{-}1)$$

where the mean number of n is equal to Ω_0 of Molière. As described in §2-2, Ω_0 is a very slowly varying function of energy E, and Ω_0 of Fig.4-7 does not differ largely from that of Fig.4-5.

Figures 4-4 ~ 4-7 show that simulated results are in good agreement with Molière's theory.

§4-4. Very small Ω_0 without Energy Loss

In the region of $\Omega_0 \lesssim 20$, Molière's treatment becomes inappropriate and approximation by Keil et al. must be applied, as discussed in Chapter II. However, Keil et al. have not presented

the formula for projected-angle distribution, and moreover the contribution of "no scattering" term is omitted in their theory. In contrast to the theoretical difficulties, the present simulation method easily gives information concerning both the projected-angle distribution and no scattering.

The results for the case of 2.21MeV nitrogen ions upon 331μg.cm^{-2} gold foil, where Ω_0=4.03, are shown in Figs.4-8(A), 4-8(B) and 4-9: the spatial- and projected-angle distributions and histogram of n, respectively. Theoretical curves of F(θ) and w(n) are drawn also, but there is no theory to calculate f(ϕ) in this case.

We find from Fig.4-9 that about 1.8% of all the projectiles experience no scattering. A contribution of no scattering is seen at ϕ=0 of f(ϕ) in Fig.4-8(B). However, the absolute value of f(0) has little meaning because it depends on the width of the graduated angle. It should be noted that the events of no scattering are experimentally unrealistic and the real contribution of them would be distributed around θ=0 (or ϕ=0).

If the no scattering component is neglected, the simulated F(θ) is in good agreement with that from Keil et al.'s theory. This indicates that Keil et al.'s procedure of summing up the single-scattering events is adequate enough.

§4-5. Small Ω_0 Including Energy Loss Process

We have also calculated on the case of Ω_0=9.85, taking the energy loss process of the projectile into account. The theory of Molière cannot be applied to this case, but the contribution of no scattering is negligibly small.

The initial beam is assumed to be monochromatic in energy, as described in §4-2 and straggling in the energy loss process is

neglected. The results for nitrogen ions of initially 4.52MeV upon silver foil of 401$\mu g \cdot cm^{-2}$ are presented: the angular distributions in Fig.4-10 and the histogram of number of scatterings in Fig.4-11. Since these are based upon a large number of histories, statistical errors are small. In Fig.4-10(A), the curve according to Keil et al.'s theory is drawn for the mean energy, $E=(E_1+E_f)/2$ (cf. (3-2-2)). Though the energy loss in the foil is large, a good accordance with the theoretical curve is seen in this case. Molière's projected-angle distribution is drawn in Fig.4-10(B) for the sake of comparison. Some deviation from the simulated result is seen because of small Ω_0. The histogram of number of scatterings in Fig.4-11 shows a good accordance with Poisson distribution.

Figure 4-12 shows the energy spectrum of outgoing particles. Though the peak energy is nearly equal to the observed value of E_f, the shape is unrealistically sharp. This is because we have neglected the energy spread of initial beam, the energy straggling in the foil, the energy resolution of the particle detector, the nonuniformity of foil thickness and others. If we introduce these effects and use more accurate approximation for -dE/dx than the coarse one described in the preceding section, the energy spectrum experimentally obtained will be reproduced.

§4-6. Effect of Geometry of Slit

So far, only the cases of pin-hole slit and longitudinal slit of infinite length have been treated. The result for the case of longitudinal slit of finite length is described in this section. The method of this simulation has been described in §4-2(v). The case of d=5mm and D=482mm is taken here.

The resultant angular distribution, $F_e(\theta)$, is shown in Fig.4-13. The ion-foil combination is exactly the same as that in Fig.4-10. Since $d \ll D$, the distribution is nearly equal to that of initially pin-hole beam (i.e. spatial-angle distribution $F(\theta)$), but the possibility of simulation on different slit geometries is understood from this simulation.

§4-7. Discussion

We have simulated some multiple scattering processes using the single-scattering cross section proposed by Molière. The adequacy of our method has been certified in several cases —— of a few values of Ω_0, with and without energy loss, and with three geometries of slit. The results show good agreement with the known theories. This means that the simulation using Monte Carlo method is useful even when the analytical expression of summing up the single-scattering events is not known. The small deviations of theoretical predictions from the experimental results found for small values of Ω_0, which have been discussed in Chapter III, are confirmed to be attributable to the underestimation of Molière's single-scattering cross section for small scattering angles.

The statistical errors of $F(\theta)$ near $\theta=0$ in all the cases presented in this chapter are rather large because of small angular intervals of graduation. However, if we sacrifice the angular resolution to some extent, the errors will be reduced.

The present simulation method can be applied to many cases. For example, the angular distribution around $\theta=0$ will give an important information to the measurement of impact parameter dependence of inner shall ionization. The simulation on the motion of impurity particles in single crystal will be possible,

because the position of the particle can be predicted easily. The simulations in this chapter have been made by means of direct method. This is also applicable to simulations on scattering due to other types of potentials, if the related differential cross sections are appropriately given.

Lindhard et al.(LNS)[18] have derived a formula of cross section of atom-atom collision using classical model, and Meyer[17] has obtained a new spatial-angle distribution function of multiple scattering. However, the number of collisions is extremely large because he has counted the collisions of even very small angular deflections (cf. §2-5). In this case, the cut-off angle becomes significant if we insist on using the direct method, as Ishitani et al.[50] have predicted, and the methods developed by Berger[46] and other authors would be appropriate.

Chapter V. Conclusional Remarks

Multiple scattering of MeV protons and nitrogen ions on aluminium, copper, silver and gold foils has been studied experimentally and by simulation using Monte Carlo method.

The experimental data agree fairly well with theories of Molière and Keil et al. with the use of Thomas-Fermi radius which takes account of both projectile and target atom. The slight deviations found when the mean number of scatterings is small, i.e. for $\Omega_0 \lesssim 20$, are attributed to an underestimation of Molière's single-scattering cross section in the small angle region. This conclusion has been confirmed by the simulations. The theory of NSW shows a large discrepancy from the observations and that of Meyer gives a little deviation for $\Omega_0 \lesssim 10$.

The projected-angle distributions for small Ω_0 and angular distributions including energy loss and considering effect of longitudinal slit of finite length etc., all of which cannot be given from the known theories, have been obtained by the simulation method.

Molière's single-scattering theory can be used safely when the phenomenon contains many scattering events. The substantial difference between protons and nitrogen ions has not been found. Moreover, the deviations of theoretical prediction from our experimental results have been found to be almost independent of projectile energy over the present energy range.

In the lower energy region (i.e. very large α region), Meyer's theory is reported to be appropriate.[24,25] However, there is an exception of Andersen et al.[53] Their experimental $\theta_{1/2}$'s in the cases of heavy ions on gold foils are much smaller than

Meyer's prediction, τ's in their experiment being very small ($\tau \lesssim 2.5$). This tendency (ignoring the absolute value) is consistent with our result in Chapter III. It will be interesting to study further about this energy region, though there are difficult problems of thin foil preparation and of relatively large energy loss as Högberg and Norden[43] have predicted. The examination of the boundary energy between the regions of applicability for the theories of Molière-Keil et al. and Meyer will be more interesting.

The actual path length of each projectile in foil is a little longer than the foil thickness because of multiple scattering, and this influences the energy loss in the medium. Yang[54] examined this effect for the case of electrons using the rough Gaussian approximation for multiple scattering. For heavy ions, Tschalär and Bichsel[55] reported an extensive study about this effect using the theory of NSW-Marion, but only for the special arrangements of energy measurement. The general research about this effect by the use of Molière-Keil et al.'s theory will become important when the accuracy of energy measurement is improved.

DeWames et al.[56,57] have shown that the effect of binding of lattice atoms on multiple scattering in the foil of single crystal is important even at large particle energies because the potential is long range. Then they calculated this effect using the rough Gaussian approximation for multiple scattering. More detailed studies using Molière's theory and experiment on this phenomenon will be of great interest.

This report is a product of the study by "multiple scattering group" in the Department of Nuclear Enginerring of Kyoto

University. The members of the group should be listed here.

Prof. M. Sakisaka

Dr. F. Fukuzawa

T. Yamazaki

Mr. M. Takasaki

Dr. S. Nakamoto

Acknowledgements

This work has been done by the help of many persons.

Prof. M. Sakisaka has guided the author throughout the present work. The author has been taught very much by his enthusiasm for science. The author would like to thank him sincerely for his continuous cooperation, advices, suggestions, encouragement, and so on.

Mr. M. Takasaki is also gratefully acknowledged. Without his continuous cooperation for a long time, it would not have been possible to complete this investigation. The present report includes some data in his report.[58]

Our experiment on multiple scattering was first carried out with the suggestion and the guide of Dr. F. Fukuzawa using the Kyoto University Cyclotron in the Institute of Chemical Research and by the use of nuclear emulsions.[59] He is of course to be acknowledged all the more for his advices and encouragement until present.

All the experiments described in this report were practised using the "Special Apparatus for Heavy Ion Research" of Kyoto University. The author wishes to acknowledge Messrs. K. Yoshida, M. Tomita, K. Ogino and K. Norisawa for their cooperative contribution to this work. The author would like to thank Dr. S. Nakamoto and Dr. K. Shima for cooperation and discussion. The author is also grateful to Prof. T. Hyodo for his critical reading of the manuscript.

Mr. Y. Tanaka of Ritsumeikan University kindly lent us a multiple beam interferometer so that we could calibrate the quartz oscillator for foil thickness measurement. Messrs. I. Makino

and S. Gotoh helped the author to calibrate. He wishes to thank them very much.

The author is deeply indebted to several members of the Radioactivity and High Energy Section of Electrotechnical Laboratory. He wishes to express his gratitude to Mr. O. Yura, the Chief of the section, and to Dr. T. Tomimasu for their continuous advices and encouragement during the data processing and completion of this work. The author takes pleasure in acknowledging Messrs. T. Mikado, S. Sugiyama, T. Noguchi, M. Chiwaki, and all the other members of the section for discussion with him. Thanks are also offered to Misses N. Ohmatsu and Y. Yamamoto for their help in the course of preparation of figures and manuscripts.

The data processing and simulations were accomplished by means of FACOM 230-60, -50 and -75 in the Data Processing Center in Kyoto University and the Computational Center of Electrotechnical Laboratory. The author is grateful to Mr. S. Kashioka, now in Hitachi Co., for his considerable assistance with the computer programs.

Appendix I.

An example of the computer programs to obtain a_c's from experimental values of F(0) and $\theta_{1/2}$ are presented here. The a_c's are given according to the theory of Keil et al. The values of $G(\vartheta)$, which have been obtained prior to this calculation are given as DATA. The interpolation operation by means of Lagrange's method is done in the SUBROUTINE YLAG. The similar program is used to obtain a_c's according to the theory of Molière.

```
      DOUBLE PRECISION AI,AF,ALPHA,A,CHI0,CHIC,CHIA,EC,EI,HBAR,OMEGA,ZI,
     1PAI,@NO,@K,@LMDA,ROW,SIGMA,THICK,THIKL,V,ZF,PAC
      DOUBLE PRECISION RTET(70),G(30,70)
      DOUBLE PRECISION FOE,TEHFE
      DOUBLE PRECISION WM(30),FGI(30),GHF,FG(30),RTETI(30),RTETHF,RAC1,
     1FINT(30),FGIE,FINTE,WMM(30),OMC1,FINTI(30),OMC2,AC1,AC2,ACM,RAC2,
     2RACM,FGII(30)
      M=10
      @NO=6.0248D23
      HBAR=1.05443D-27
      EC=4.8026D-10
      PAI=3.14159265358979323D0
      READ(5,180)(RTET(J),J=1,51)
  180 FORMAT(4D17.10)
      READ(5,179)((G(I,J),J=1,51),I=1,25)
  179 FORMAT(4D17.10)
      DO 60 I=1,25
      WM(I)=DBLE(FLOAT(I))
      FGI(I)=G(I,1)**WM(I)
      GHF=G(I,1)/2.0D0
      DO 61 J=1,51
      IF(GHF.GT.G(I,J))GO TO 62
   61 CONTINUE
   62 DO 65 K=1,10
      KJ=J+5-K
      FG(K)=G(I,KJ)
      RTETI(K)=RTET(KJ)
   65 CONTINUE
      CALL YLAG(RTETHF,M,GHF,FG,RTETI)
      FINT(I)=RTETHF/DSQRT(WM(I))
   60 CONTINUE
C  MOLIERE,S CONSTANTS
      DO 42 KK=1,7
      READ(5,100)EI,ZI,AI,ZF,AF,ROW,THICK
  100 FORMAT(D15.8/2D15.8/2D15.8/D15.8/D15.8)
      WRITE(6,200)EI,AI,ZI,AF,ZF,ROW,THICK
  200 FORMAT(1H1,15HA TABLE OF DATA/1H ,10HEINC      =D15.8,5H  MEV/1H ,1
     10HAINC      =D15.8/1H ,10HZINC      =D15.8/1H ,10HAFOIL     =D15.8/1H
     2 ,10HZFOIL     =D15.8/1H ,10HDENSITY   =D15.8,8H  G*CM-3/1H ,10HTHIC
     3KNESS=D15.8,8H  G*CM-2///)
      V=DSQRT(3.20412D-6*@NO*EI/AI)
      ALPHA=ZI*ZF*EC**2/HBAR/V
      @K=V/HBAR*AI/@NO
      A=0.885341900*5.29172D-9/DSQRT(ZI**(2.0D0/3.0D0)+ZF**(2.0D0/3.0D0)
     1)
      CHI0=1.0D0/@K/A
      CHIC=2.0D0*EC**2*ZI*ZF/HBAR/@K/V*DSQRT(PAI*@NO*THICK/AF)
      PAC=1.1300+3.76D0*ALPHA**2
      CHIA=CHI0*DSQRT(PAC)
      OMEGA=(CHIC/CHIA)**2
   11 SIGMA=16.0D0*PAI*ALPHA**2/@K/@K/CHIA/CHIA/(4.0D0+CHIA**2)
      @LMDA=AF/@NO/ROW/SIGMA
      THIKL=THICK/ROW
      WRITE(6,212)THIKL
  212 FORMAT(1H ,10HTHICKNESS=D17.10)
```

```
      WRITE(6,299)A
  299 FORMAT(1H ,10HA THEORY =D17.10)
      WRITE(6,259)OMEGA
  259 FORMAT(1H ,10HOMEGA    =D17.10)
      READ(5,120)FOE,TEHFE
  120 FORMAT(2D15.8)
      FGIE=2.0D0*PAI*FOE*CHIC**2
      FINTE=TEHFE/CHIC
      IF(FOE.EQ.0.0D0)GO TO 40
      DO 66 I=3,25
      IF(FGIE.GT.FGI(I))GO TO 67
   66 CONTINUE
      I=25
   67 IF(I.GT.21)I=21
      IF(I.LT.9)I=9
      DO 68 J=1,10
      JJ=I+5-J
      WMM(J)=WM(JJ)
      FGII(J)=FGI(JJ)
   68 CONTINUE
      CALL YLAG(OMC1,M,FGIE,FGII,WMM)
      IF(OMC1.GT.0.0D0)GO TO 41
   40 OMC1=0.0D0
   41 AC1=DSQRT(OMC1*PAC)/CHIC/WK
      RAC1=AC1/A
      WRITE(6,255)
  255 FORMAT(1H0,42HKEIL ET AL,S A CORRECTED FROM F(0),THETAHF)
      WRITE(6,250)FOE,TEHFE
  250 FORMAT(1H0,10HF(0) EXPT=D17.10/1H ,10HTETHF,E, =D17.10/)
      WRITE(6,256)AC1,RAC1
  256 FORMAT(1H0,10HA CO.F(0)=D17.10,4H  CM/1H ,10HAC/A F(0)=D17.10)
      WRITE(6,260)OMC1
  260 FORMAT(1H ,10HOMEGA CO.=D17.10)
      IF(FINTE.GT.1.5D0)GO TO 71
      DO 64 I=3,25
      IF(FINTE.LT.FINT(I))GO TO 69
   64 CONTINUE
      I=25
   69 IF(I.GT.21)I=21
      IF(I.LT.9)I=9
      DO 70 J=1,10
      JJ=I-6+J
      WMM(J)=WM(JJ)
      FINTI(J)=FINT(JJ)
   70 CONTINUE
      CALL YLAG(OMC2,M,FINTE,FINTI,WMM)
      IF(OMC2.LT.0.0D0)OMC2=0.0D0
      AC2=DSQRT(OMC2*PAC)/CHIC/WK
      ACM=(AC1+AC2)/2.0D0
      RAC2=AC2/A
      RACM=ACM/A
      WRITE(6,257)AC2,RAC2
  257 FORMAT(1H0,10HA CO.TEHF=D17.10,4H  CM/1H ,10HAC/A TEHF=D17.10)
      WRITE(6,261)OMC2
  261 FORMAT(1H ,10HOMEGA CO.=D17.10)
```

```
)*
      WRITE(6,258)ACM,RACM
  258 FORMAT(1H0,10HA CO.MEAN=D17.10,4H  CM/1H ,10HAC/A MEAN=D17.10)
      GO TO 42
   71 WRITE(6,999)
  999 FORMAT(1H0,22HTETHF WA MOLIERE DA YO)
   42 CONTINUE
      STOP
      END
```

```
      SUBROUTINE YLAG(P,N,V,X,F)
      DOUBLE PRECISION P,V,X(N),F(N),A,B,C
      A=1.0D0
      C=0.0D0
      DO 3000 I=1,N
      IF(V.NE.X(I)) GO TO 1000
      P=F(I)
      RETURN
 1000 A=A*(V-X(I))
      B=1.0D0
      DO 2000 J=1,N
      IF(I.NE.J) B=B*(X(I)-X(J))
 2000 CONTINUE
      C=C+F(I)/(B*(V-X(I)))
 3000 CONTINUE
      P=A*C
      RETURN
      END
```

Appendix II.

An example of the computer programs of simulation on multiple scattering by means of Monte Carlo method is presented here. This program includes energy loss process and three geometries of slit. Uniform random numbers are given by means of SUBROUTINE KUNIRN of the Data Processing Center of Kyoto University.

```
      DIMENSION NT(50),NP(50),NPE(50),NY(50),NS(202),CTP(50),CY(50),CYP(
     150),YPW(50),TR(50),PN(50),YP(50),FT(50),PEN(50),NN(202)
      DIMENSION YPN(500),ACT(500)
      DIMENSION @LENG(30)
      DIMENSION EL(30),DEDXG(30),DEDX(30),A(30),BA(30),CA(30),
     1NPAR(500),CCH(500)
     2,NPARX(100),CCHX(100)
C     CALCULATION OF CONSTANTS
      READ(5,100)EI,AI,ZI,AF,ZF,ROW,THICK
  100 FORMAT(F12.0/2F12.0/2F12.0/F12.0,E15.7)
      READ(5,101)DIS,DSL
  101 FORMAT(2F12.0)
      READ(5,102)AW
  102 FORMAT(E15.8)
      READ(5,103)(EL(I),DEDXG(I),I=1,18)
  103 FORMAT(2F10.0)
      DO 40 I=1,18
      DEDX(I)=1.0E3*ROW*DEDXG(I)
   40 CONTINUE
      READ(5,104)CHANL,CHANU,CHANW
  104 FORMAT(3F12.0)
      READ(5,106)RXL,RXU,RXW
  106 FORMAT(3E15.8)
      DO 41 J=1,17
      A(J)=(DEDX(J+1)-DEDX(J))/(EL(J+1)-EL(J))
      BA(J)=DEDX(J)/A(J)
      CA(J)=BA(J)-EL(J)
      @LENG(J)=ALOG((EL(J+1)+CA(J))/BA(J))/A(J)
   41 CONTINUE
      NCH=(CHANU-CHANL)/CHANW+1
      DO 42 I=1,NCH
      NPAR(I)=0
      CCH(I)=CHANL+CHANW*FLOAT(I-1)
   42 CONTINUE
      NCHX=(RXU-RXL)/RXW+1
      DO 99 I=1,NCHX
      NPARX(I)=0
      CCHX(I)=RXL+RXW*FLOAT(I-1)
   99 CONTINUE
      READ(5,105)EOI
  105 FORMAT(F12.0)
      DO 43 I=1,17
      IF(EOI.LE.EL(I+1))GO TO 44
   43 CONTINUE
      GO TO 45
   44 NRI=I
      @N0=6.02486E23
      HBAR=1.05443E-27
      EC=4.80286E-10
      PAI=3.1415927
      WRITE(6,200)EI,AI,ZI,AF,ZF,ROW,THICK
  200 FORMAT(1H1,15HA TABLE OF DATA/1H ,10HEINC     =F15.8,5H  MEV/1H ,1
     10HAINC     =F15.8/1H ,10HZINC     =F15.8/1H ,10HAFOIL    =F15.8/1H
     2 ,10HZFOIL    =F15.8/1H ,10HDENSITY  =F15.8,8H  G*CM-3/1H ,10HTHIC
     3KNESS=E15.8,8H  G*CM-2///)
```

```
      WRITE(6,214)EOI
  214 FORMAT(1H0,10HEOI       =,F15.8,5H  MEV/)
      G=AF/(AI+AF)
      VP2=3.20412E-6*QNO/AI
      V=SQRT(EI*VP2)
      EICM=EI*G
      AICM=AI*G
      ALPHAP=ZI*ZF*EC**2/HBAR
      ALP2=ALPHAP**2
      ALPHA=ALPHAP/V
      AI2=AI**2
      AF2=AF**2
      AIAF=AI*AF*2.0
      QK=V/HBAR*AI/QNO
      QKCMP=AICM/HBAR/QNO
      QKP2=QKCMP**2
      QKCM=QKCMP*V
      CHIOP=CBRT(128.0/9.0/PAI**2)*SQRT(CBRT(ZI**2)+CBRT(ZF**2))*9.1083E
     1-28/HBAR**2*EC**2
      CHIOP2=CHIOP**2
      CHIO=CHIOP/QK
      CHIOCM=CHIOP/QKCM
      CHIC=2.0*EC**2*ZI*ZF/HBAR/QK/V*SQRT(PAI*QNO*THICK/AF)
      CHICCM=CHIC*QK/QKCM
      CHIA=CHIO*SQRT(1.13+3.76*ALPHA**2)
      CHIACM=CHIOCM*SQRT(1.13+3.76*ALPHA**2)
      OMEGA=(CHIC/CHIA)**2
C     CALCULATION OF B VALUE
      C=0.1544-ALOG(OMEGA)
      B=1.153+2.583*ALOG10(OMEGA)
   10 ERR=B-ALOG(B)+C
      IF(ABS(ERR).LT.1.0E-5)GO TO 11
      B=B*(1.0-ERR/(B-1.0))
      GO TO 10
   11 SIGMAP=16.0*PAI
      SIGMA=SIGMAP*ALPHA**2/QK**2/CHIA**2/(4.0+CHIA**2)
      QLMDAP=AF/QNO/ROW
      QLMDAI=QLMDAP/SIGMA
      WRITE(6,201)V,EICM,AICM,ALPHA,QK,QKCM,CHIO,CHIOCM,CHIC,CHICCM,CHIA
     1,CHIACM,OMEGA,B,SIGMA,QLMDAI
  201 FORMAT(1H0,10HV         =E15.8,8H  CM*S-1/1H ,10HEICM      =E15.8,5H
     1  MEV/1H ,10HAICM      =E15.8/1H ,10HALPHA     =E15.8/1H ,10HK
     2  =E15.8,6H  CM-1/1H ,10HKCM       =E15.8,6H  CM-1/1H ,10HCHIO
     3=E15.8,8H  RADIAN/1H ,10HCHIOCM    =E15.8,8H  RADIAN/1H ,10HCHIC
     4  =E15.8,8H  RADIAN/1H ,10HCHICCM    =E15.8,8H  RADIAN/1H ,10HCHIA
     5    =E15.8,8H  RADIAN/1H ,10HCHIACM    =E15.8,8H  RADIAN/1H ,10HOME
     6GA     =E15.8/1H ,10HB          =E15.8/1H ,10HSIGMA     =E15.8,6H  CM+
     72/1H ,10HLAMBDA    =E15.8,4H  CM///)
      THICK=THICK/ROW
      WRITE(6,212)THICK
  212 FORMAT(1H ,10HTHICKNESS=,E15.8,4H  CM)
      K=13978104282
      CALL KUNIRN(R,IR,K)
      SL=DSL/2.0
      DO 26 J=1,50
```

```
      CTP(J)=FLOAT(J-1)*AW
      CTU=CTP(J)+AW/2.0
      IF(J.EQ.1)GO TO 30
      CTL=CTP(J)-AW/2.0
      GO TO 31
   30 CTL=0.0
   31 ACT(J)=2.0*PAI*(COS(CTL)-COS(CTU))
   26 CONTINUE
      DO 12 I=1,202
      NS(I)=0
   12 CONTINUE
      NBS=0
      DO 13 I=1,50
      NB(I)=0
      NP(I)=0
      NPE(I)=0
   13 CONTINUE
      NLE=0
      NUE=0
      NLZX=0
      NUZX=0
      KO=0
      V2=E0I*VP2
      ALPHA2=ALP2/V2
      QKCM2=QKP2*V2
      CHIA2=CHI0P2/QKCM2*(1.13+3.76*ALPHA2)
      QLMDAI=QLMDAP/SIGMAP/ALPHA2*QKCM2*CHIA2*(4.0+CHIA2)
      RRI=ALOG((E0I+CA(NRI))/BA(NRI))/A(NRI)
C     PATHS OF 100 PARTICLES
      DO 14 I=1,10000
      E0=E0I
      NR=NRI
      RL=THICK
      RR=RRI
      QLMDA=QLMDAI
      THETA=0.0
      PHI=0.0
      Z=0.0
      COQ=1.0
      ZX=0.0
C     A PATH OF ONE PARTICLE
      DO 15 K=1,1000
      CALL KUNIRN(R,IR)
      Z1=-QLMDA*ALOG(1.0-R)
      ZX=ZX+Z1
      Z=Z+Z1*COQ
      IF(Z.LE.0.0)GO TO 32
      IF(Z.GE.THICK)GO TO 47
      IJ=1
      GO TO 58
   47 IJ=2
      Z1=RL/COQ
   58 Z2=RR-Z1
      IF(Z2.GE.0.0)GO TO 46
      IF(NR.LE.1)GO TO 48
```

```
      E0=EL(NR)
      NR=NR-1
      Z1=-Z2
      RR=QLENG(NR)
      GO TO 58
   48 KO=KO+1
      GO TO 14
   46 E0=(E0+CA(NR))*EXP(-A(NR)*Z1)-CA(NR)
      IF(IJ.EQ.2)GO TO 16
      RR=Z2
      RL=THICK-Z
      V2=E0*VP2
      ALPHA2=ALP2/V2
      QKCM2=QKP2*V2
      CHIA2=CHIOP2/QKCM2*(1.13+3.76*ALPHA2)
      QLMDA=QLMDAP/SIGMAP/ALPHA2*QKCM2*CHIA2*(4.0+CHIA2)
      CALL KUNIRN(R,IR)
      CO=1.0-2.0*R*CHIA2/(4.0*(1.0-R)+CHIA2)
      CO=(AI+AF*CO)/SQRT(AI2+AIAF*CO+AF2)
      ATETA=ARCOS(CO)
      CALL KUNIRN(R,IR)
      APHI=2.0*PAI*R
      IF(APHI.GT.PAI)APHI=APHI-2.0*PAI
      COQ=COS(THETA)*CO-SIN(THETA)*SIN(ATETA)*COS(APHI)
      THETA=ARCOS(COQ)
      IF(THETA.EQ.0.0)GO TO 17
      SI=SIN(ATETA)*SIN(APHI)/SIN(THETA)
      IF(ABS(SI).GE.1.0) GO TO 50
      PHI=PHI+ARSIN(SI)
      GO TO 18
   50 PHI=PHI+SIGN(PAI/2.0,SI)
      GO TO 18
   17 PHI=0.0
   18 IF(PHI.GT.PAI)PHI=PHI-2.0*PAI
      IF(PHI.LT.PAI*(-1.0))PHI=PHI+2.0*PAI
   15 CONTINUE
      GO TO 14
C     DETECTION OF A PARTICLE
   16 IF(K.GT.201)GO TO 19
      NS(K)=NS(K)+1
      GO TO 20
   19 NS(202)=NS(202)+1
   20 IF(THETA.GT.1.57)GO TO 14
      JT=IFIX(THETA/AW+1.5)
      TA=TAN(THETA)*SIN(PHI)
      TA=ABS(TA)
      RPHI=ATAN(TA)
      JP=IFIX(RPHI/AW+1.5)
      X=DIS*TAN(THETA)*COS(PHI)
      X=ABS(X)
      IF(JT.EQ.1)GO TO 21
      IF(JT.GT.50)GO TO 22
      NT(JT)=NT(JT)+1
      GO TO 22
   21 NT(JT)=NT(JT)+2
```

```
 22 IF(JP.EQ.1)GO TO 23
    IF(JP.GT.50)GO TO 56
    NP(JP)=NP(JP)+1
    IF(X.LE.SL)NPE(JP)=NPE(JP)+1
    GO TO 56
 23 NP(JP)=NP(JP)+2
    IF(X.LE.SL)NPE(JP)=NPE(JP)+2
 56 JCH=IFIX((E0-CHANL)/CHANW+1.5)
    IF(JCH-0)51,51,52
 51 NLE=NLE+1
    GO TO 14
 52 IF(JCH-NCH-1)54,54,55
 55 NUE=NUE+1
    GO TO 14
 54 NPAR(JCH)=NPAR(JCH)+1
    JCHX=IFIX((ZX-RXL)/RXW+1.5)
    IF(JCHX-0)98,98,97
 98 NLZX=NLZX+1
    GO TO 14
 97 IF(JCHX-NCHX-1)96,96,95
 95 NUZX=NUZX+1
    GO TO 14
 96 NPARX(JCHX)=NPARX(JCHX)+1
    GO TO 14
 32 NBS=NBS+1
 14 CONTINUE
    HISTOGRAMS AND DISTRIBUTION FUNCTIONS
    WRITE(6,260)KO
260 FORMAT(1H0,4HKO =,2X,I5)
    NTSUM=0
    NPSUM=0
    NPESUM=0
    DO 27 J=2,50
    NTSUM=NTSUM+NT(J)
    NPSUM=NPSUM+NP(J)
    NPESUM=NPESUM+NPE(J)
 27 CONTINUE
    WRITE(6,250)NTSUM,NPSUM,NPESUM
250 FORMAT(1H0,7HNTSUM =,I10,2X,7HNPSUM =,I10,2X,8HNPESUM =,I10)
    TSUM=FLOAT(NTSUM)+FLOAT(NT(1))/2.0
    PSUM=(FLOAT(NPSUM)+FLOAT(NP(1))/2.0)*AW
    PESUM=(FLOAT(NPESUM)+FLOAT(NPE(1))/2.0)*AW
    WRITE(6,251)TSUM,PSUM,PESUM
251 FORMAT(1H0,6HTSUM =,E15.8,2X,6HPSUM =,E15.8,2X,7HPESUM =,E15.8)
    DO 28 J=1,50
    TR(J)=FLOAT(NT(J))/TSUM/AW
    FT(J)=FLOAT(NT(J))/TSUM/ACT(J)
    IF(J.EQ.1)FT(J)=FT(J)/2.0
    PN(J)=FLOAT(NP(J))/PSUM
    PEN(J)=FLOAT(NPE(J))/PESUM
 28 CONTINUE
    PRINTING OF THE RESULTS
    WRITE(6,202)
202 FORMAT(1H1,5X,5HTHETA,8X,7HN(TETA),7X,9HFR(THETA),8X,8HF(THETA),8X
   1,6HN(PHI),5X,7HNE(PHI),8X,6HF(PHI),11X,7HFE(PHI)/1H ,6X,3HPHI//)
```

```
      WRITE(6,203)(CTP(I),NT(I),TR(I),FT(I),NP(I),NPE(I),PN(I),PEN(I),I
     1=1,50)
203   FORMAT(1H ,E15.8,2X,I10,2X,E15.8,2X,E15.8,2X,I10,2X,I10,2X,E15.8,2
     1X,E15.8)
      DO 29 I=2,202
      NN(I)=I-1
 29   CONTINUE
      WRITE(6,206)NS(1)
206   FORMAT(1H1,31HNUMBER OF NO SCATT. PARTICLES =,I8//)
      WRITE(6,207)
207   FORMAT(1H ,1X,5(6HSCATT.,3X,6HNUMBER,3X)/)
      WRITE(6,208)(NN(I),NS(I),I=2,201)
208   FORMAT(1H ,(5(I8,I10)))
      WRITE(6,209)NS(202)
209   FORMAT(1H0,26HNUMBER OF OVER 200 SCATT =,I12//)
      WRITE(6,213)NBS
213   FORMAT(1H0,23HNUMBER OF BACK SCATTER=,I12//)
      WRITE(6,210)IR
210   FORMAT(1H0,20HLAST RANDOM NUMBER =,I12)
      WRITE(6,215)
215   FORMAT(1H1,5X,6HENEPGY,9X,4HN(E)//)
      WRITE(6,216)(CCH(I),NPAR(I),I=1,NCH)
216   FORMAT(1H ,F15.8,2X,I10)
      WRITE(6,217)KO,NLE,NUE
217   FORMAT(1H0,10HSTOPPED  =,I10/1H ,10HLOWER E. =,I10/1H ,10HUPPER E.
     1 =,I10//)
      WRITE(6,218)(CCHX(I),NPARX(I),I=1,NCHX)
218   FORMAT(1H ,F15.8,2X,I10)
      WRITE(6,219)NLZX,NUZX
219   FORMAT(1H0,17HLORWER THAN RXL =,I10/1H ,17HHIGHER THAN RXU =,I10/)
 45   STOP
      END
```

References

1) E. Rutherford: Phil. Mag. 12 (1906) 143.

2) E. Rutherford: Phil. Mag. 21 (1911) 669.

3) F. Mayer: Ann. Phys. (Germany) 41 (1913) 931.

4) N. Bohr: K. Danske Vidensk. Selsk. mat.-fys. Medd. 18 (1948) No.8.

5) E. J. Williams: Proc. Roy. Soc. A169 (1939) 531.

6) E. J. Williams: Phys. Rev. 58 (1940) 292.

7) S. Goudsmit and J. L. Saunderson: Phys. Rev. 57 (1940) 24.

8) S. Goudsmit and J. L. Saunderson: Phys. Rev. 58 (1940) 36.

9) G. Molière: Z. Naturforsch. 2a (1947) 133.

10) G. Molière: Z. Naturforsch. 3a (1948) 78.

11) H. S. Snyder and W. T. Scott: Phys. Rev. 76 (1949) 220.

12) H. W. Lewis: Phys. Rev. 78 (1950) 526.

13) H. Bethe: Phys. Rev. 89 (1953) 1256.

14) E. Keil, E. Zeitler and W. Zinn: Z. Naturforsch. 15a (1960) 1031.

15) B. P. Nigam, M. K. Sundaresan and Ta-You Wu: Phys. Rev. 115 (1959) 491.

16) J. B. Marion and B. A. Zimmerman: Nuclear Instrum. and Methods 51 (1967) 93.

17) L. Meyer: Phys. Status solidi b44 (1971) 253.

18) J. Lindhard, V. Nielsen and M. Scharff: K. Danske Vidensk. Selsk. mat.-fys. Medd. 36 (1968) No.10.

19) A. O. Hanson, L. H. Lanzl, E. M. Lyman and M. B. Scott: Phys. Rev. 84 (1951) 634.

20) L. Voyvodic and E. Pickup: Phys. Rev. 85 (1952) 91.

21) L. B. Strong and R. R. Roy: Phys. Rev. 131 (1963) 198.

22) W. G. Simon: Phys. Rev. 136 (1964) B410.

23) N. O. Lassen and A. Ohrt: K. Danske Vidensk. Selsk. mat.-fys. Medd. 36 (1967) No.9.

24) F. Bernhard, J. Lippold, L. Meyer, S. Schwabe and R. Stolle: Atomic Collision Phenomena in Solids, ed. D. W. Palmar et al. (North-Holland, 1970) p.663.

25) H. H. Andersen and J. Bøttiger: Phys. Rev. B4 (1971) 2105.

26) H. Bichsel: Phys. Rev. 112 (1958) 182.

27) A. A. Bednyakov, A. N. Boyarkina, I. A. Savanko and A. F. Tulinov: Soviet Physics - JETP 15 (1962) 515.

28) A. A. Bednyakov, V. N. Dvoretskii, I. A. Savanko and A. F. Tulinov: Soviet Physics - JETP 19 (1964) 1280.

29) A. A. Bednyakov, V. S. Nikolaev, A. V. Rudchenko and A. F. Tulinov: Soviet Physics - JETP 23 (1966) 391.

30) M. Sakisaka, T. Yamazaki, M. Takasaki and S. Nakamoto: J. Phys. Soc. Japan 29 (1970) 1551.

31) T. Yamazaki, M. Takasaki and M. Sakisaka: J. Phys. Soc. Japan, to be published.

32) T. Yamazaki, M. Takasaki, S. Kashioka and M. Sakisaka: J. Phys. Soc. Japan, to be published.

33) G. Wentzel: Ann. Phys. (Germany) 69 (1922) 335.

34) W. T. Scott: Rev. mod. Phys. 35 (1963) 231.

35) S. Leisegang: Z. Phys. 132 (1952) 183.

36) R. H. Dalitz: Proc. Roy. Soc. A206 (1951) 509.

37) 沢木 司: 真空蒸着 (日刊工業社, 1965).

38) L. Holland: Vacuum Deposition of Thin Films (John Wiley & Sons, 1960).

39) L. C. Northcliffe and R. F. Schilling: Nuclear Data Tables A7 (1970) 233.

40) S. K. Allison and S. D. Warshaw: Rev. mod. Phys. 25 (1953) 779.

41) J. L. Goldberg, H. S. Snyder and W. T. Scott: Phys. Rev. 100 (1955) 1013.

42) L. Meyer and P. Krygel: Nuclear Instrum. and Methods 98 (1972) 381.

43) G. Högberg and H. Norden: Nuclear Instrum. and Methods 90 (1970) 283.

44) D. Kerr, G. Sigert, K. Kürzinger, E. Konecny and H. Ewald: Z. Naturforsch. 22a (1967) 1799.

45) For example, R. R. Wilson: Phys. Rev. 86 (1952) 261.

46) For example, M. J. Berger: Methods in Computational Physics, ed. B. Alder et al. (Academic Press, 1963) Vol.1, p.135.

47) M. T. Robinson and O. S. Oen: Phys. Rev. 132 (1963) 2385.

48) T. Ishitani and R. Shimizu: Japan J. appl. Phys. 10 (1971) 821.

49) T. Ishitani, K. Murata and R. Shimizu: Japan J. appl. Phys. 10 (1971) 1464.

50) T. Ishitani, R. Shimizu and K. Murata: Japan J. appl. Phys. 11 (1972) 125.

51) J. Lindhard, M. Scharff and H. E. Schiøtt: K. Danske Vidensk. Selsk. mat.-fys. Medd. 33 (1963) No.14.

52) T. H. Naylor, J. L. Balintfy, D. S. Burdick and K. Chu: Computer Simulation Techniques (John Wiley & Sons, 1968).

53) H. H. Andersen, J. Bøttiger and H. Knudsen: Radiation Effects 13 (1972) 203.

54) C. N. Yang: Phys. Rev. 84 (1951) 599.

55) C. Tschalär and H. Bichsel: Nuclear Instrum. and Methods 62 (1968) 208.

56) R. E. DeWames and W. F. Hall: Phys. Rev. Letters 17 (1966) 122.

57) R. E. DeWames, W. F. Hall and G. W. Lehman: Phys. Rev. 148

(1966) 181.

58) 高崎　稔：p, N イオンの多重散乱(京都大学修士学位論文, 1970).

59) 山崎鉄夫：速い荷電粒子の多重散乱の研究(京都大学修士学位論文, 1968)

Table I. Multiple scattering data for protons.

Foil	E (MeV)	ρt ($\mu g.cm^{-2}$)	α	χ_α (10^{-2} rad.)	Ω_o	F(0)	$\theta_{1/2}$ (10^{-2} rad.)	$\frac{F(2\theta_{1/2})}{F(0)}$
Al	0.479	192	2.97	0.210	46.6	319	2.42	0.104
	0.491	156	2.93	0.205	37.7	461	2.02	0.102
	0.491	156	2.93	0.205	37.7	473	1.95	0.108
	0.975	375	2.08	0.105	87.9	669	1.71	0.0900
	0.975	375	2.08	0.105	87.9	671	1.69	0.0894
	1.02	270	2.04	0.101	63.1	988	1.42	0.0859
	1.45	562	1.71	0.0718	128	820	1.54	0.0884
	1.45	562	1.71	0.0718	128	709	1.58	0.100
Cu	0.410	869	7.15	0.682	57.5	27.1	8.33	0.116
	0.462	579	6.74	0.606	38.3	54.0	5.95	0.0969
	0.471	424	6.68	0.595	28.1	79.5	4.74	0.116
	0.854	869	4.96	0.329	57.2	108	4.08	0.109
	0.944	869	4.72	0.298	57.1	113	4.00	0.110
	1.44	869	3.82	0.196	56.7	280	2.46	0.112
	1.44	869	3.82	0.196	56.7	287	2.42	0.117
Ag	0.440	820	11.2	1.19	23.9	28.6	8.04	0.112
	0.448	736	11.1	1.17	21.5	29.0	7.82	0.115
	0.489	316	10.6	1.07	9.21	*	3.97	0.116
	0.871	820	7.96	0.604	23.8	103	4.10	0.112
	0.996	823	7.44	0.528	23.9	119	3.78	0.117
	1.46	820	6.15	0.361	23.8	275	2.54	0.109
	1.52	736	6.03	0.347	21.3	308	2.36	0.113

(to be continued)

(continued)

Foil	E (MeV)	ρt ($\mu g \cdot cm^{-2}$)	α	χ_α (10^{-2} rad.)	Ω_o	F(0)	$\theta_{1/2}$ (10^{-2} rad.)	$\frac{F(2\theta_{1/2})}{F(0)}$
Au	0.473	606	18.1	2.19	7.00	55.8	5.30	0.147
	0.501	236	17.6	2.07	2.72	*	2.67	0.177
	0.966	206_9	12.7	1.07	23.9	30.6	7.64	0.111
	0.991	606	12.5	1.05	6.99	206	2.70	0.141
	1.45	110_2	10.4	0.715	12.7	130	3.80	0.0970
	1.50	206_9	10.2	0.695	23.8	70.2	5.03	0.103

E is the average energy in the laboratory system.

The values of * were not measured. Other notations are described in the text.

Table II. Multiple scattering data for nitrogen ions.

Foil	E (MeV)	ρt ($\mu g.cm^{-2}$)	α	χ_α (10^{-2} rad.)	Ω_o	F(0)	$\theta_{1/2}$ (10^{-2} rad.)	$\frac{F(2\theta_{1/2})}{F(0)}$
Al	1.33	67.1	46.5	0.619	12.0	265	2.49	0.120
	1.36	33.1	46.1	0.607	5.90	796	1.25	0.182
	1.39	90.9	45.5	0.591	16.2	175	2.96	0.126
	2.22	90.9	36.0	0.371	16.2	421	2.07	0.111
	2.27	89.7	35.6	0.362	16.0	538	1.79	0.112
	4.18	118	26.2	0.197	21.1	1200	1.24	0.0983
Cu	1.28	116	106	1.70	6.15	73.7	4.60	0.130
	1.60	424	94.5	1.37	22.5	17.8	9.44	*
	2.29	116	79.1	0.956	6.15	219	2.70	0.129
	4.40	290	57.1	0.498	15.4	*	2.78	*
	4.50	142	56.4	0.487	7.55	*	1.16	*
Ag	1.32	113	169	3.03	2.78	110	3.44	0.165
	1.83	316	143	2.18	7.76	31.2	6.94	0.137
	2.37	113	126	1.69	2.78	275	2.14	0.159
	4.47	283	91.7	0.896	6.95	*	2.43	0.181
Au	2.29	220	215	3.38	2.24	95.2	3.70	0.167
	4.37	606	156	1.77	6.16	*	4.26	0.190
	4.59	330	152	1.69	3.36	*	2.35	0.259

Table III. Parameters of Molière and NSW for 1.45 MeV protons on Al of 562 $\mu g.cm^{-2}$ thick.

	Molière	NSW	
		μ=1.12	μ=1.80
α	1.71	1.71	1.71
χ_o (rad.)	2.06×10^{-4}	2.06×10^{-4}	2.06×10^{-4}
χ_μ (rad.)	*	2.31×10^{-4}	3.72×10^{-4}
χ_α (rad.)	7.18×10^{-4}	2.30×10^{-4}	3.68×10^{-4}
χ_c (rad.)	8.12×10^{-3}	8.12×10^{-4}	8.12×10^{-4}
Ω_o	1.28×10^{2}	1.23×10^{3}	4.77×10^{2}
B	6.58	9.19	8.17

* The parameter χ_μ does not appear in the theory of Molière.

Table IV. Parameters of Molière and NSW for 4.18 MeV nitrogen ions on Al of 118 $\mu g.cm^{-2}$ thick.

	Molière	NSW	
		μ=1.12	μ=1.80
α	26.2	26.2	26.2
χ_o (rad.)	3.87×10^{-5}	3.87×10^{-5}	3.87×10^{-5}
χ_μ (rad.)	*	4.33×10^{-5}	6.96×10^{-5}
χ_α (rad.)	1.97×10^{-3}	4.23×10^{-5}	6.72×10^{-5}
χ_c (rad.)	9.03×10^{-3}	9.03×10^{-3}	9.03×10^{-3}
Ω_o	2.11×10^{1}	4.35×10^{4}	1.69×10^{4}
B	4.37	13.1	12.1

* The parameter χ_μ does not appear in the theory of Molière.

Figure Captions

Fig.2-1. Illustration of spatial angle θ and projected angles ϕ_x and ϕ_y.

Fig.2-2. Scattering cross sections represented by $f(\eta)$ against η. Three cross sections given by Rutherford, Molière and LNS are shown.

Fig.3-1. Schematic view of experimental arrangement.

Fig.3-2. Block diagram of measuring system.

Fig.3-3. Schematic view of vacuum evaporation system.
S: source material, B: tungsten boat, G: glass slide,
Q: head of foil thickness monitor, C: shutter, J: bell jar.

Fig.3-4. Foil thicknesses from MBI method vs. those from quartz crystal method, in Å units. The calibration factor for each element is shown in the table.

Fig.3-5. Stopping power for protons. Curves from other authors are also drawn. Solid curves are from the table of ref.39 and the dashed curve is from that of ref.40.

Fig.3-6. Stopping power for nitrogen ions. Curves from other authors are also drawn. Solid curves are from the table of ref.39 and the dashed curve is obtained from the interpolation of the same table.

Fig.3-7. Multiple scattering distribution of 1.45MeV protons scattered from an aluminium foil of 562μg.cm^{-2}. Curves calculated according to Molière's theory using a_{TF} of (2-2-3) and according to NSW's theory using μ=1.12 and 1.80 are also drawn for comparison.

Fig.3-8. Multiple scattering distribution of 4.18MeV nitrogen ions scattered from an aluminium foil of 118μg.cm^{-2}. Curves calculated according to Molière's theory using a_{TF} of (2-2-3) and according to NSW's theory using μ=1.12 and 1.80 are also drawn for comparison. The curve according to Keil et al.'s theory is also drawn for reference.

Fig.3-9. Multiple scattering distributions of (A) 1.39MeV nitrogen ions scattered from an aluminium foil of 90.9μg.cm^{-2}, and of (B) 1.32MeV nitrogen ions scattered from a silver foil of 113 μg·cm^{-2}. Theoretical curves are drawn also. In (A), Keil et al.'s distribution functions, as obtained from (2-2-2) (noted as eq.(2)) and (2-2-3) (noted as eq.(3)), are compared. In (B), the treatments according to Keil et al. with the use of (2-2-3) and according to Meyer are compared.

Fig.3-10. $\chi_\alpha{}^2 F(0)$ as a function of Ω_0. The same marks for ion-atom combinations are used in Figs.3-11～3-17. Typical experimental errors are shown by bars.

Fig.3-11. $\theta_{1/2}/\chi_\alpha$ as a function of Ω_0.

Fig.3-12. $F(2\theta_{1/2})/F(0)$ as a function of Ω_0. Note the suppressed

origin of the ordinate.

Fig.3-13. Ratio of experimental F(0) to the theoretical value against Ω_o.

Fig.3-14. Ratio of experimental $\theta_{1/2}$ to the theoretical value against Ω_o.

Fig.3-15. Ratio of experimental $F(2\theta_{1/2})/F(0)$ to the theoretical value against Ω_o.

Fig.3-16. Ratio a_c/a_{TF} from experimental F(0) against Ω_o.

Fig.3-17. Ratio a_c/a_{TF} from experimental $\theta_{1/2}$ against Ω_o.

Fig.4-1. Simplified model of ion trajectories in the simulation.

Fig.4-2. Schematic arrangement for the measurement of spatial-angle distribution. Actually in the simulation, the plane A is a sphere whose center is the beam spot on the foil.

Fig.4-3. Schematic arrangement for the measurement of projected-angle distribution; the case of longitudinal slit of length d. Actually in the simulation, the line L is a circle whose center is the center of the beam spot, O, on the foil.

Fig.4-4. Simulated multiple-scattering angular distributions of 0.407MeV protons upon copper foil of 869$\mu g \cdot cm^{-2}$, based on 40500 histories: the spatial-angle distribution in (A) and the

projected-angle one in (B). The curves are calculated according to Molière's theory. Typical statistical errors are shown by bars.

Fig.4-5. Histogram of the number of scatterings for multiple scattering of Fig.4-4.

Fig.4-6. Simulated multiple-scattering angular distributions of 1.45MeV protons upon copper foil of 869μg.cm^{-2}, based on 15000 histories: the spatial-angle distribution in (A) and projected-angle one in (B).

Fig.4-7. Histogram of the number of scatterings for multiple scattering of Fig.4-6.

Fig.4-8. Simulated multiple-scattering angular distributions of 2.21MeV nitrogen ions upon gold foil of 331μg.cm^{-2}, based on 20000 histories. The spatial- and projected-angle distributions are shown in (A) and (B), respectively. The curve in (A) is drawn according to Keil et al.'s theory.

Fig.4-9. Histogram of the number of scatterings for multiple scattering of Fig.4-8.

Fig.4-10. Simulated multiple-scattering angular distributions of nitrogen ions upon silver foil of 401μg.cm^{-2}, based on 700000 histories. Here, energy loss process is taken into account. Initial beam-energy is 4.52MeV.

The spatial-angle distribution is shown in (A) where the

curve is drawn according to Keil et al.'s theory. The projected-angle distribution is shown in (B). The curve according to Molière's treatment is presented for the sake of comparison; here a small deviation is seen because $\Omega_o < 20$. Both the theoretical curves are drawn for the average energy in the foil (3.92MeV).

Fig.4-11. Histogram of the number of scatterings for multiple scattering of Fig.4-10. Statistical errors are very small.

Fig.4-12. Calculated energy spectrum of outgoing nitrogen ions of Fig.4-10, based on 640000 histories. The incident beam is assumed to be monochromatic.

Fig.4-13. Multiple-scattering angular distribution, $F_e(\theta)$, of initially longitudinal beam of 5mm length. Other initial conditions are the same as those in Fig.4-10. This result is based on 700000 histories, but actually only 11871 particles enter the plane P of Fig.4-3.

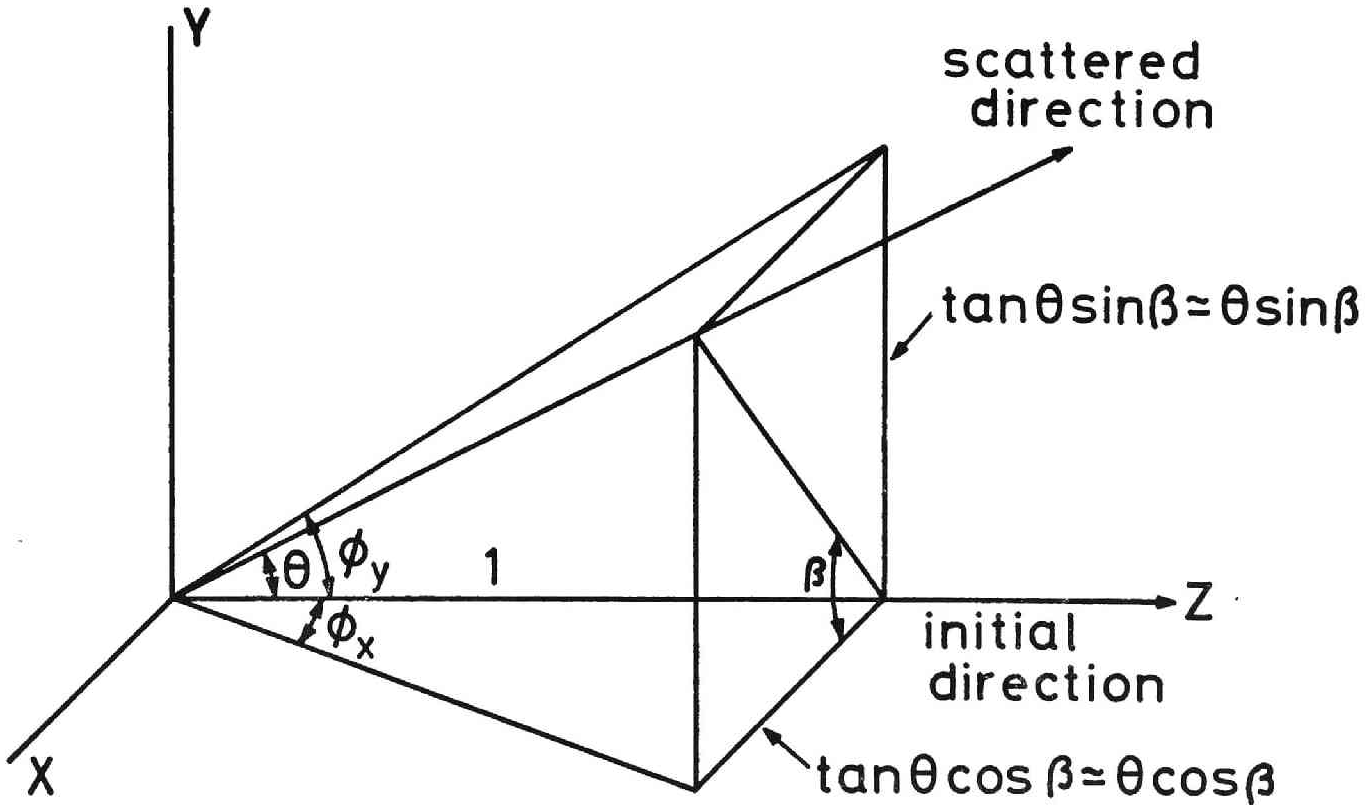
Y
scattered
direction
tanθsinβ≈θsinβ
θ
ϕ_y
1
β
Z
ϕ_x
initial
direction
X
tanθcosβ≈θcosβ

Fig.2-1

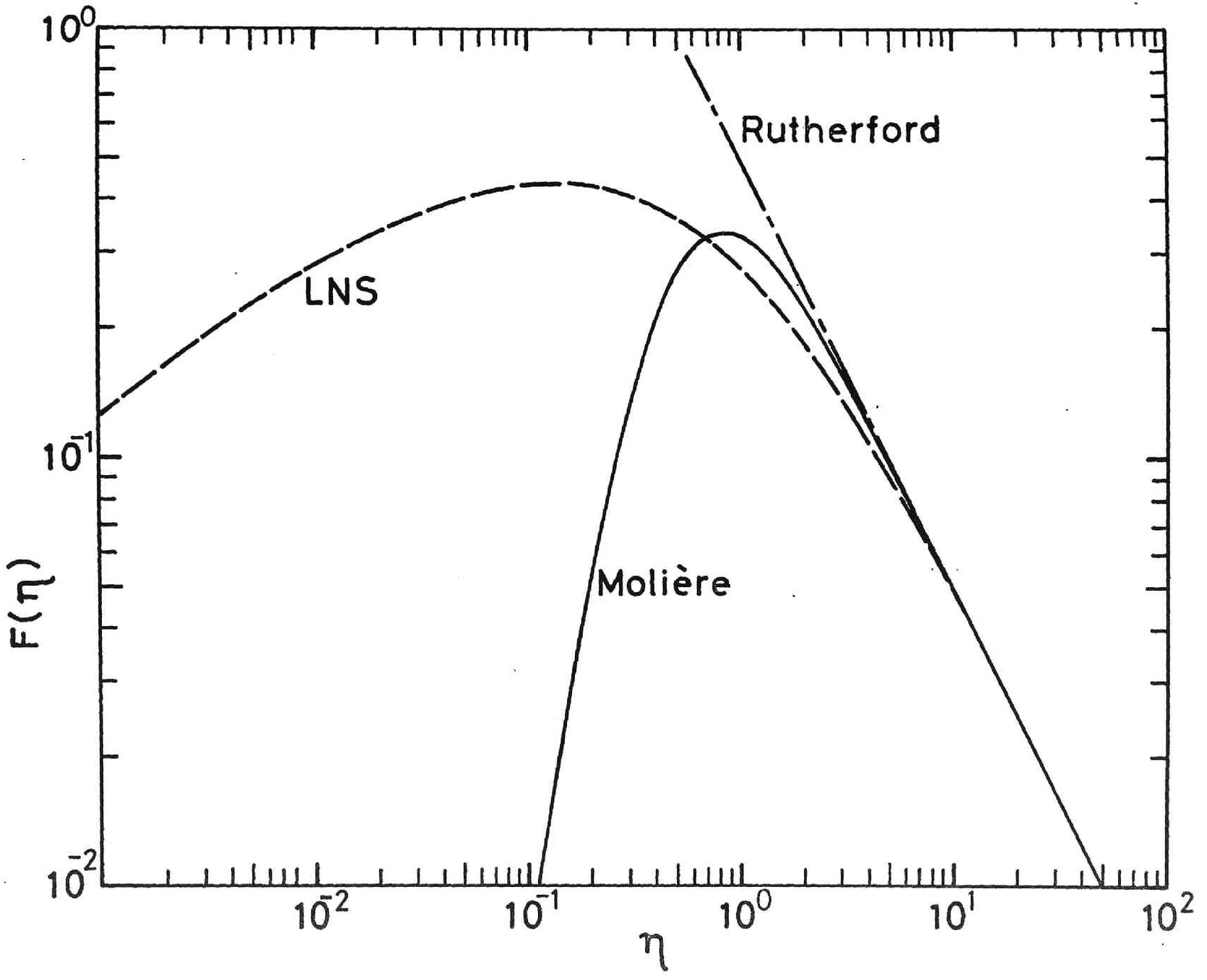

Fig.2-2

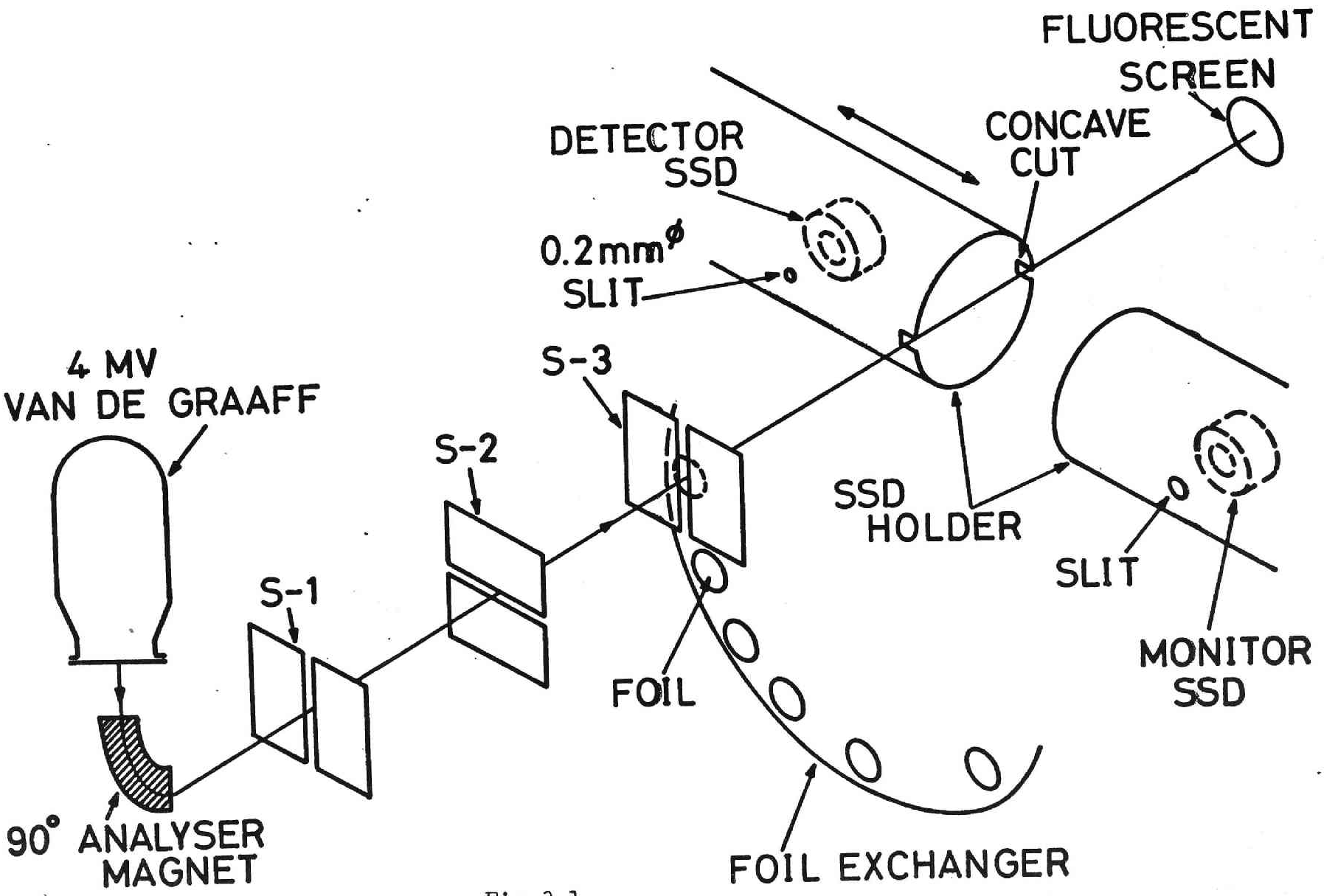
FLUORESCENT
SCREEN
CONCAVE
CUT
DETECTOR
SSD
0.2mmφ
SLIT
4 MV
VAN DE GRAAFF
S-3
S-2
S-1
SSD
HOLDER
SLIT
MONITOR
SSD
FOIL
90° ANALYSER
MAGNET
FOIL EXCHANGER

Fig.3-1

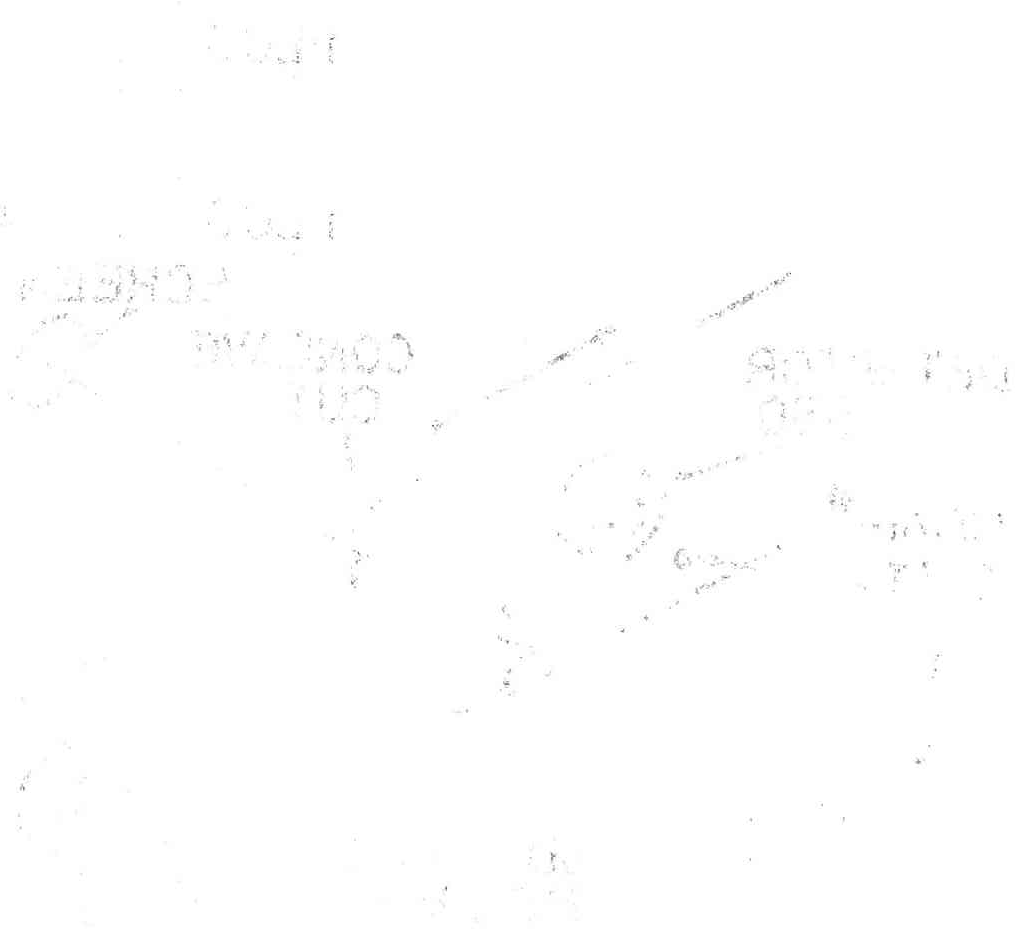

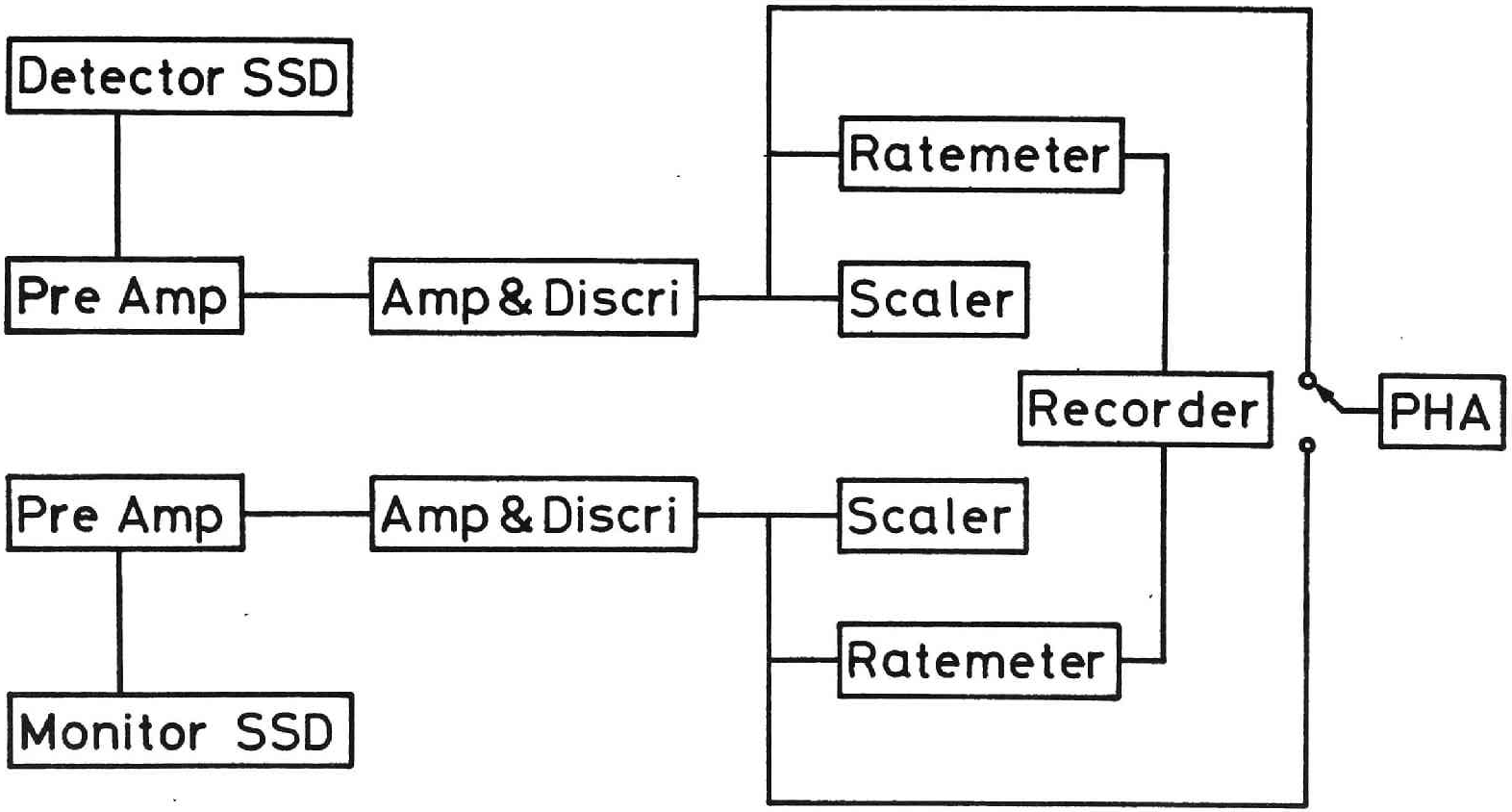
Detector SSD
Pre Amp
Amp & Discri
Ratemeter
Scaler
Recorder
PHA
Pre Amp
Amp & Discri
Scaler
Ratemeter
Monitor SSD

Fig.3-2

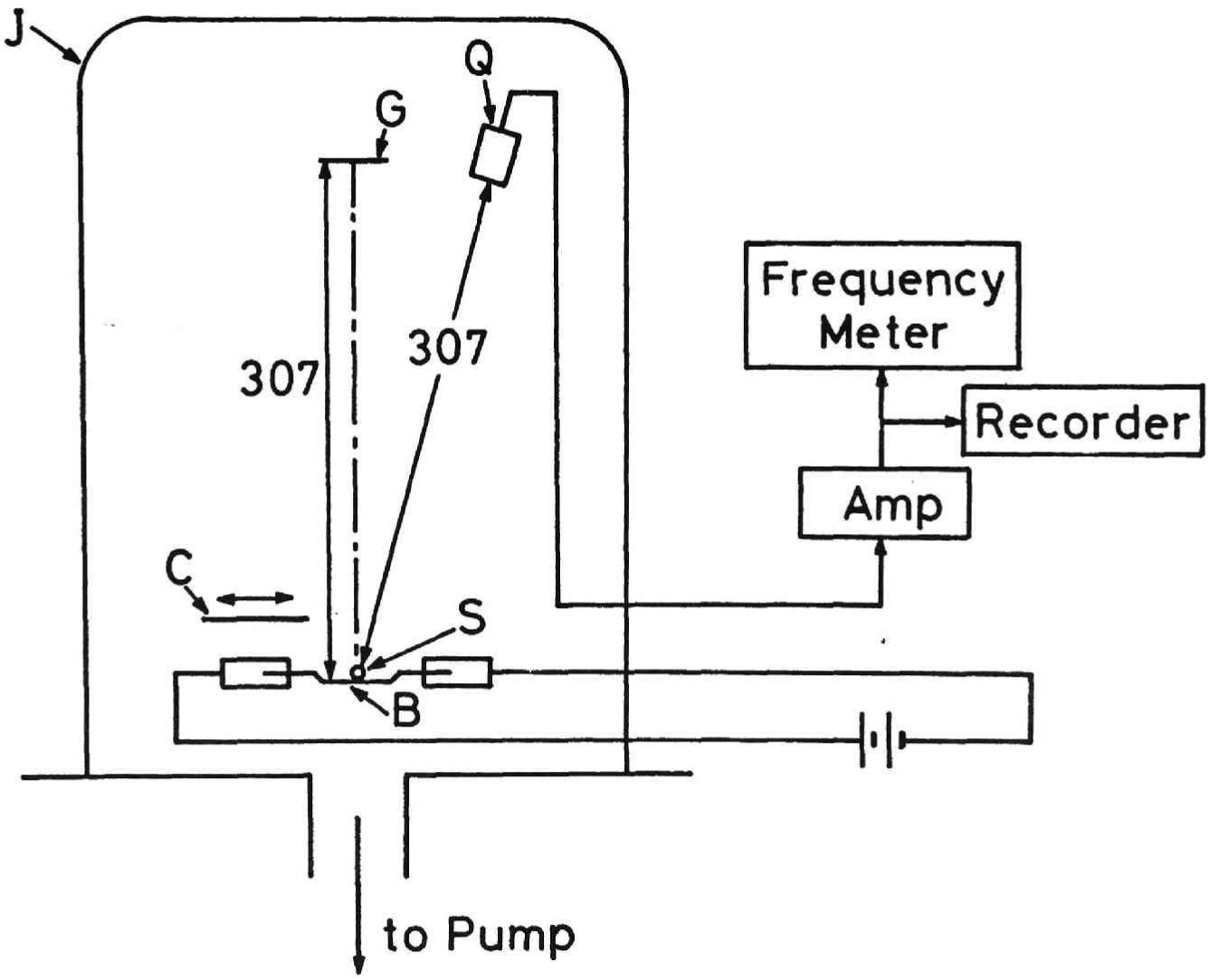

Fig.3-3

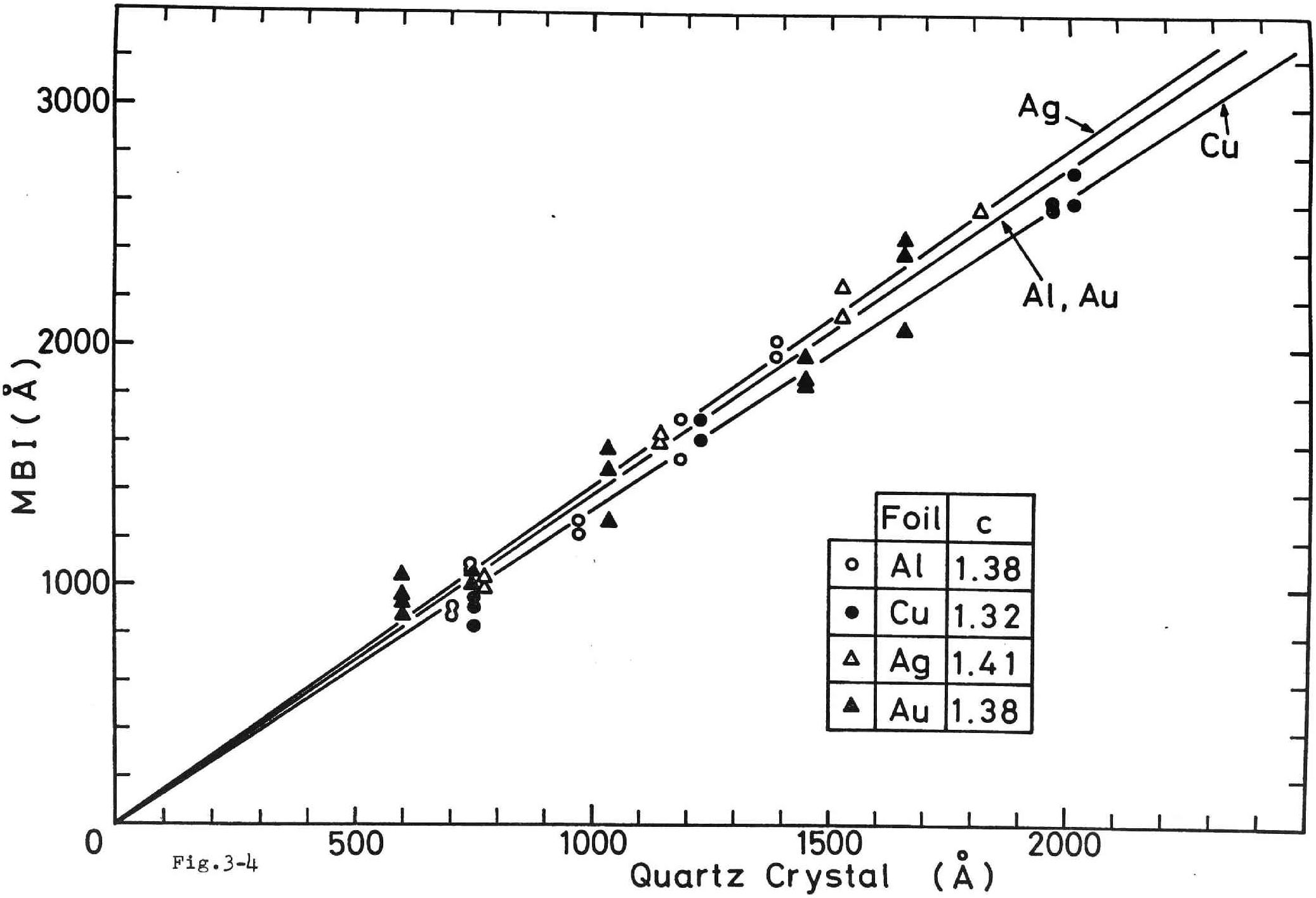
3000
2000
1000
0
MBI (Å)
500
1000
1500
2000
Quartz Crystal (Å)
Ag
Cu
Al, Au
Foil
c
Al
1.38
Cu
1.32
Ag
1.41
Au
1.38

Fig.3-4

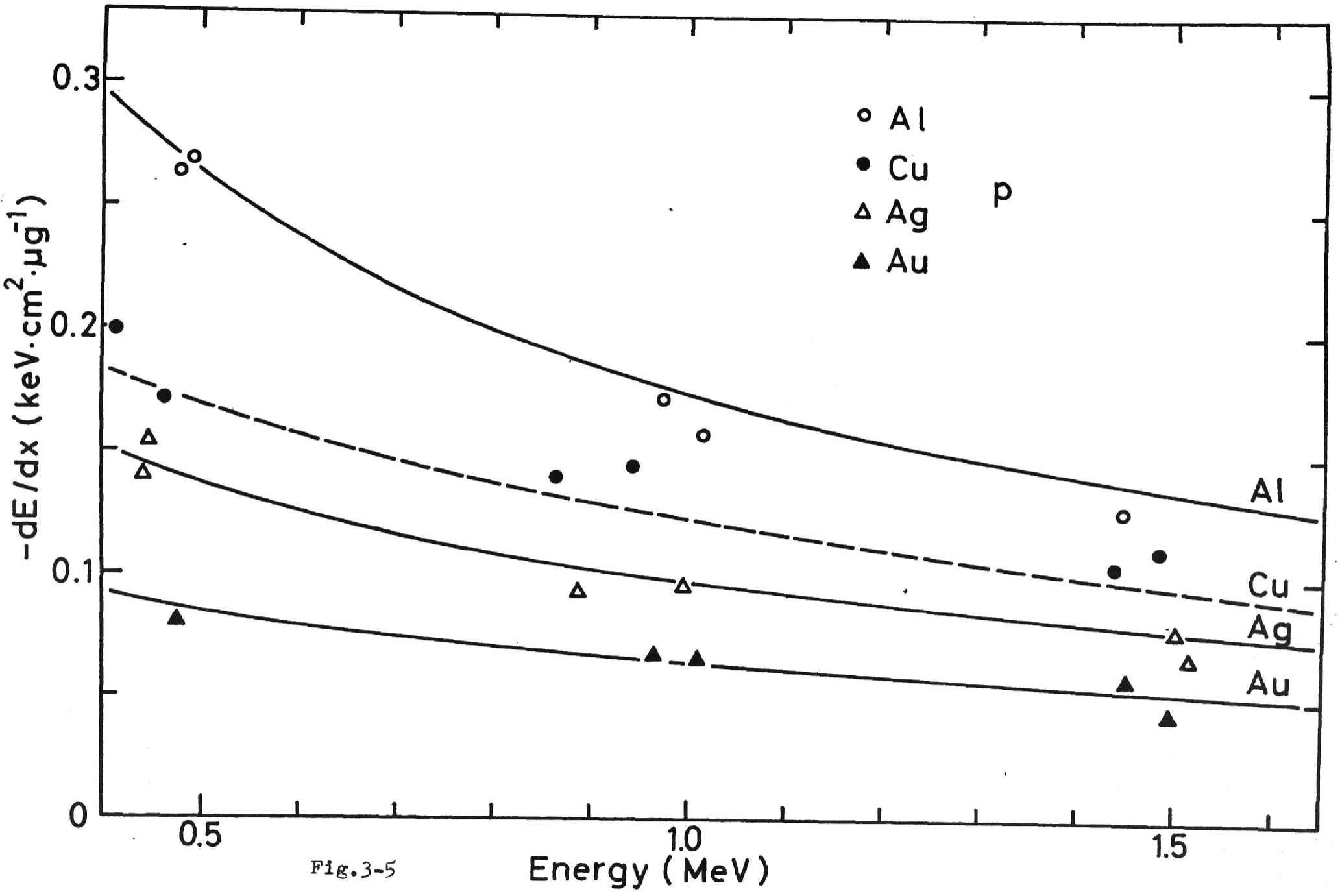
0.3
0.2
0.1
0
0.5
1.0
1.5
-dE/dx (keV·cm²·μg⁻¹)
Energy (MeV)
Al
Cu
Ag
Au
p
Al
Cu
Ag
Au

Fig.3-5

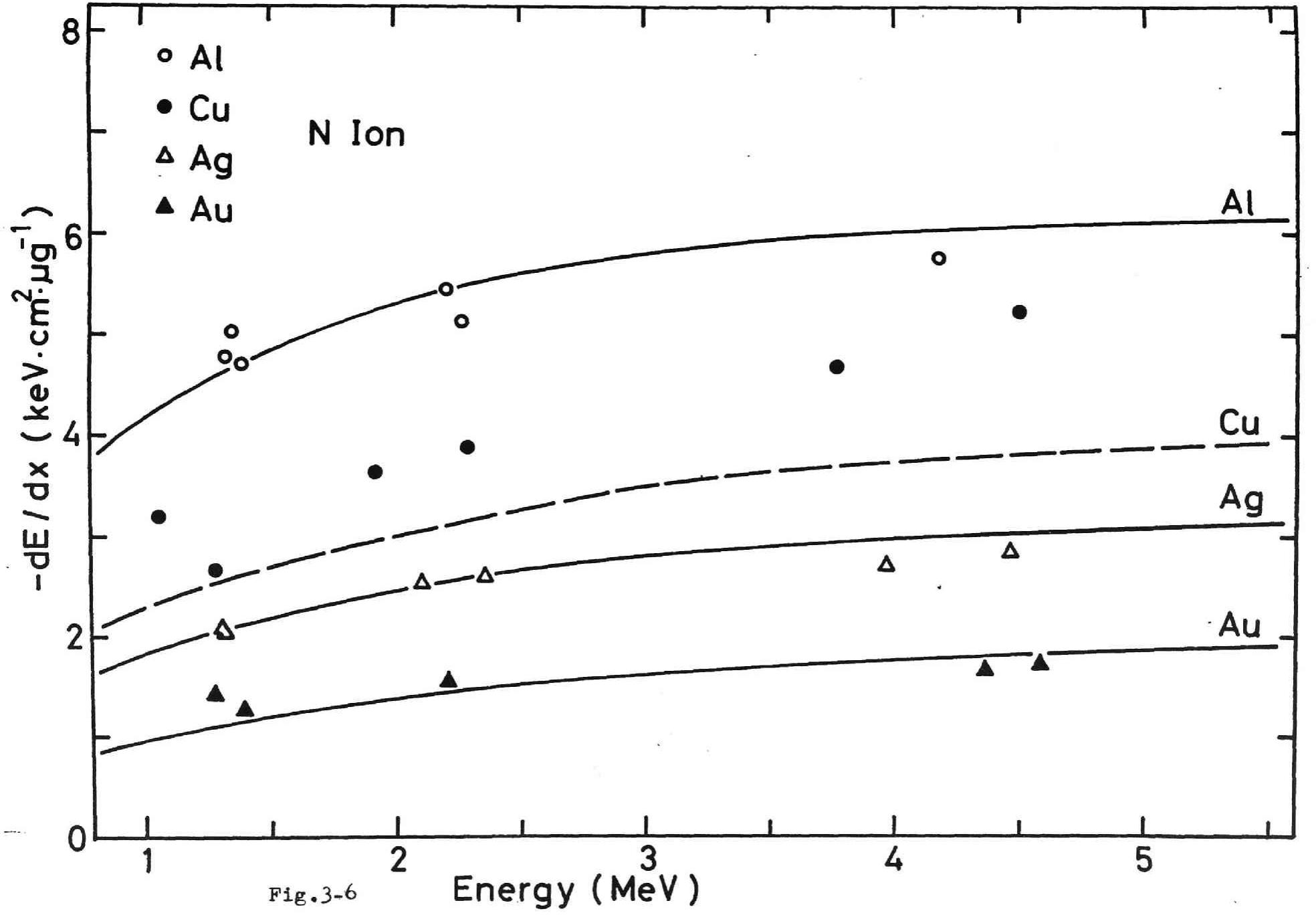
o Al
● Cu
△ Ag
▲ Au
N Ion
Al
Cu
Ag
Au
-dE / dx (keV·cm²·μg⁻¹)
Energy (MeV)
0
2
4
6
8
1
2
3
4
5

Fig.3-6

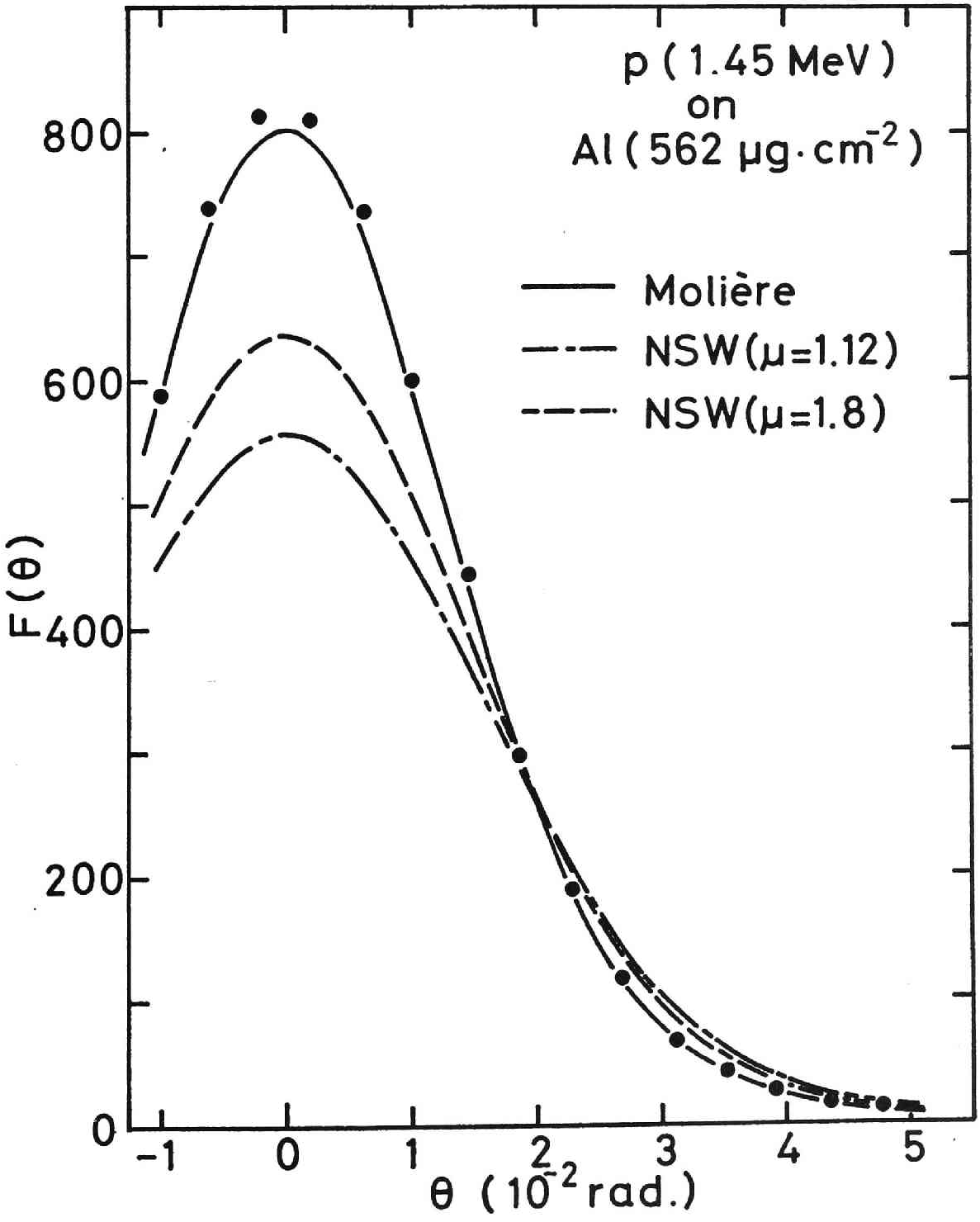
p (1.45 MeV)
on
Al (562 μg·cm⁻²)
Molière
NSW(μ=1.12)
NSW(μ=1.8)
F(θ)
800
600
400
200
0
-1
0
1
2
3
4
5
θ (10⁻² rad.)

Fig.3-7

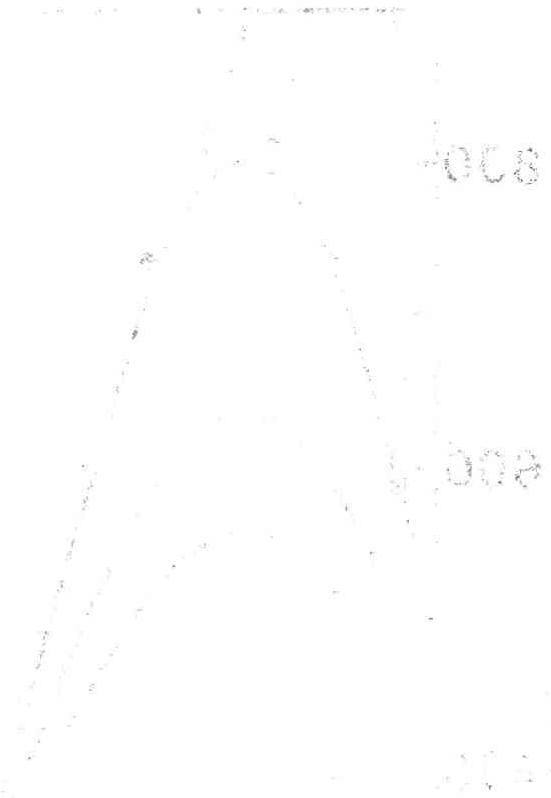

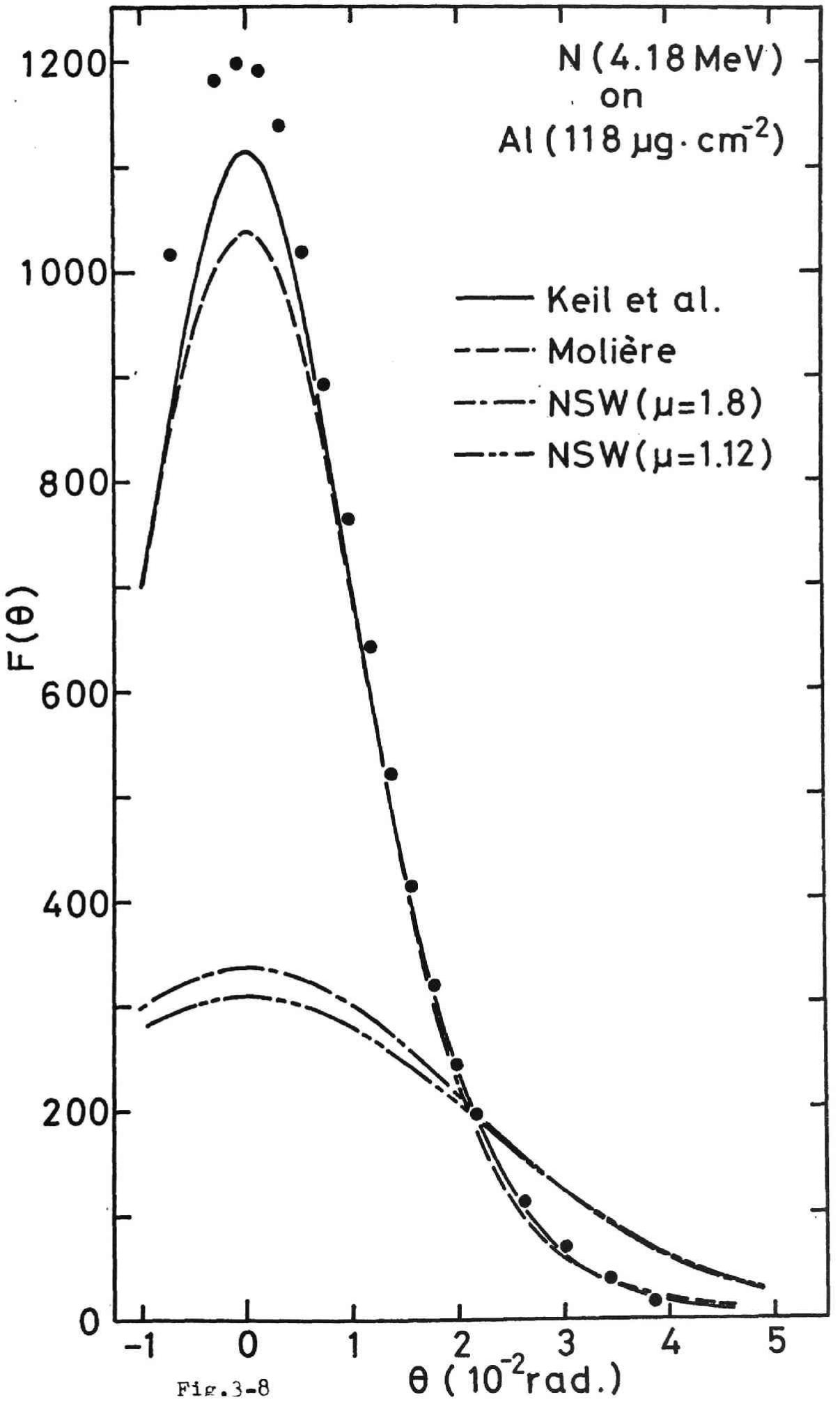
N (4.18 MeV)
on
Al (118 μg · cm⁻²)
Keil et al.
Molière
NSW (μ=1.8)
NSW (μ=1.12)
F(θ)
θ (10⁻² rad.)
0
200
400
600
800
1000
1200
-1
0
1
2
3
4
5

Fig.3-8

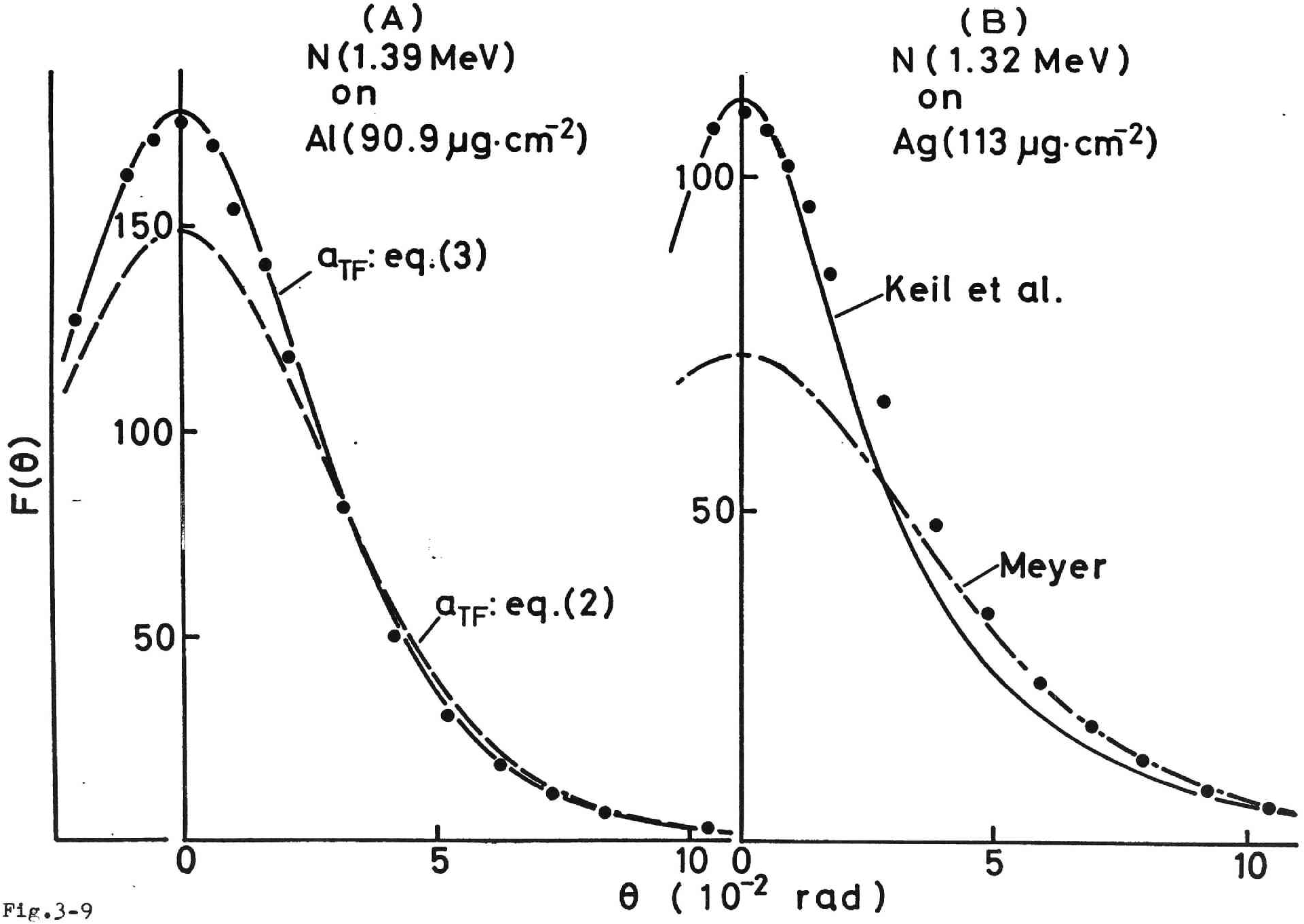
(A)
N(1.39 MeV)
on
Al(90.9 μg·cm⁻²)
150
100
50
F(θ)
a_{TF}: eq.(3)
a_{TF}: eq.(2)
0
5
10
(B)
N(1.32 MeV)
on
Ag(113 μg·cm⁻²)
100
50
Keil et al.
Meyer
0
5
10
θ (10⁻² rad)

Fig.3-9

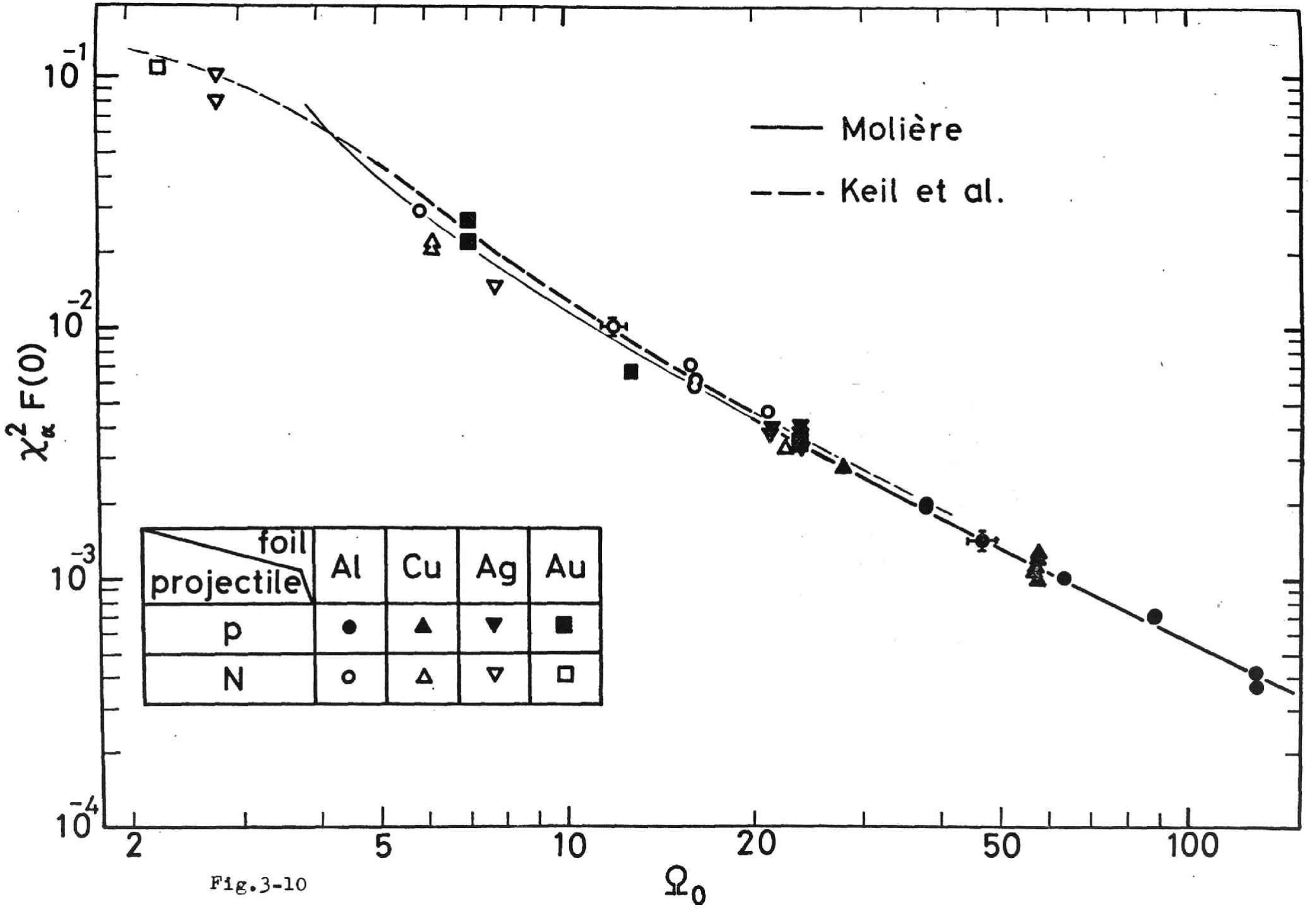
Molière
Keil et al.
$\chi_\alpha^2 F(0)$
Ω_0
10^{-1}
10^{-2}
10^{-3}
10^{-4}
2
5
10
20
50
100
foil
projectile
Al
Cu
Ag
Au
p
N

Fig.3-10

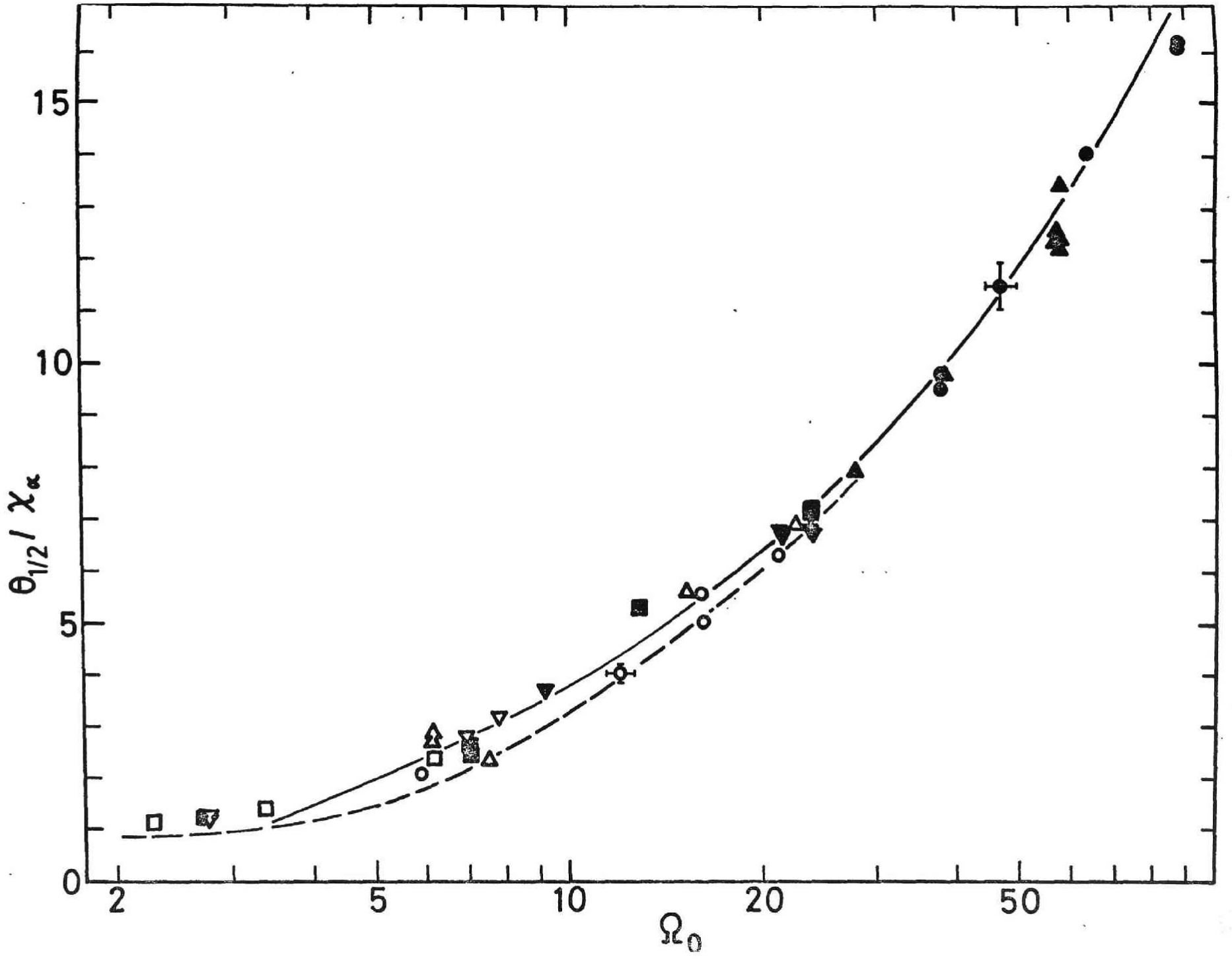

Fig.3-11

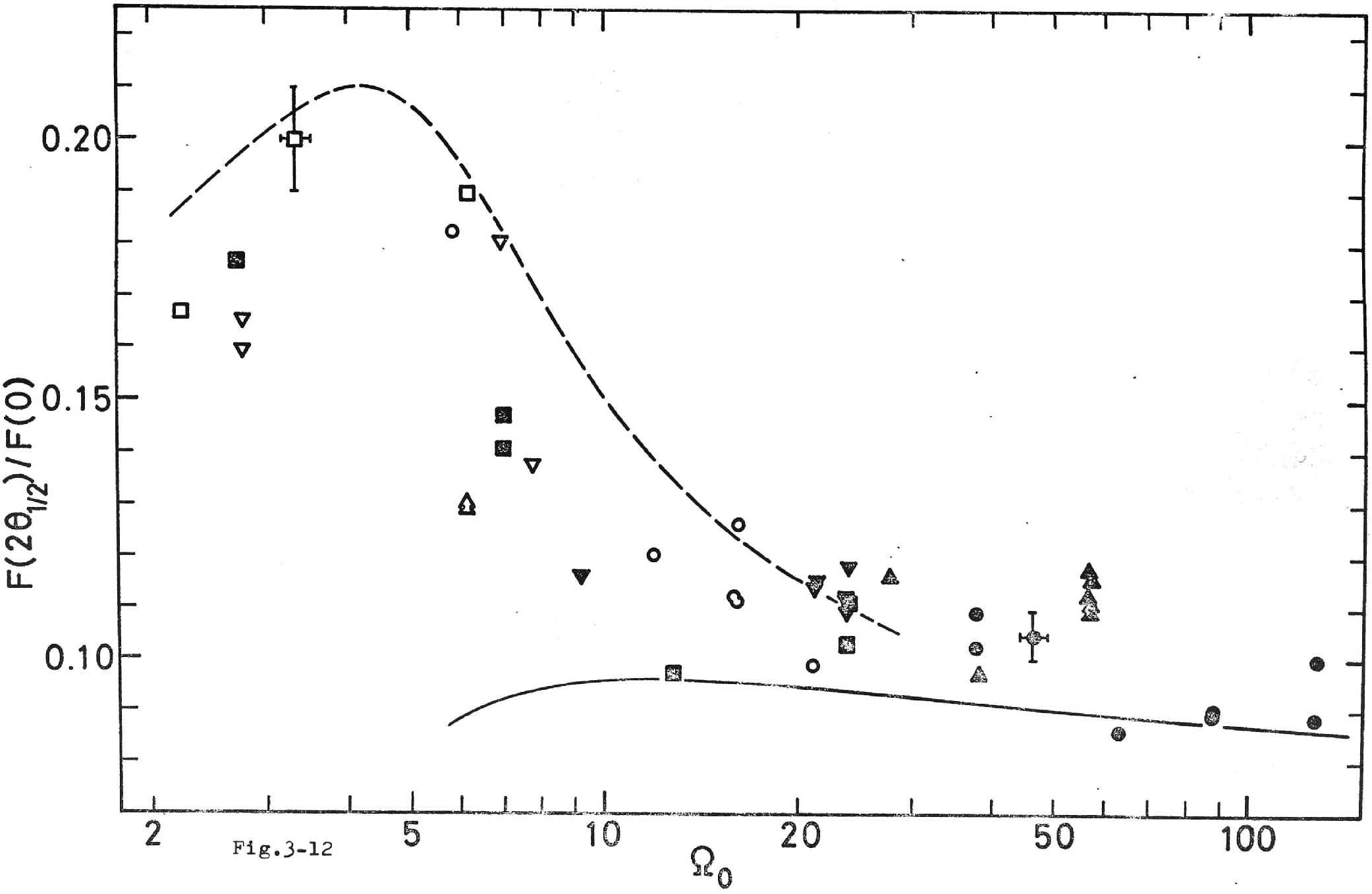

Fig.3-12

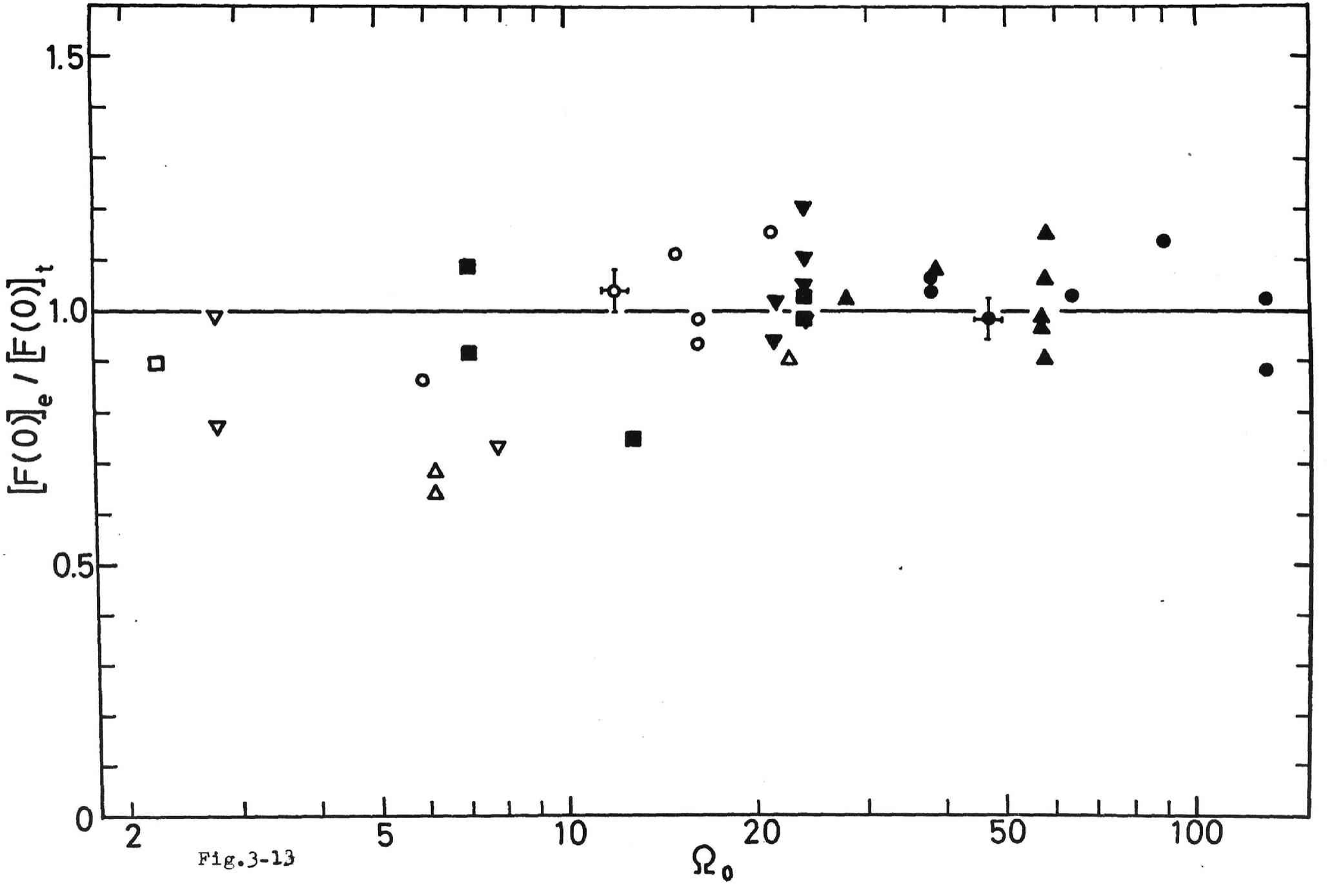

Fig.3-13

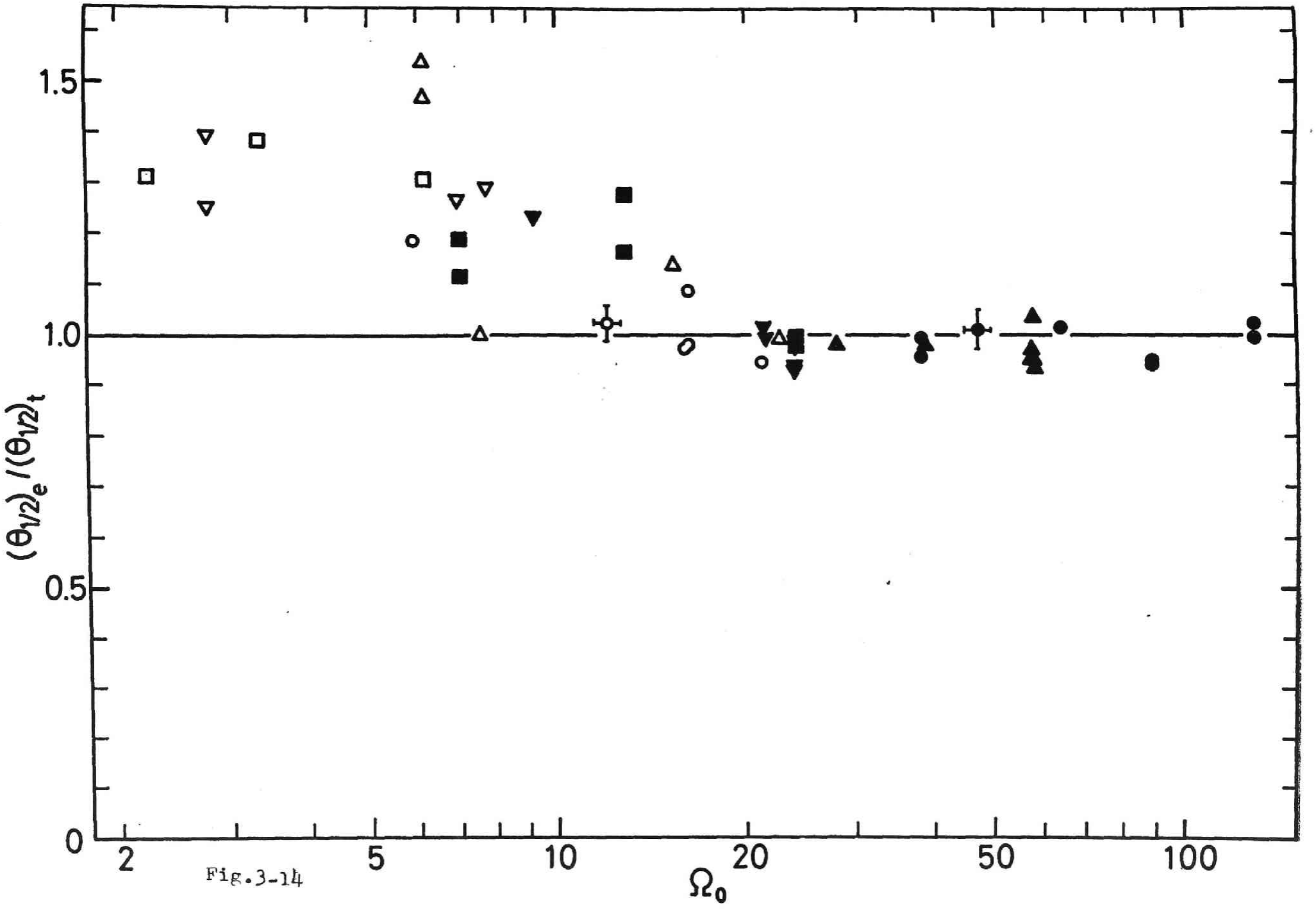

Fig.3-14

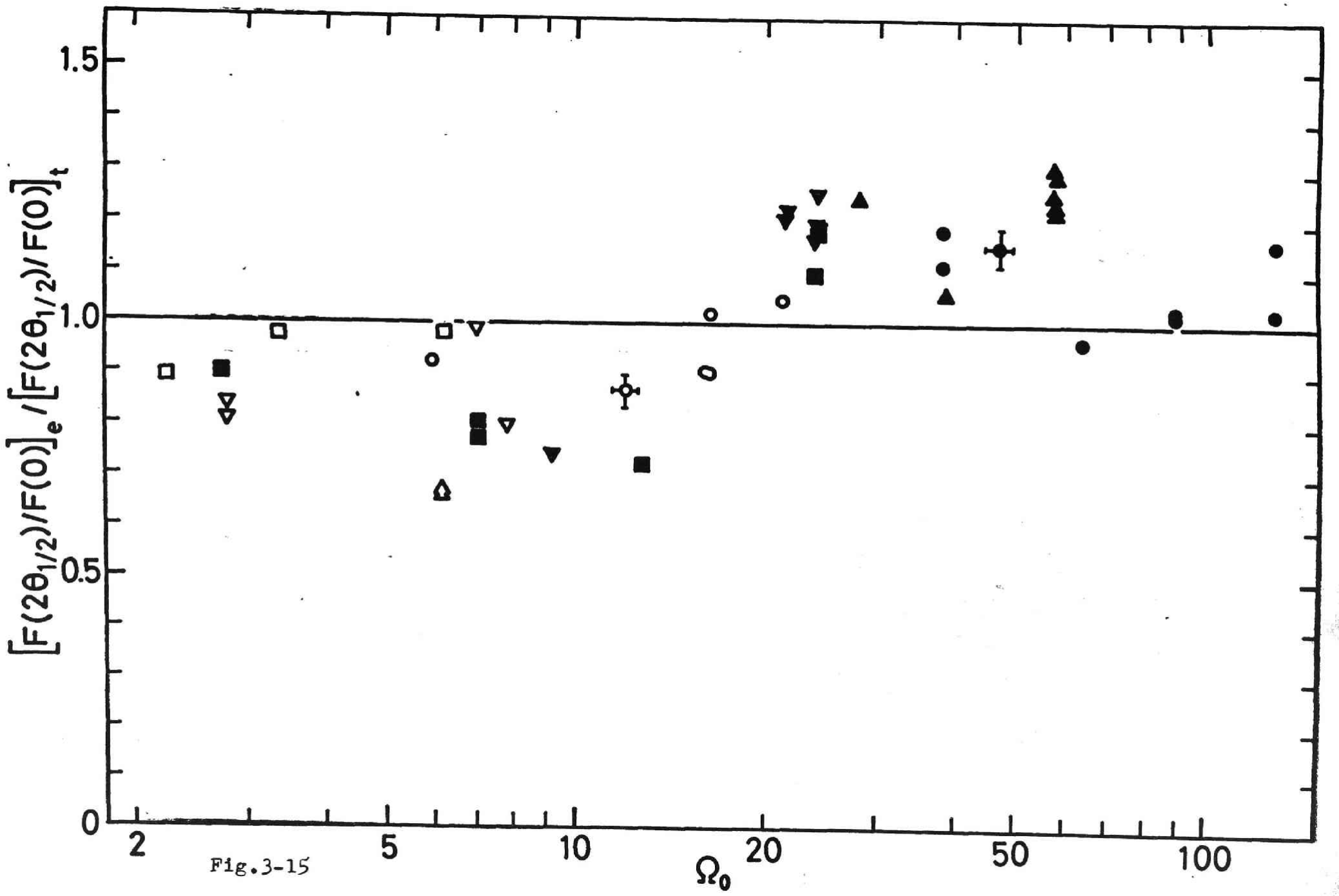

Fig.3-15

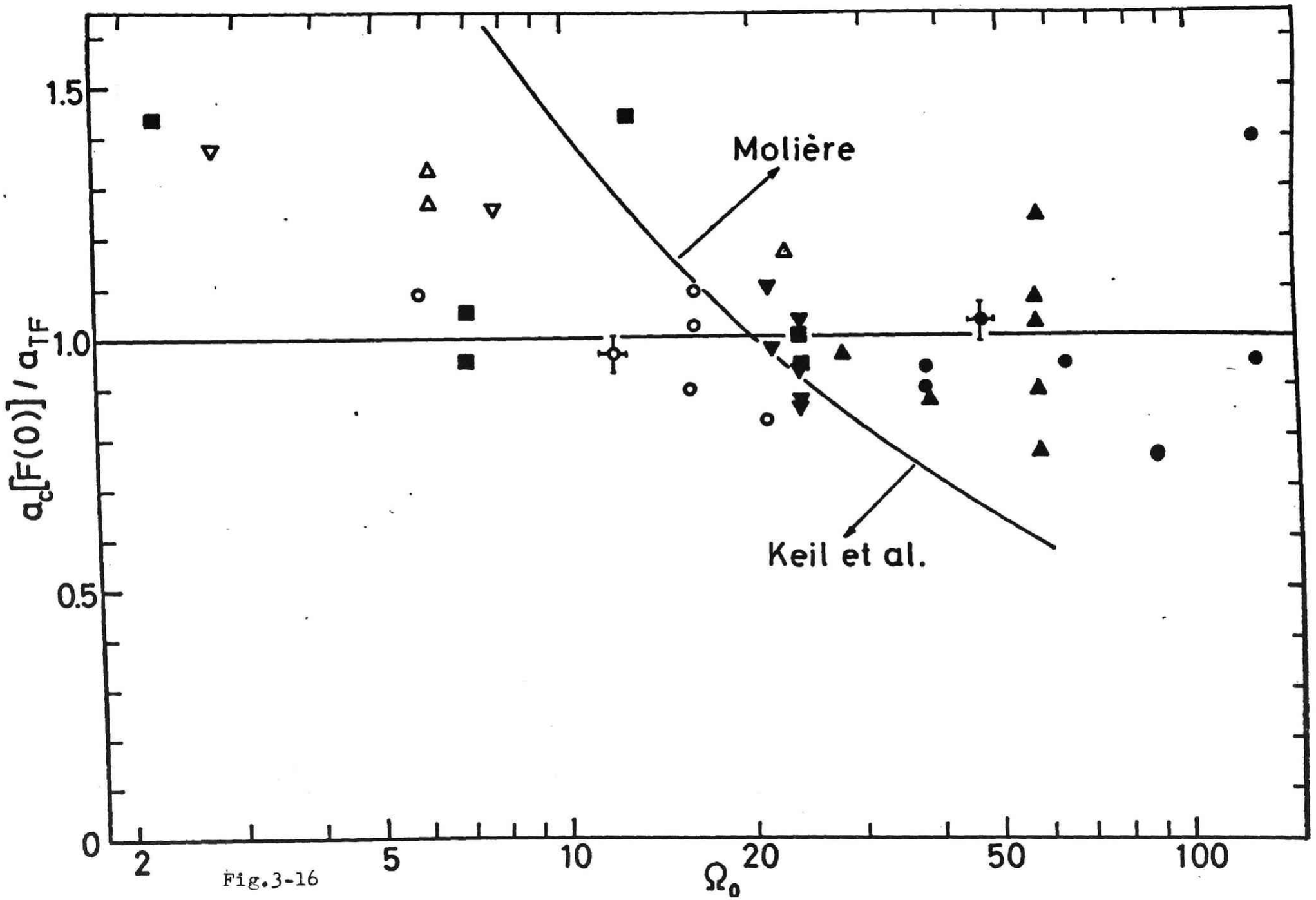

Fig.3-16

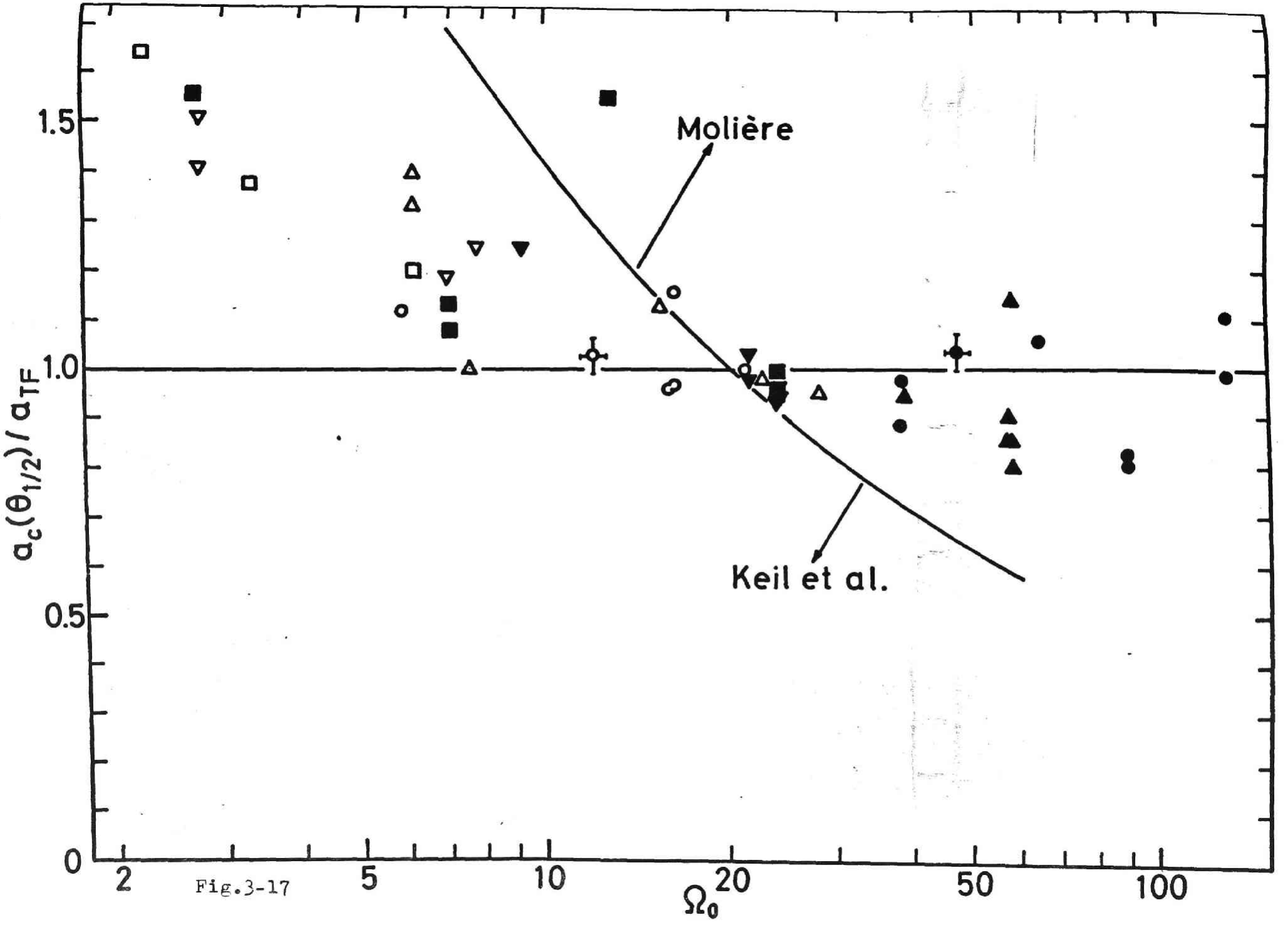
Molière
Keil et al.
$a_c(\theta_{1/2}) / a_{TF}$
1.5
1.0
0.5
0
2
5
10
20
50
100
Ω_0

Fig.3-17

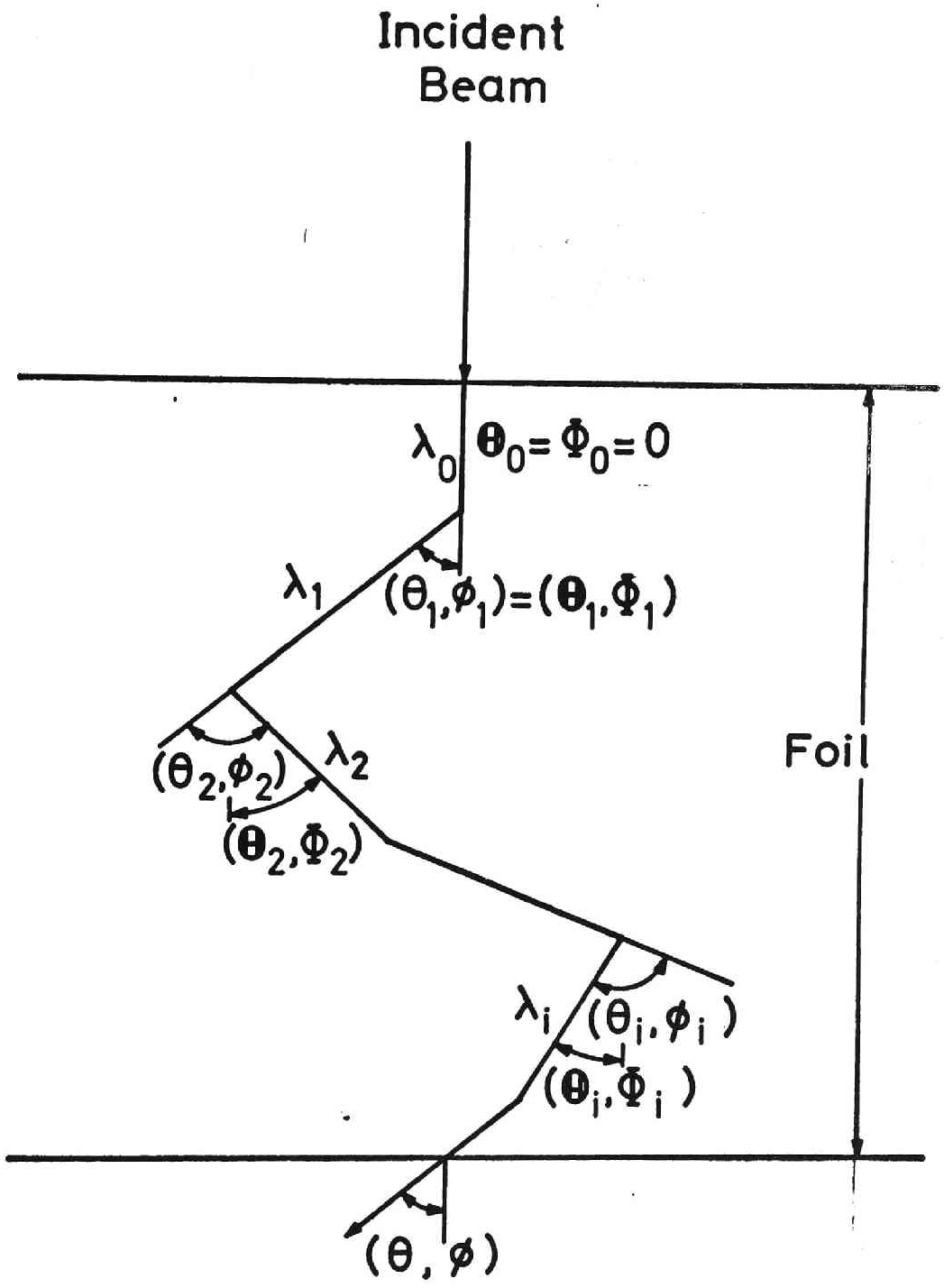
Incident
Beam
λ_0 $\theta_0=\Phi_0=0$
λ_1 $(\theta_1,\phi_1)=(\theta_1,\Phi_1)$
(θ_2,ϕ_2)
λ_2
(θ_2,Φ_2)
Foil
λ_i (θ_i,ϕ_i)
(θ_i,Φ_i)
(θ,ϕ)

Fig.4-1

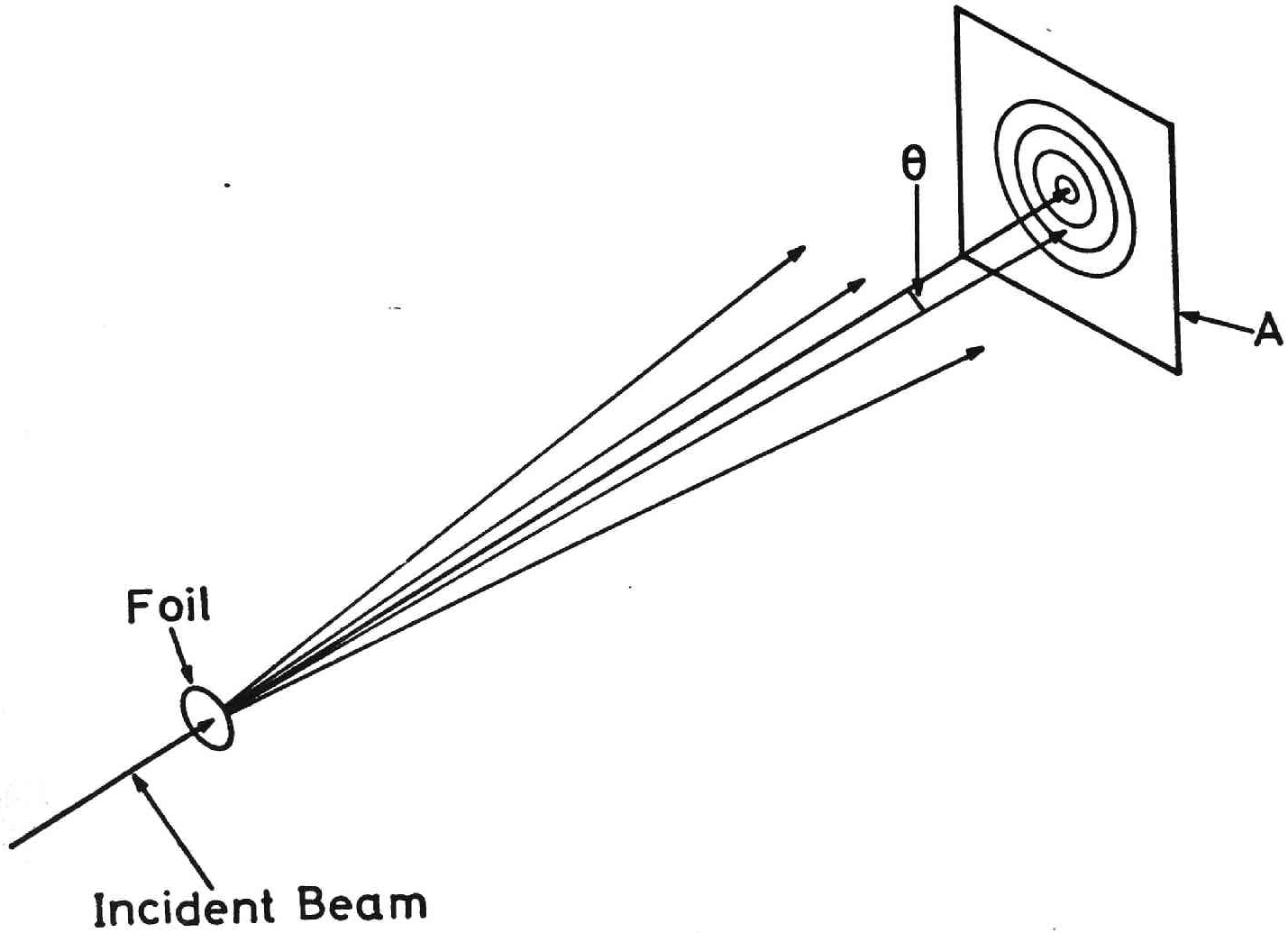

Fig.4-2

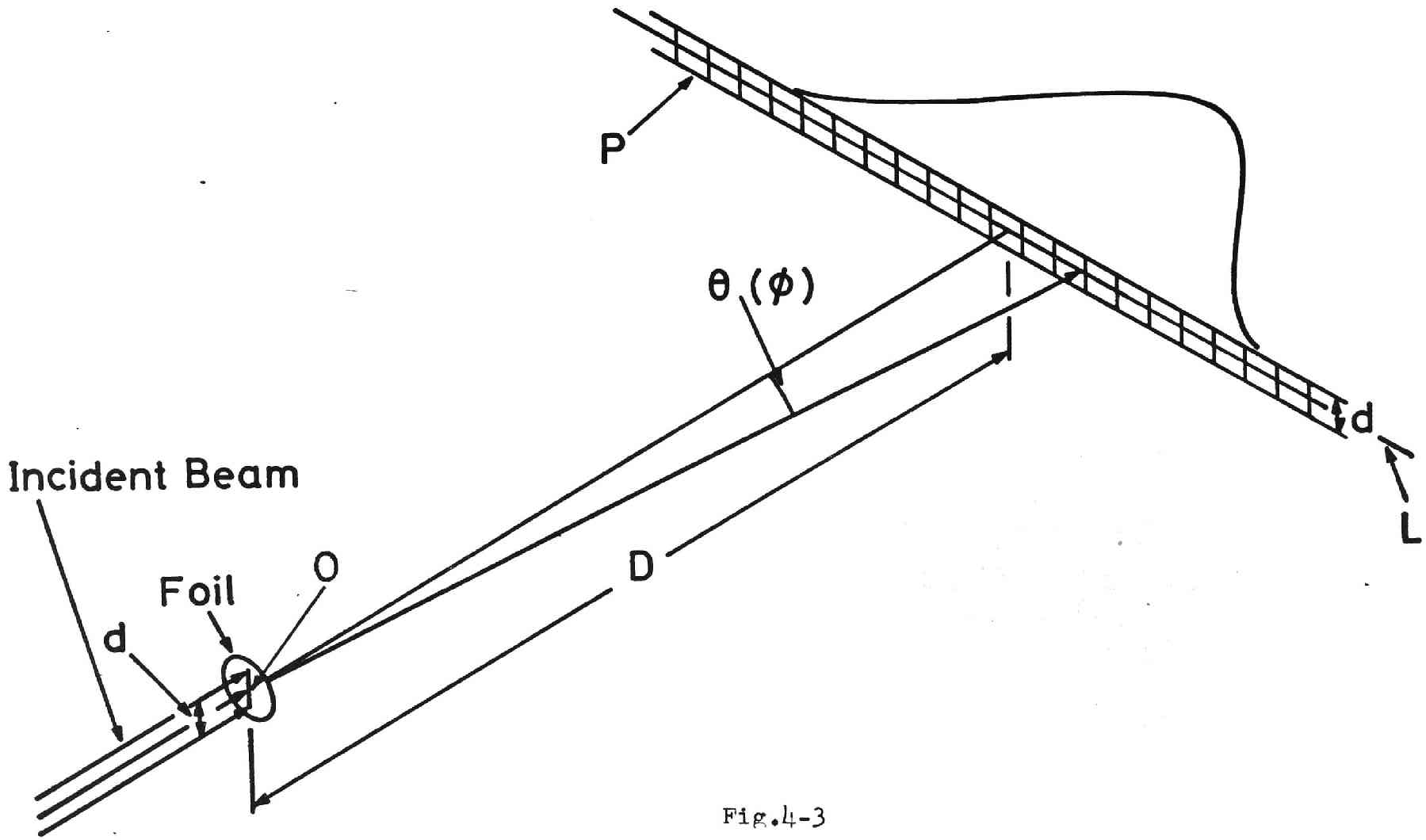

Fig.4-3

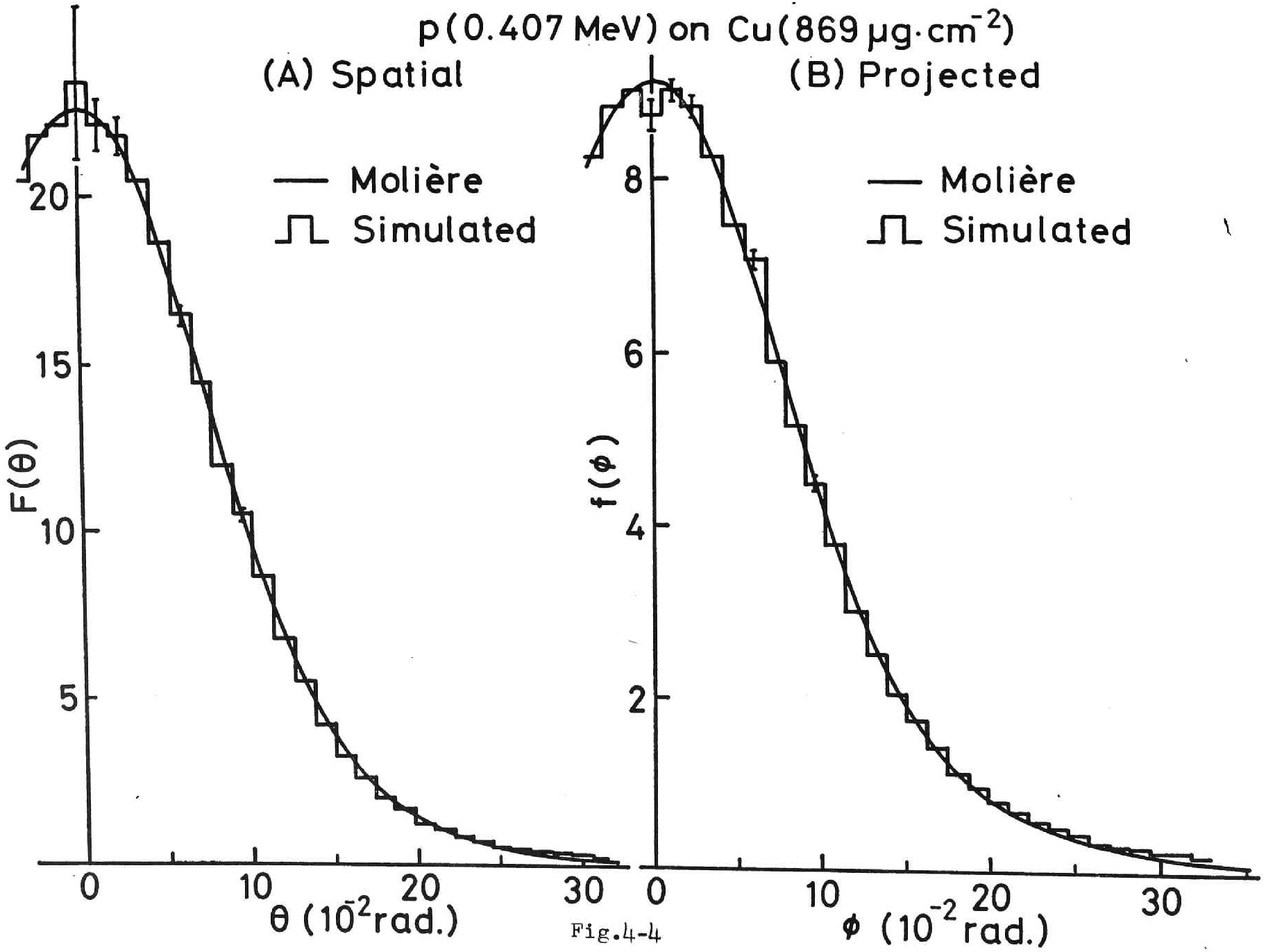
p(0.407 MeV) on Cu(869 μg·cm⁻²)
(A) Spatial
(B) Projected
Molière
Simulated
Molière
Simulated
F(θ)
f(φ)
θ (10⁻²rad.)
φ (10⁻² rad.)
0
10
20
30
5
10
15
20
2
4
6
8

Fig.4-4

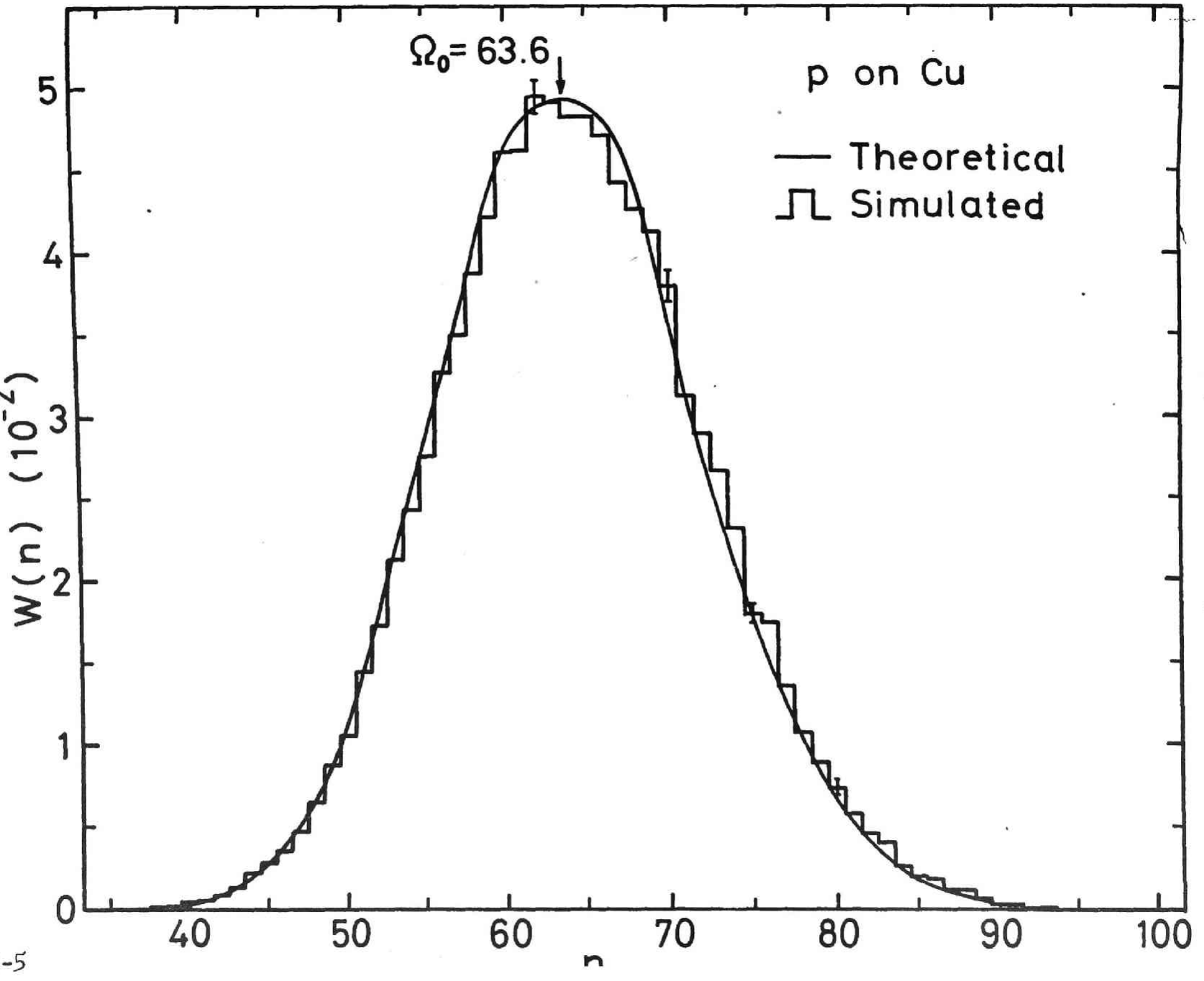
Ω_0= 63.6
p on Cu
Theoretical
Simulated
W(n) (10^{-2})
n
0
1
2
3
4
5
40
50
60
70
80
90
100

Fig.4-5

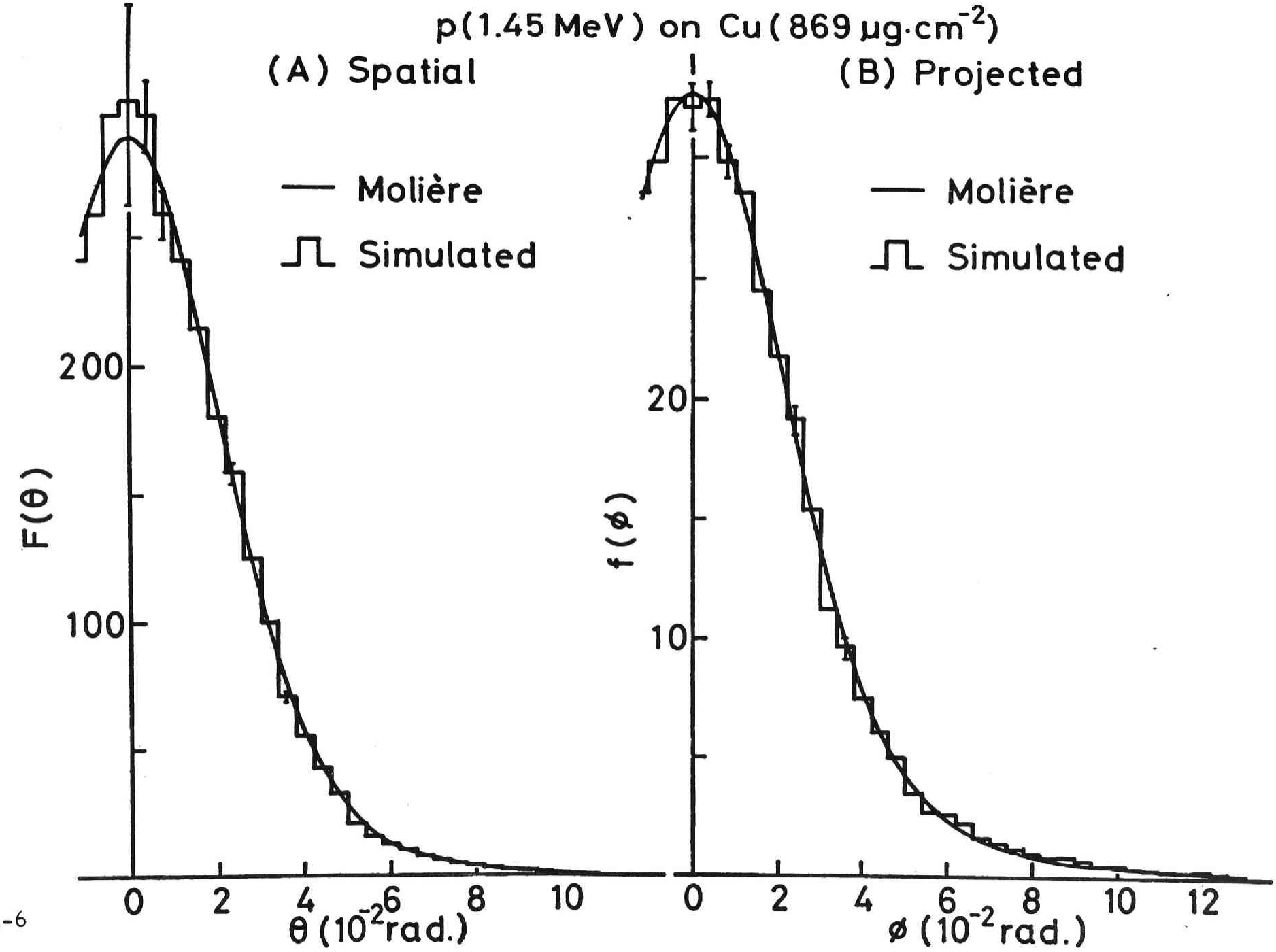
p(1.45 MeV) on Cu(869 μg·cm⁻²)
(A) Spatial
(B) Projected
Molière
Simulated
Molière
Simulated
F(θ)
f(φ)
200
100
20
10
0
2
4
6
8
10
12
θ (10⁻² rad.)
φ (10⁻² rad.)

Fig.4-6

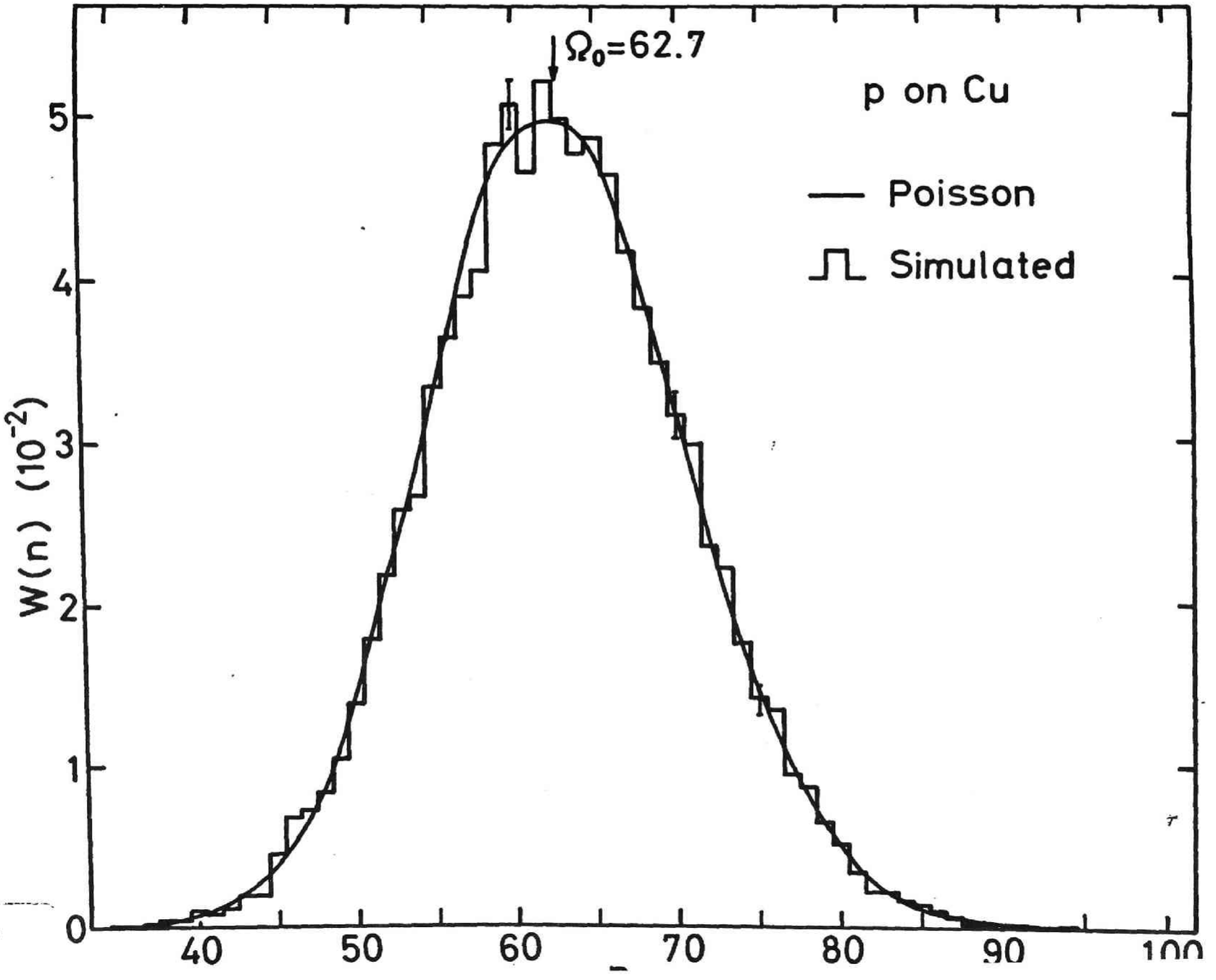
Ω_0=62.7
p on Cu
Poisson
Simulated
W(n) (10^{-2})
0
1
2
3
4
5
40
50
60
70
80
90
100

Fig.4-7

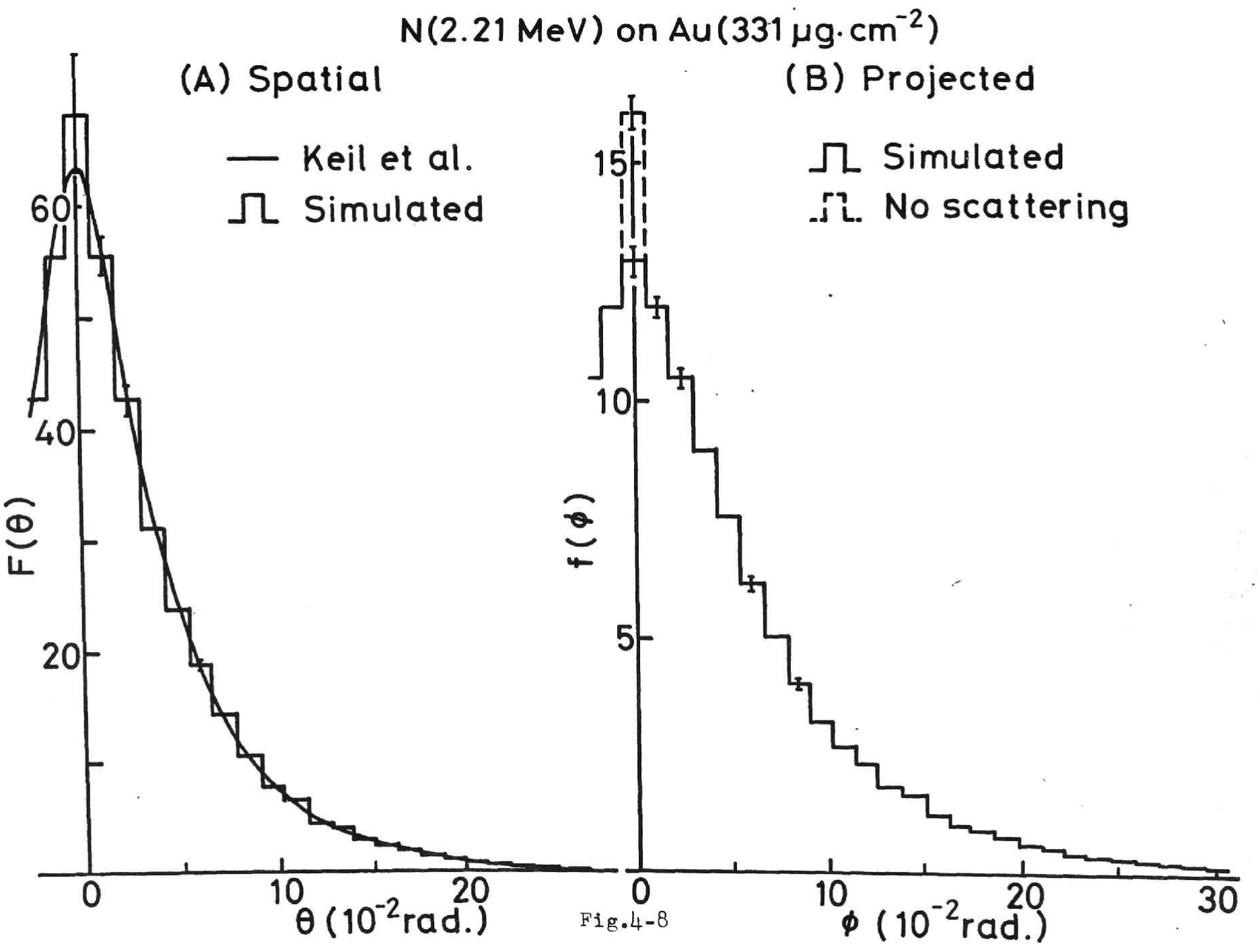
N(2.21 MeV) on Au(331 μg·cm⁻²)
(A) Spatial
(B) Projected
Keil et al.
Simulated
Simulated
No scattering
F(θ)
f(φ)
θ (10⁻²rad.)
φ (10⁻²rad.)
60
40
20
15
10
5
0
10
20
30

Fig.4-8

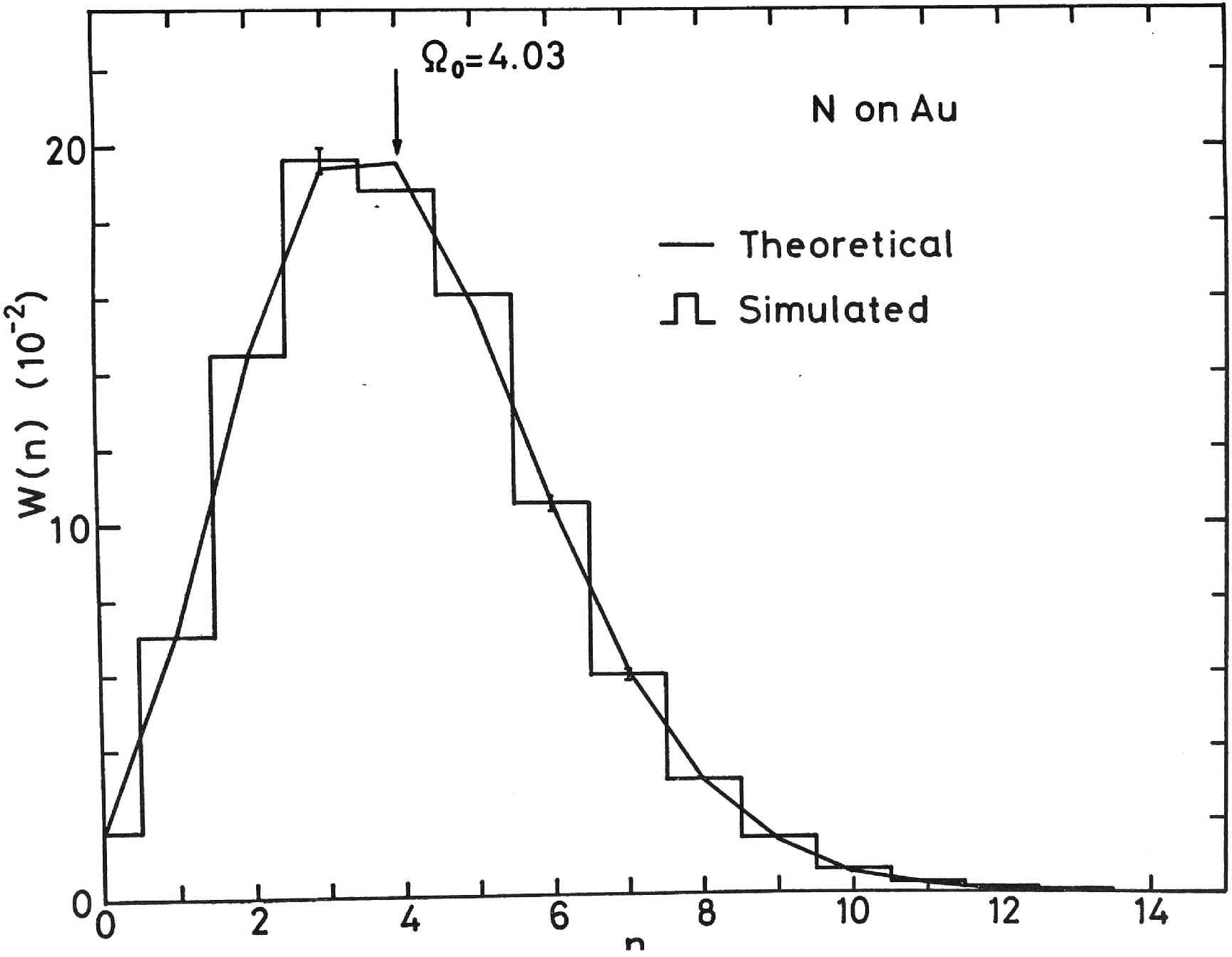
Ω_0=4.03
N on Au
Theoretical
Simulated
W(n) (10^{-2})
20
10
0
0
2
4
6
8
10
12
14
n

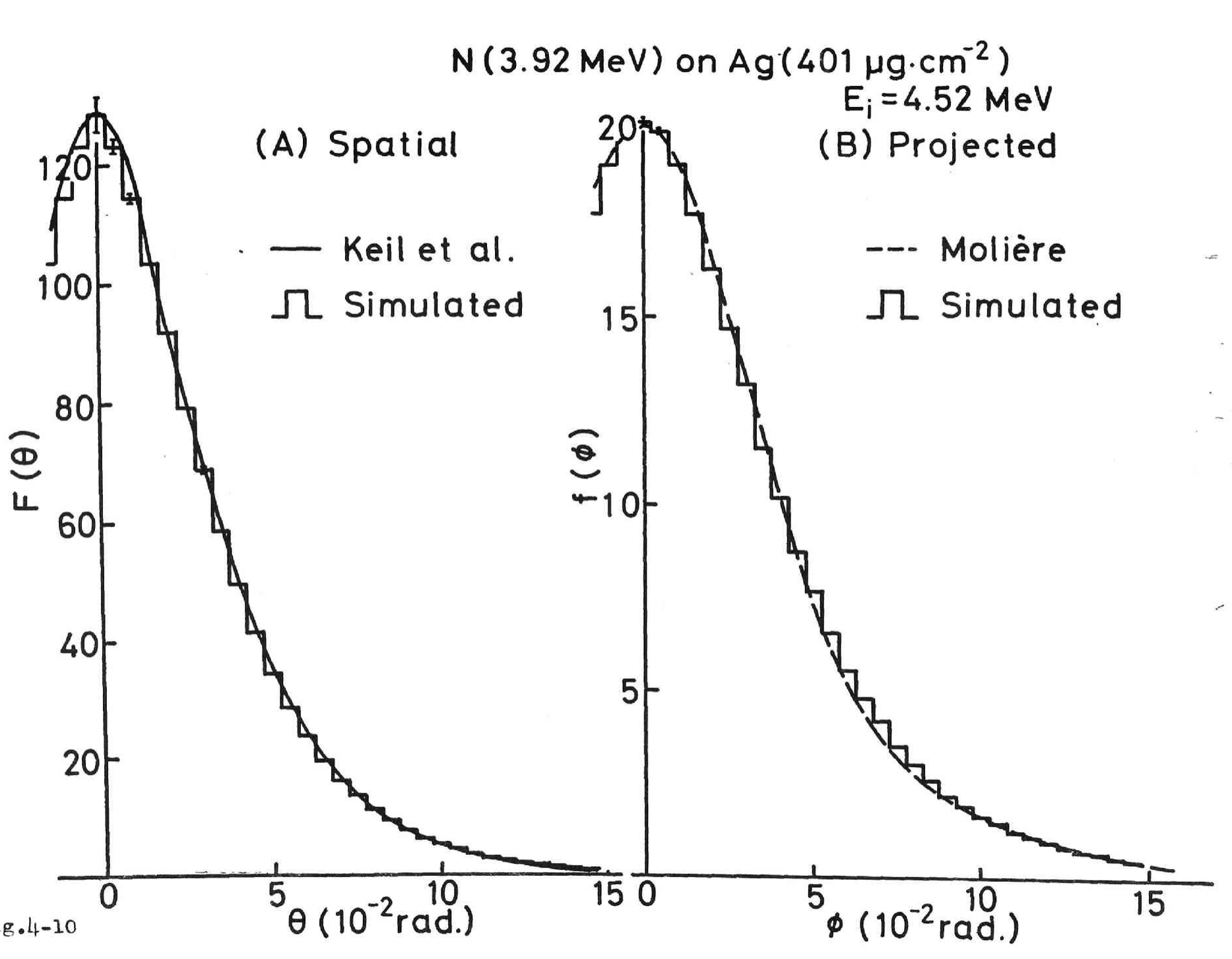
N(3.92 MeV) on Ag(401 μg·cm⁻²)
E_i = 4.52 MeV
(A) Spatial
(B) Projected
Keil et al.
Simulated
Molière
Simulated
F(θ)
f(φ)
θ (10⁻² rad.)
φ (10⁻² rad.)
120
100
80
60
40
20
20
15
10
5
0
5
10
15

Fig.4-10

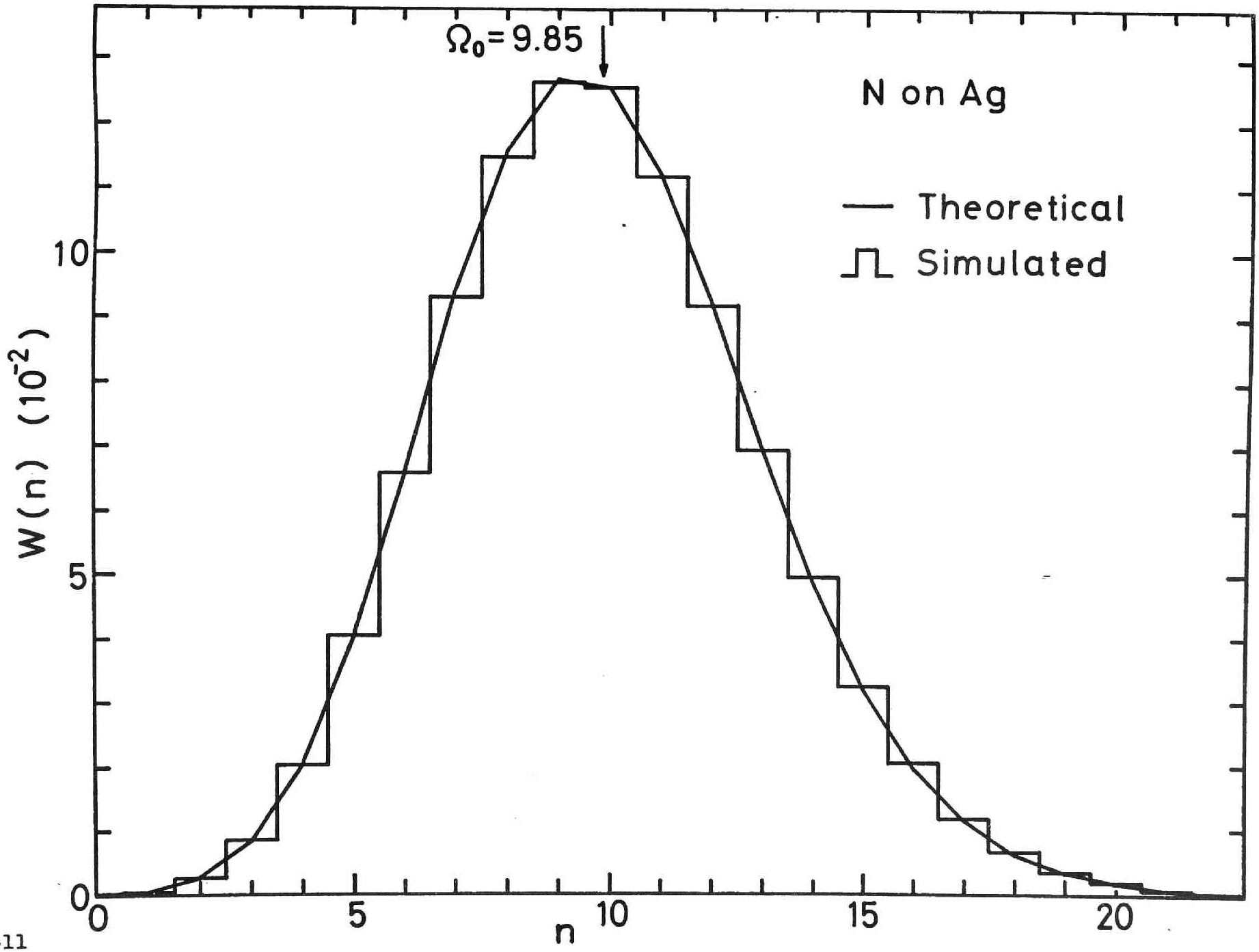
$\Omega_0 = 9.85$
N on Ag
Theoretical
Simulated
W(n) (10^{-2})
0
5
10
n
0
5
10
15
20

Fig.4-11

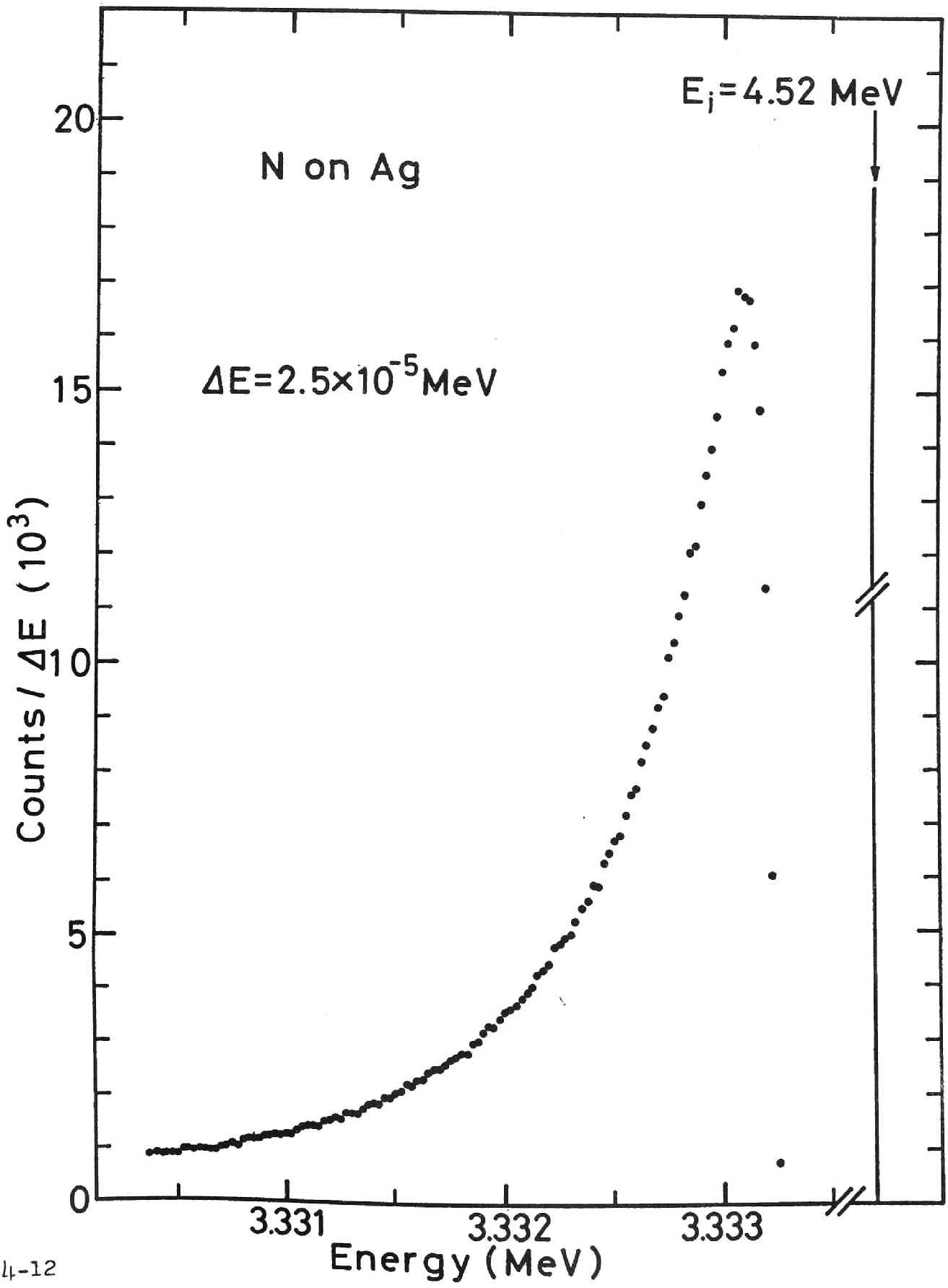
E_i=4.52 MeV
N on Ag
$\Delta E=2.5\times10^{-5}$MeV
Counts / ΔE (10^3)
20
15
10
5
0
3.331
3.332
3.333
Energy (MeV)

Fig.4-12

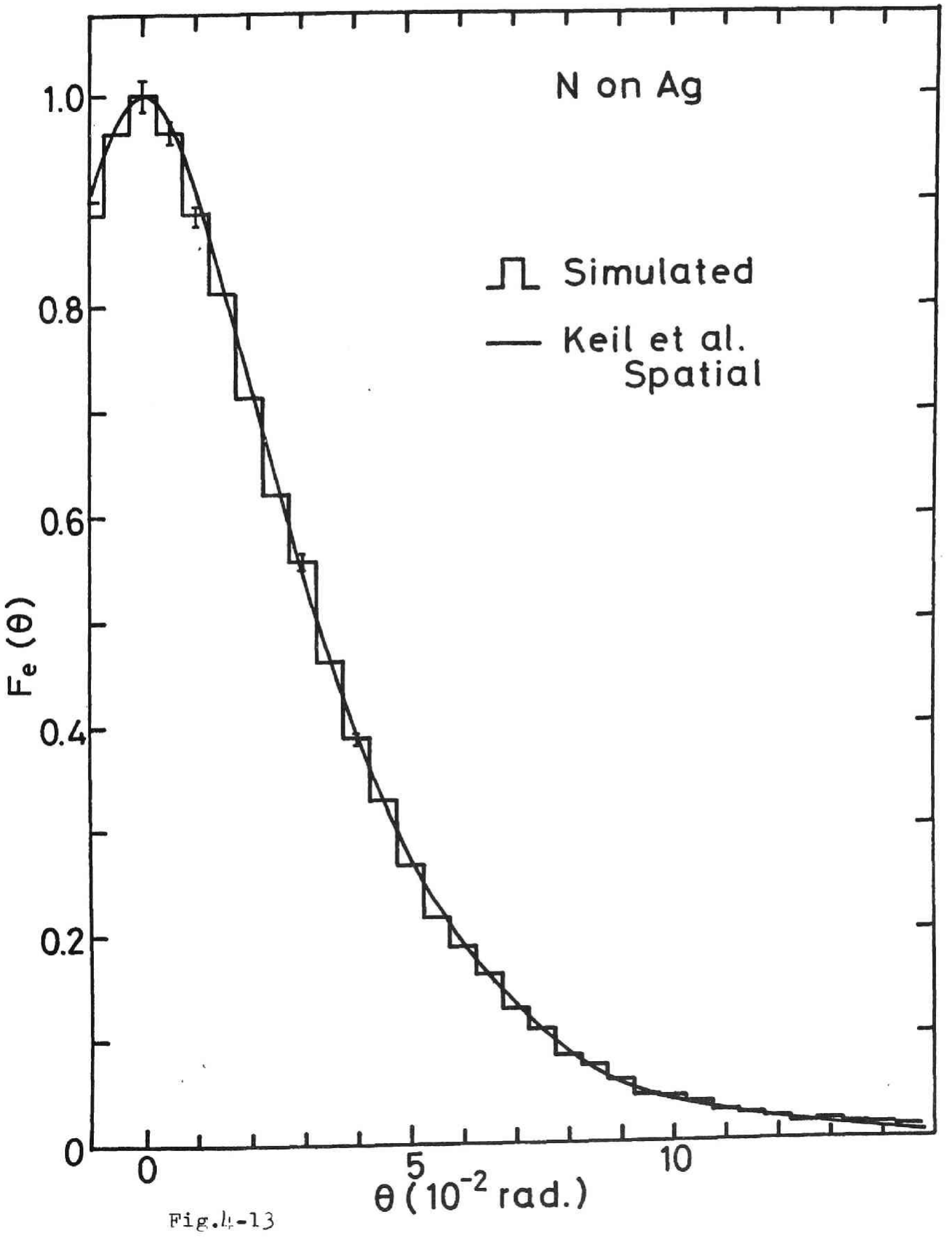
N on Ag
Simulated
Keil et al.
Spatial
1.0
0.8
0.6
0.4
0.2
0
$F_e(\theta)$
0
5
10
θ (10^{-2} rad.)

Fig.4-13